MASTER COPY

...COPY FOR REPRODUCTION PURPOSES

REPORT DOCUMENTAT

AD-A276 022

Approved
...o 0704-0188

(2)

1. AGENCY USE ONLY (Leave blank)	2. REPORT DATE	3. REPORT ...
	January 25, 1994	...D

4. TITLE AND SUBTITLE

"Optical and Image Transmission through Desert Atmospheres"

5. FUNDING NUMBERS

DAAL03-89-G-0108

6. AUTHOR(S)

Carlos McDonald, Luis Carrillo, Gerardo Carrillo, Miguel Nunez, Rick Gamboa, and Jerry Flores

7. PERFORMING ORGANIZATION NAME(S) AND ADDRESS(ES)

University of Texas at El Paso
Electrical Engineering Department
El Paso, TX 79968

8. PERFORMING ORGANIZATION REPORT NUMBER

9. SPONSORING / MONITORING AGENCY NAME(S) AND ADDRESS(ES)

U. S. Army Research Office
P. O. Box 12211
Research Triangle Park, NC 27709-2211

10. SPONSORING / MONITORING AGENCY REPORT NUMBER

ARO 27259.2-GS-SAH

11. SUPPLEMENTARY NOTES

The view, opinions and/or findings contained in this report are those of the author(s) and should not be construed as an official Department of the Army position, policy, or decision, unless so designated by other documentation.

12a. DISTRIBUTION / AVAILABILITY STATEMENT

Approved for public release; distribution unlimited.

12b. DISTRIBUTION CODE

13. ABSTRACT *(Maximum 200 words)*

ABSTRACT

Based on a unique experimental technique, measurement results are presented on the passive, remote sensing of the optical modulation transfer function of desert atmospheres (MTF_A), including the DC, low and high spatial cutoff frequency components which are attributed to contrast, aerosol, and turbulence respectively. In particular, use of this technique has made it possible, for the first time, to directly measure the low spatial frequency cutoff of the aerosol component. This technique is based on utilizing digital image processing of remote video scenes which include two, optically identical, castellated targets which are located at different distances and are contrasted against the horizon sky. Ratios of apparent contrast and FFT calculations are used to determine the MTF_A components, including the spatial cutoff frequencies of the aerosol and turbulence components, independent of the imaging system and actual properties of the targets. The experimental technique is described along with current MTF_A component measurements.

14. SUBJECT TERMS

Optical Modulation transfer function of the atmosphere, aerosols, turbulence, contrast, light extinction

15. NUMBER OF PAGES

144

16. PRICE CODE

17. SECURITY CLASSIFICATION OF REPORT	18. SECURITY CLASSIFICATION OF THIS PAGE	19. SECURITY CLASSIFICATION OF ABSTRACT	20. LIMITATION OF ABSTRACT
UNCLASSIFIED	UNCLASSIFIED	UNCLASSIFIED	UL

NSN 7540-01-280-5500

Standard Form 298 (Rev. 2-89)
Prescribed by ANSI Std. Z39-18
298-102

Optical and Image Transmission Through Desert Atmospheres

Final Report

by

Carlos McDonald,

Gerardo Carrillo, Luis Carrillo, Miguel Nunez,

Rick Gamboa, and Jerry Flores

January 25, 1994

U.S. Army Research Office

Grant No. DAAL03-89-G-0108

The University of Texas at El Paso

Electrical Engineering Department

El Paso, Texas 79968

APPROVED FOR PUBLIC RELEASE;

DISTRIBUTION UNLIMITED

THE VIEWS, OPINIONS, AND/OR FINDINGS CONTAINED IN THIS REPORT ARE THOSE OF THE AUTHOR(S) AND SHOULD NOT BE CONSTRUED AS AN OFFICIAL DEPARTMENT OF THE ARMY POSITION, POLICY, OR DECISION, UNLESS SO DESIGNATED BY OTHER DOCUMENTATION.

ABSTRACT

Based on a unique experimental technique, measurement results are presented on the passive, remote sensing of the optical modulation transfer function of desert atmospheres (MTF_A), including the DC, low and high spatial cutoff frequency components which are attributed to contrast, aerosol, and turbulence, respectively. In particular, use of this technique has made it possible, for the first time, to directly measure the low spatial frequency cutoff of the aerosol component. This technique is based on utilizing digital image processing of remote video scenes which include two, optically identical, castellated targets which are located at different distances and are contrasted against the horizon sky. Ratios of apparent contrast and FFT calculations are used to determine the MTF_A components, including the spatial cutoff frequencies of the aerosol and turbulence components, independent of the imaging system and actual properties of the targets. The experimental technique is described along with current MTF_A component measurements.

TABLE OF CONTENTS

LIST OF FIGURES

LIST OF FIGURES
APPENDIX A

1. SUMMARY OF RESEARCH STUDY

An experimental research study was conducted for the purpose of measuring the overall optical modulation transfer function of desert atmospheres (MTF_A), including, for the first time, the low spatial frequency component of the MTF_A attributed to aerosols, MTF_p; the high frequency component due to turbulence, MTF_t; and the DC component of the MTF_A which is related to contrast, MTF_b.

MTF_A measurements were performed with a unique, passive, remote sensing system. This unique system is based on digital image processing of remote video scenes which ideally include two, optically identical, castellated targets, located along a horizontal direction at different distances from a high resolution CCD video camera, and which are contrasted against the horizon sky.

The basic theory of the MTF_A is summarized in section 2, the experimental approach and measuring system is described in section 3, a summary of the most important results are included in section 4, conclusions and recommendations for future research are included in section 5, and lists of all related grant publications and participants are included in sections 6 and 7, respectively. A summary of the MTF_A data, obtained over a two year period, and analysis results are included in appendix A.

2. THEORY

The atmospheric modulation transfer function, MTF_A, is a quality measure of optical imaging or "seeing" through the atmosphere. It corresponds to a low pass filter and may be expressed approximately by the following product of independent components,[1]

$$MTF_A = (MTF_b) \cdot (MTF_t) \cdot (MTF_p) \cdot (MTF_m) \ , \qquad (1)$$

where,

MTF_b = modulation transfer due to contrast,

MTF_t = modulation transfer function due to atmospheric turbulence,

MTF_p = modulation transfer function due to scattering and absorption by aerosols and particulates, and

MTF_m = modulation transfer function due to molecular absorption and scattering.

MTF_b, the contrast component, is independent of spatial frequency and has a DC component related to extinction; MTF_t, the turbulence component, exhibits a high spatial frequency component measuring thousands of cycles/radian; MTF_p, the aerosol component,

has a very low spatial frequency varying from tens to hundreds of cycles/radian and MTF_m, the molecular scattering component, primarily due to isotropic, Raleigh scattering, is independent of spatial frequency and is negligible compared to scattering, having a value of approximately one, i.e., $MTF_m \approx 1$.

This report describes a unique experiment which has been used to measure the MTF_A components of contrast, turbulence, and for the first time, the direct measurement of the low spatial cutoff frequency of the aerosol component.[2,3,21] Current results of the measurements of MTF_A components are presented.

2.1 Background

Consider a video scene recording of a two dimensional object viewed through the atmosphere. Neglecting electronic noise contributed to the imaging system, the observed image, $f'(x,y)$ may be expressed by the following relation,[4]

$$f'(x,y) = f(x,y) * PSF(x,y) \ , \qquad (2)$$

where,

$f'(x,y)$ = Brightness distribution of image observed through the imaging system and the atmosphere,

$f(x,y)$ = Inherent object brightness free of imaging system and atmospheric degradation,

$PSF(x,y)$ = Optical point spread function which is a measure of the camera's imaging performance and of atmospheric degradation, and

$*$ = Convolution operator.

The optical transfer function, $OTF(f_x,f_y)$, of the imaging system/atmosphere is given by the two-dimensional spatial Fourier transform of $PSF(x,y)$, $\mathcal{F}[PSF(x,y)]$, and is related to the Fourier transforms of the image and object brightness distributions as follows:

$$OTF(f_x, f_y) = \mathcal{F}[PSF(x,y)] = \frac{\mathcal{F}[f'(x,y)]}{\mathcal{F}[f(x,y)]} \quad . \tag{3}$$

Generally, the atmosphere behaves like a spatial low pass filter, attenuating the high spatial frequencies and resulting in the degradation or blurring of the image. The MTF_A magnitudes and spatial cutoff frequencies are related to scattering, turbulence, and path and background radiance.

The modulus of the OTF is defined as the total modulation transfer function of the imaging system and atmosphere, MTF_T, and is given by,

$$MTF_T = | OTF(f_x, f_y) | = (MTF_I) \cdot (MTF_A) \ , \qquad (4)$$

where,

MTF_I = Modulation Transfer Function of Imaging System, and

MTF_A = Modulation Transfer Function of the Atmosphere.

As given by equation (1), the MTF_A may be expressed as the product of the MTF_A components due to contrast, turbulence, aerosols, and molecular scattering.

Consider a camera that is simultaneously focused on two, optically identical target images which are located at different distances from a camera. If MTF_{TF} and MTF_{TN} represent the MTF of the imaging system/atmosphere of the far and near target, respectively, it follows from equation (4) that this ratio is given the following expression,

$$\frac{MTF_{TF}}{MTF_{TN}} = \frac{MTF_{AF}}{MTF_{AN}} \ . \qquad (5)$$

From the above expression , it follows that the ratio of the MTF's is independent of the optical transfer function of the imaging system, and is only a function of the ratio of the atmosphere modulation transfer function of the two targets.

2.2 Aerosol MTF

Light scattering by aerosols is a function of the relative particle size compared to the optical wavelength.[5] If the size of the particle is small compared to the wavelength, the scattering of light will be at large angles with respect to the direction of propagation, and the effect of the scattering is primarily attenuation. If the particle size is comparable or larger than the incident wavelength, more of the light is diffracted primarily in the forward direction. This results in multiple random forward scattering of light to be incident on the receiver, causing degradation and blurring of the image, similar to the effect of atmospheric turbulence.

The MTF for forward scattering, MTF_p, is given theoretically by the following expressions,[5,6,7,8,9,20]

$$MTF_p = e^{-(\frac{f_\theta}{f_c})^2 \cdot \tau_s}, \qquad f_\theta < f_c, \tag{6}$$

$$MTF_p = e^{-\tau_s}, \qquad f_\theta > f_c, \tag{7}$$

where,

f_θ = spatial frequency (cycles/radian),

f_c = a/λ, spatial frequency cutoff (cycles/radian),

λ = optical wavelength (m),

a = effective particle radius (m),

τ_s = $\sigma_s r$ (optical depth),

σ_s = scattering coefficient (m^{-1}), and

r = horizontal path length (m).

The above expressions strictly hold for small angle scattering for the case when the particle radius is comparable or greater than the optical wavelength. It should be noted that there is quite a variation in the models by the various authors, depending on what assumptions are made. Also, the scattering coefficient, σ_s, approximately corresponds to extinction, and may be estimated from contrast transmittance measurements.[17]

The asymptotic cutoff spatial frequency, f_c, where the MTF_p approaches $\exp(-\tau_s)$, was experimentally determined for polystyrene microspheres and is given by the following expression,[9]

$$f_c = 24.4\left(\frac{D}{\lambda}\right)^{.75} \quad cycles/radian, \tag{8}$$

where D is the particle diameter.

Assuming dusty desert conditions so that $D/\lambda \approx 10$, in the visible range,

$$f_c = 137 \quad cycles/radian. \tag{9}$$

For approximately clear desert conditions, $D = \lambda$, giving a value of f_c as follows,

$$f_c \approx 24.4 \quad cycles/radian. \tag{10}$$

The cutoff frequency given by equation (8) also applies when $D/\lambda<1$, resulting in anisotropic multiple scattering.[8,9]

From the above expressions, it can be concluded that the cutoff spatial frequency is observable in windy desert environments when the particulate size is comparable or greater than the optical wavelength. As the spatial frequency approaches zero, the aerosol MTF approaches one.

A relation between the spatial frequency in cycles per radian, f_θ, and the spatial frequency, f_x, in cycles/length is established from the relation between the distances of the image and object planes of the imaging system:

$$\theta = \frac{\Delta X}{S} = \frac{\Delta X'}{S'}, \tag{11}$$

where S and S' correspond to the distances to object and image planes, respectively. The displacements, ΔX and $\Delta X'$, correspond to

the displacements subtended by the view angle θ at the object and image planes, respectively. If ΔX corresponds to one spatial wavelength period, it follows that:

$$f_\theta = \frac{1}{\theta} = \frac{S}{\Delta X} = \frac{S'}{\Delta X'} \ \ cycles/radian, \tag{12}$$

$$f_x = \frac{1}{\Delta X} \ ; \qquad f'_x = \frac{1}{\Delta X'} \ \ cycles/radian, \tag{13}$$

$$f_\theta = f_x S = f'_x S' \ \ cycles/length. \tag{14}$$

2.3 Turbulence MTF

The modulation transfer function component of the atmosphere due to turbulence, MTF_T, is caused by random fluctuations of the atmospheric refractive index which result from random changes in temperature and pressure along the propagation path. As a result, the high spatial frequencies are attenuated, resulting in the

blurring of the observed image. The MTF_T has been studied extensively as it is the primary degradation of imaging in astronomy.

The MTF for atmospheric turbulence, MTF_T, for a horizontal path may be described by the following expression[10,11,12,13]:

$$MTF_T = \exp[-57.44 f_\theta^{\frac{5}{3}} \lambda^{-\frac{1}{3}} C_n^2 r] \ , \qquad (15)$$

where,

λ = optical wavelength (cm),

r = horizontal path length (cm),

C_n^2 = refractive index structure function $cm^{-2/3}$, and

f_θ = spatial frequency (cycles/radian) of angular field of view.

C_n^2 may be expressed in terms of atmospheric pressure P and the temperature structure function, C_T^2, as described below[14]:

$$C_n^2 = (79X10^{-6}\frac{P}{T^2})^2 C_T^2 \ , \qquad (16)$$

where P is the pressure in millibars and T is the temperature in degrees Kelvin. Near the surface, C_T^2 is a function of the air temperature vertical gradient.

At low spatial frequencies, $MTF_T \rightarrow 1$. The MTF_T behaves like a low pass spatial filter and decreases with increasing spatial frequency. The high cutoff frequency, f_{ct}, where MTF_T decreases to e^{-1}, follows from Equation (15):

$$f_{ct} = [57.44\lambda^{-\frac{1}{3}} C_n^2 r]^{-\frac{3}{5}} . \qquad (17)$$

For a typical summer noon day in the local desert, $C_n^2 \sim 10^{-14}$ $cm^{-2/3}$.[14] Assuming a horizontal path with r = 1000 m and λ = 5.5 x 10^{-5} cm (visible), the cutoff frequency is

$$f_{ct} = 3{,}250 \ cycles/radian . \qquad (18)$$

The turbulence MTF has the highest cutoff frequency of the MTF components.

2.4 Contrast MTF

The atmospheric MTF is also degraded by radiance from the target background as well as from the intervening atmosphere, resulting in contrast reduction between the target and background. This effect can be expressed in terms of the MTF_b, the modulation transfer function due to contrast, and is given by the following expression[13]:

$$MTF_b = \frac{B_t' - B_b'}{B_t' + B_b'} = \frac{(B_t - B_b)\, T_{r_j}}{(B_t + B_b)\, T_{r_j} + 2B_h} , \qquad (19)$$

where B'_t and B'_b are the apparent target and background brightness measured at a horizontal range r_j; B_t and B_b are the inherent target and background brightness; B_h is the measured horizon sky brightness corresponding to the scattered radiation along the path; Finally, T_{r_j} is the contrast transmittance measured at r_j.

The contrast transmittance and the target and background brightness are expressed by the following fundamental relationships[15,16]:

$$T_{r_j} = \frac{B_t' - B_b'}{B_t - B_b} = e^{-\sigma r_j} , \qquad (20)$$

$$B_t' = B_t T_{r_j} + B_h \,, \tag{21}$$

$$B_b' = B_b T_{r_j} + B_h \,. \tag{22}$$

The contrast MTF is independent of spatial frequency and corresponds to the atmospheric MTF at zero spatial frequency, where all other MTF components have a value of one. It should be noted that the above target brightness values correspond to the average target brightness.

The contrast MTF may be determined from contrast transmittance measurements of multiple targets. Based on the ratio of contrast transmittance of two targets with identical inherent optical properties and located at horizontal ranges r_j and r_{j+1} with a common background, it follows that the ratio of contrast transmittances to the two targets is given by the following expression[17,18]:

$$\frac{T_{r_{(j+1)}}}{T_{r_j}} = \frac{B'_{t_{(j+1)}} - B'_{b_{(j+1)}}}{B'_{t_j} - B'_{b_j}} = e^{-\sigma(r_{(j+1)} - r_j)} \,. \tag{23}$$

From the above expression, the extinction, σ, may be determined from only the apparent average target and background brightness of the targets located at the known ranges r_j and r_{j+1}, respectively, and appearing on the same video image. Once the extinction is calculated from Equation (23), Equation (20) is used to determine the contrast transmittance T_{r_j} at r_j. The horizon sky brightness B_h can be measured from the same video scene. Equations (21) and (22) may then be used to remotely determine the values of the inherent brightness of the targets and background, B_t and B_b, respectively. The values corresponding to B_h, B_b, B_t, and T_{r_j} may be used in Equation (19) to determine the contrast MTF at zero spatial frequency.

The background may correspond to the white strips of a castellated target, or it may correspond to the horizon sky brightness. For the latter case, $B'_{bj} = B'_{b(j+1)} = B_h$.

3. EXPERIMENTAL APPROACH

Two black and white castellated targets are horizontally located at one and two km from a digital video camera (see Figures 1 and 2). The targets were constructed so that their castellations generate identical spatial frequencies ranging from DC to approximately 80,000 cycles/radian. Both targets are contrasted against

the sky and positioned so that they are both digitally recorded on the same video scene, as shown in Figure 2.

Horizontal line FFT's are generated at corresponding target locations, as explained below. The ratios of the corresponding spectral components of the far target to the near target yields the MTF_A. The MTF_A components due to contrast, aerosols, and turbulence will then be determined from contrast measurements and from the low and high spatial frequency responses, respectively. For validation of theoretical or laboratory models, ancillary measurements were taken of atmosphere scattering and vertical temperature gradient.

3.1 Target Configuration

Figure 1 shows the target configuration. It consists of two castellated targets located at radial distances of 1 and 2 Km. from the video camera. The radial distances to the targets are displaced by a small view angle, θ, in order to allow both targets to be viewed by the video camera in the same scene. Ideally the center of both targets is located at the same height from the horizontal ground. Both targets are assured to have identical inherent optical properties as viewed by the camera by constructing the targets of the same material and by having equal solid angles subtended by both targets when viewed by the camera. This requires that the area of the target be in proportion to the square of the

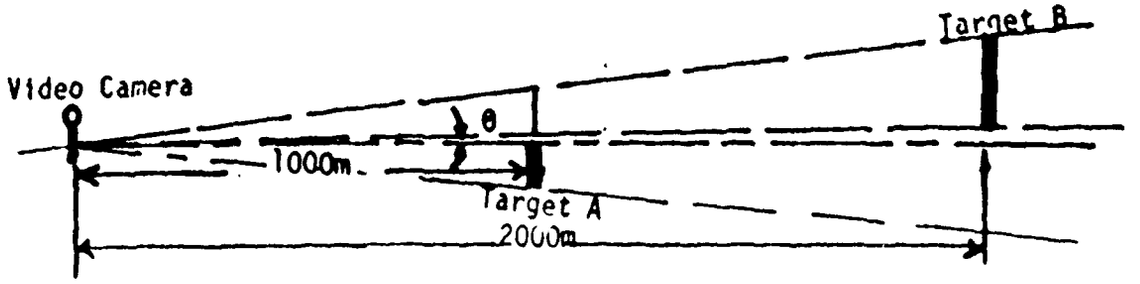

Figure 1. Two target emplacement for MTF_A measurements.

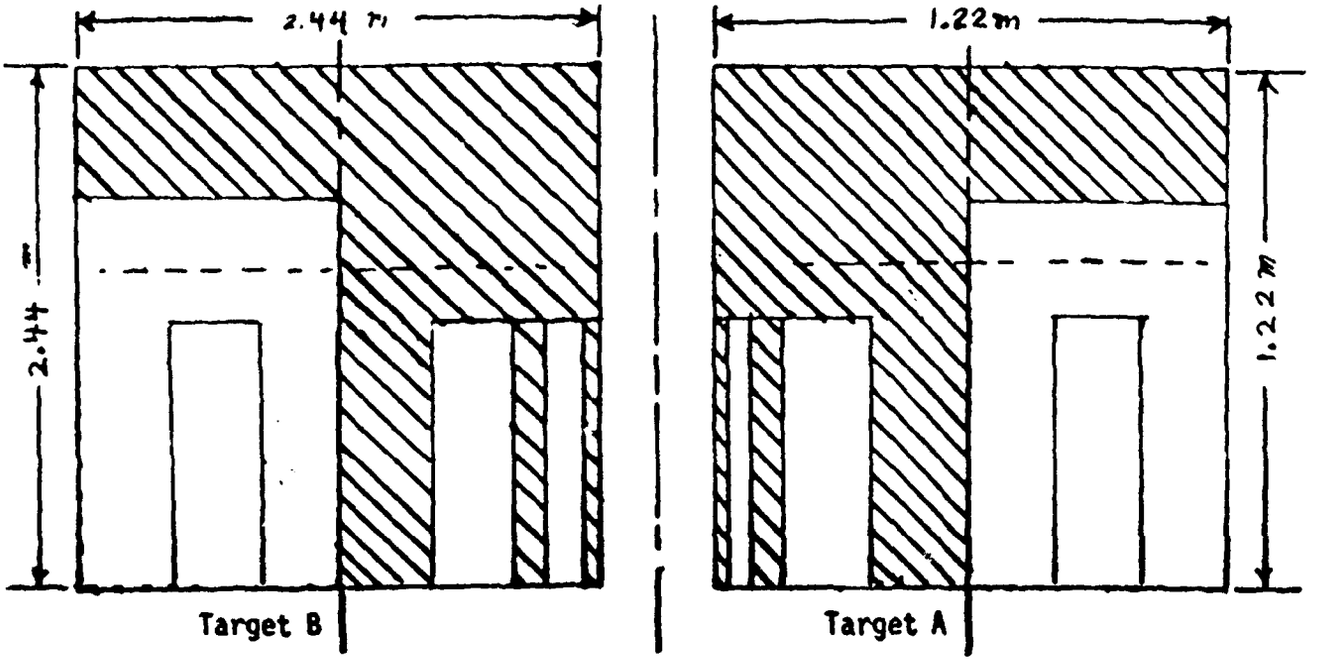

Figure 2. Camera view of the targets located at one an two km. respectively.

radial distance to the target. In order to insure that the corresponding black and white strips of both castellated targets generate the same spatial frequencies in cycles/radian at the camera location, the area of the corresponding strips on both of these targets is also proportional to the square of the radial distances to the camera.

Based on the above construction, both castellated targets were of identical size as viewed from the camera, as shown in Figure 2. Referring to Figure 2, the targets consist of castellated black and white strips for generation of identical spatial frequencies from both targets. The target at 1000 meters measures about 1.22 X 1.22 meters^2, forcing the target at 2000 meters to measure 2.44 x 2.44 meters^2.

3.2 Spatial Frequency Generation

Referring to Figure 2, the lower halves of both targets consist of castellated black and white strips of variable widths. These strips vary from 0.4 meter to 0.6 cm in width for the target located at 1000 meters and 0.8 meter to 1.2 cm for the corresponding strip widths of the target located at 2000 meters, generating identical spatial frequencies varying from 1200 to 80,000 cycles/radian at the camera location. This spatial frequency range

will adequately cover the high spatial frequency cutoff range of the turbulence MTF_A component.

The low and DC spatial frequencies are generated by the outer dimensions of the targets which measure 1.22 x 1.22 meters^2 and 2.44 x 2.44 meters^2, respectively. This fact may be shown by taking the one-dimensional, spatial Fourier transform along the horizontal path of the target. At the target, there is no atmospheric filtering, and the target is ideally in sharp contrast to the sky background. For this case, the spatial Fourier transform corresponds to a pulse and is easily calculated,[19]

$$G(f_x) = B_t \cdot W \cdot \frac{\sin \pi W f_x}{\pi W f_x} , \qquad (24)$$

where,

B_t = target brightness,

W = width of target (m), and

f_x = spatial frequency (cycles/meter).

The corresponding frequency, f_θ, in cycles/radian is related to f_x by equation (12), where S is the radial distance from the camera to the target.

From equation (24), it follows that the amplitude of the spectrum varies as (sin x)/x, generating a continuous spatial

frequency spectrum with a maximum at zero (DC) spatial frequency and decreasing to the first minimum at a spatial frequency given by

$$f_{\theta_{min}} = \frac{S}{W} \quad cycles/radian. \tag{25}$$

For the target at 1000 meters which measures 1.22 x 1.22 meters^2,

$$f_{\theta_{min}} = \frac{1000}{1.22} = 820 \quad cycles/radian. \tag{26}$$

Similarly, spatial frequencies ranging from DC and higher are also generated by the black/white, black/sky, and white/sky step transitions. It follows from the above analysis that identical spatial frequencies ranging from DC to 80,000 cycles/radian are generated by both targets described in Figures 1 and 2.

3.3 MTF_A Spatial Frequency Response

As described in the previous section, the castellated targets described in Figures 1 and 2 ideally generate identical spatial frequency components in the range from DC to 80,000 cycles/radian. However, the radial distances r_A and r_B from the video camera to the

targets A and B are 1000 meters and 2000 meters, respectively. Therefore, the spatial frequency components received by the camera from target B are filtered by an additional amount over those received by the camera from target A, located closer to the camera. This additional filtering corresponds to the intervening atmosphere in the region between the targets, $r_B - r_A$. Since both targets are observed and recorded on the same video scene, additional blurring will be observed on target B due to the spatial filtering of the atmosphere in the region between the targets.

From the brightness distributions of the solid/castellated target images recorded by the video camera, the spatial frequency response of the atmospheric MTF_A can be calculated for the atmospheric region between the targets. The spatial frequency response of the MTF_A between targets A and B may be expressed from equation (4) as follows:

$$MTF(O\text{-}A) = MTF_I \cdot MTF_A(O\text{-}A) \ , \qquad (27)$$

$$MTF(O\text{-}B) = MTF_I \cdot MTF_A(O\text{-}B) = MTF_I \cdot MTF_A(O\text{-}A) \cdot MTF_A(A\text{-}B) \ , \qquad (28)$$

where,

MTF(O-A) = apparent MTF of target A,

$MTF_A(O\text{-}A)$ = MTF_A of atmosphere between camera and target A,

MTF_I = MTF of video camera imaging system,

$MTF(O\text{-}B)$ = apparent MTF of target ,

$MTF_A(O\text{-}B)$ = MTF_A of atmosphere between camera and target B, and

$MTF_A(A\text{-}B)$ = MTF_A of atmosphere between targets A and B.

From the above equations, and equation (2), it follows that since targets A and B have the same inherent properties, $MTF_A(A\text{-}B)$, which is the MTF_A for the atmospheric region between targets A and B is given by

$$MTF_A(A\text{-}B) = \frac{MTF(O\text{-}B)}{MTF(O\text{-}A)} = \frac{|\mathcal{F}[f'_B(x,y)]|}{|\mathcal{F}[f'_A(x,y)]|}, \qquad (29)$$

where $f_B'(x,y)$ and $f_A'(x,y)$ are the apparent brightness distributions of targets A and B recorded by the video camera, respectively.

From the above expression, it is concluded that the MTF_A of the intervening atmosphere between targets A and B, $MTF_A(A\text{-}B)$, is given by the ratio of the apparent MTF's of target B to target A, or by

the ratios of the corresponding Fourier frequency components of targets A and B, respectively. This conclusion is very significant as this ratio is independent of the imaging system characteristics and the actual optical properties of the targets.

3.4 Instrumentation

The video scenes were recorded with a high resolution, 12-bit CCD camera with 512 X 1024 pixels. The CCD camera (Patterson Electronics, Tustin, CA) was cooled to -35°C in order to minimize electronic noise. An 8 inch telescope with 2 meter focal length was used to observe both targets on the same scene at high magnification. A 4 inch telescope with one meter focal length was used for visual sighting. Equal density filters were used to attenuate the brightness. For a given filter, the integration time may be increased in multiples of 10 ms until the maximum dynamic range 4095 is reached. The digital camera was interfaced with a PC-AT where the digitized images are stored and operations are performed. FFT operations were performed with an attached array floating point processor (Eighteen-Eight Labs, Boulder City, Nev.) to the PC and with MATHCAD software. (See Figure 3)

An integrating nephelometer was used to measure the local scattering coefficient. Thermocouples were used to measure the vertical temperature gradient.

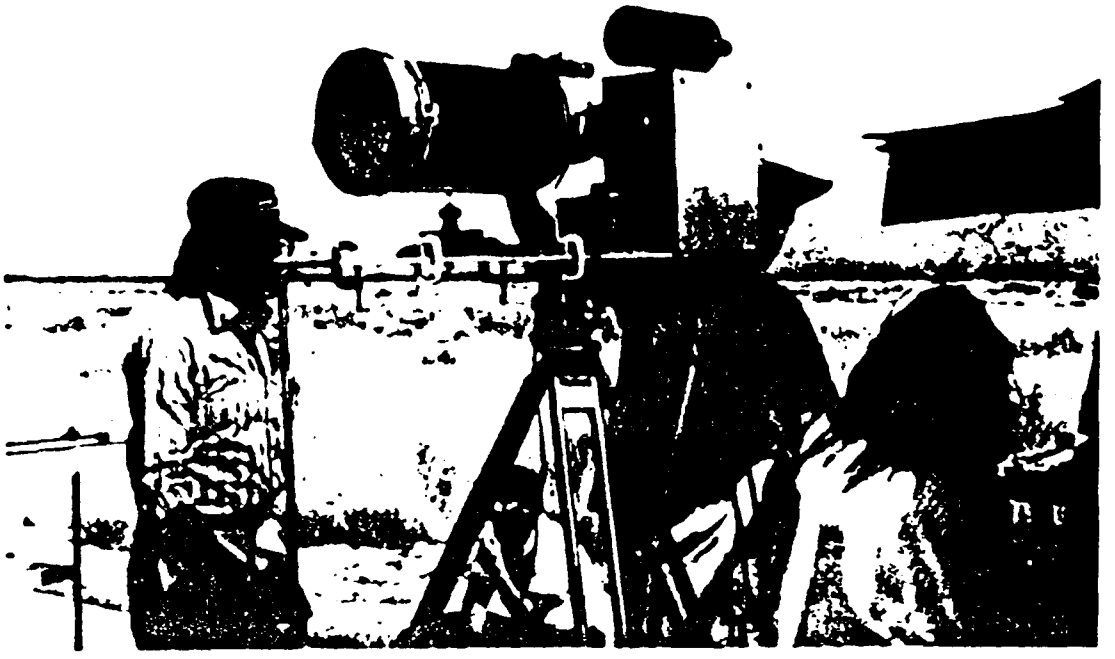

(a)

(b)

Figure 3. The top photo (a) shows the CCD digital video camera with telescopes. Photo (b) shows the PC-AT used to control tha camera and to record and analyze the digitized image.

Recording of the target video scenes was initially severely limited by wind-induced vibrations of the digital camera platform. In order to overcome this limitation, a portable wind resistant cage, measuring approximately 3x3x5 m^2, was designed and fabricated to house the CCD camera which rested on a tripod mounted on top of a six foot high platform. In addition, the pc-based monitoring and recording equipment was also housed inside the wind cage. In order to minimize its weight, the wind cage was constructed with 2"x4" wooden frame, covered with tarp, and lined inside with black plastic. Guy wires were used to secure the wind cage to ground. Since summer temperatures varied up to 110 degrees F, two evaporative air conditioners were installed to cool the air and equipment inside the cage.

The near and far targets were mounted on towers measuring 8 and 13 meters in height, respectively. The height between the towers was necessary due to the hilly terrain existing between the targets and physical constraint of maximum height of the camera. As a result, the line of sight from the camera to the targets was approximately 0.2 degrees with respect to the horizontal. The near tower was constructed with 4"x4" lumber, while the far target was constructed of 3 in^2, light structural, square tubing. Guy wires were used to secure the towers to ground. In order to clean and align the targets along the desired line of sight, the targets were mounted on rails which were attached to the towers. This allowed

the targets to be raised or lowered with winches which were operated by an electric drill. (See Figure 4)

4.0 EXPERIMENTAL RESULTS

MTF_A measurements were performed with the digital video camera/dual target system described in the previous section. Video scenes were obtained from early morning to early afternoon in order to record the relative imaging effects of aerosol and turbulence. Integration times varied from 10 ms to one second, depending on the attenuation of the equal density filter used and on the desired dynamic range.

To measure the aerosol MTF_A component, MTF_p, the low frequency component of the MTF_A, horizontal and vertical line FFT's of each target were computed from the digitized pixel data of the video scenes. These pixels were located across the portions of both targets where there are single step changes between the white and black portions of the target (see dashed lines of Figure (2)). These step changes generate a low frequency (sin x)/x spectrum, similar to equation (24). Based on equation (29), the ratio between the corresponding FFT components of the targets yields the low frequency spatial response of the aerosol component of the MTF_A between the two targets.

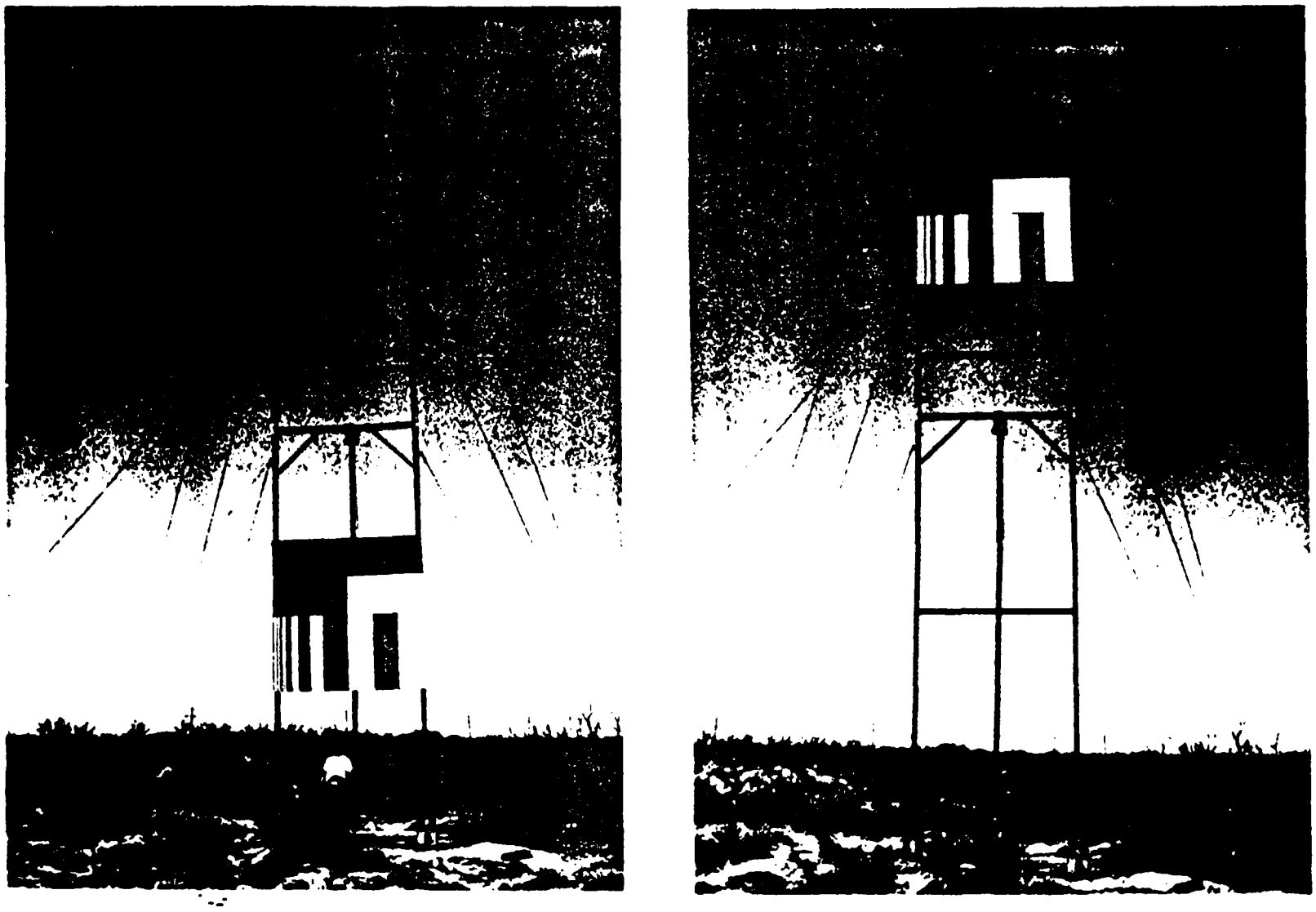

Figure 4. The above photo shows one of the two castellated targets measuring 2.24 m^2, mounted on vertical rails to a 13 m. tower. A motor driven winch is used to lift and lower the target.

The results of MTF_A measurements are summarized in Appendix A, corresponding to typical measurements obtained early morning, mid-morning, and noon, from August 1992 through August 1993. Figures 5-8 summarize typical results of the MTF_p aerosol component measurements. Referring to Figures 5-8, (a) corresponds to the pixel values in the line path through the white/black step for the near and far targets, F_i and B_i, respectively; (b) corresponds to the normalized low frequency magnitude of the FFT's computed from the pixel values shown in (a) where $|Ffft_j|$ and $|Bfft_j|$ are the FFT's of the near and far targets, respectively, and $|Ffft_0|$ and $|Bfft_0|$ are their corresponding DC components; and (c) corresponds to the normalized low frequency MTF_p, given by the ratio of magnitude of the FFT's between the far and near targets, respectively. FFT analysis yielded a maximum spatial frequency resolution of about 0.12 cycles/mrad.

Referring to (c) of Figures 5-8, the low frequency dependence of the MTF_p, below the cutoff frequency, conforms closely, within 0.5%, to the model of the aerosol component given by equation (6). However, the transition given by equation (7) was not observed, as the frequency response continued to drop for f_θ greater than f_c. This phenomena is explained below.

The estimated aerosol cutoff frequencies, f_c, and the DC components of the MTF_A, MTF_b, are also included in (c) of Figures 5-8. The cutoff frequencies were estimated from the aerosol MTF_p frequency response, equation (6), and estimates of the optical

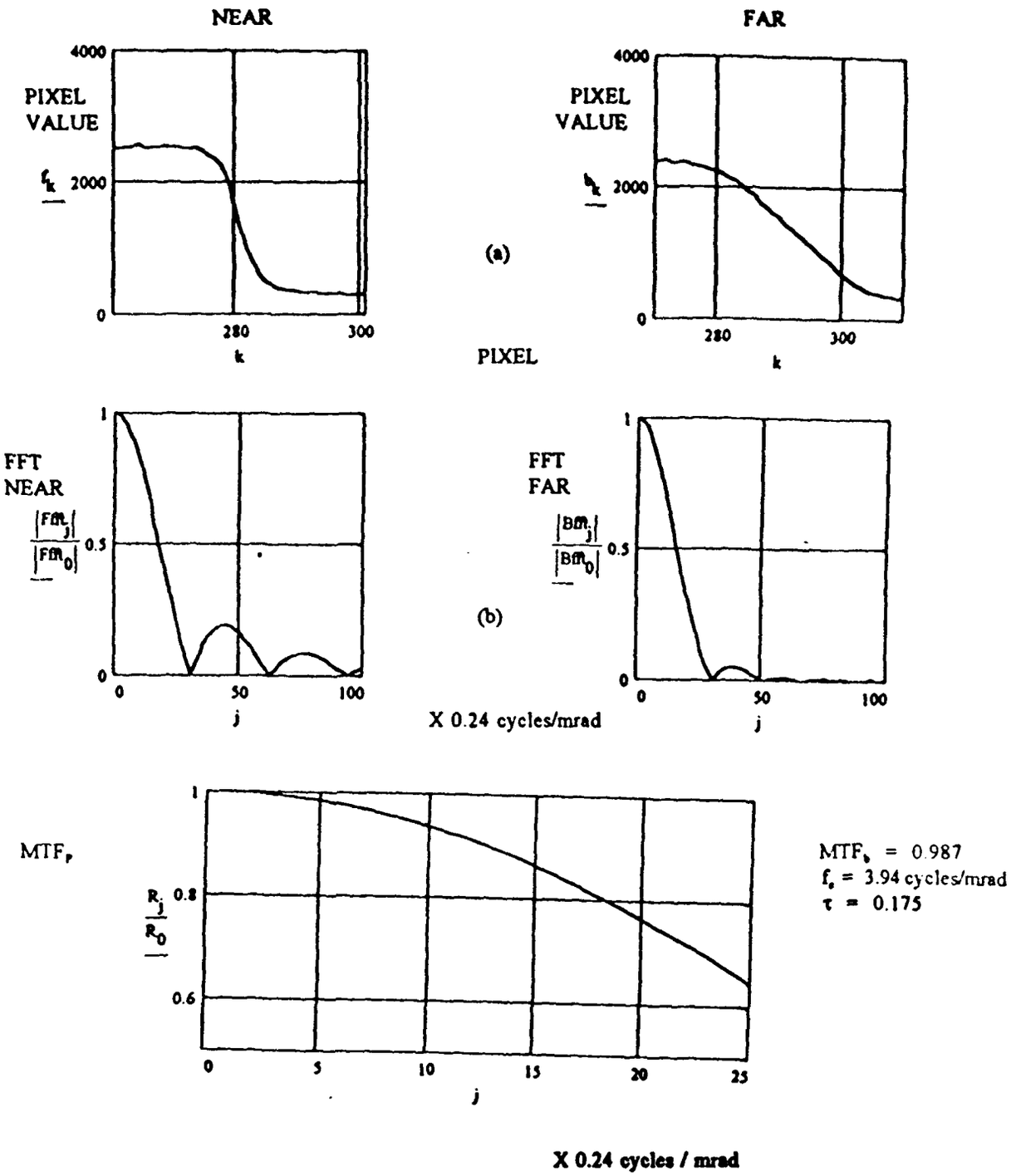

Figure 5 .Data from the morning of August 21, 1992: (a) line pixel values of the black-white steps for both targets; (b) normalized, line FFTs of both targets based on the corresponding pixel values shown; (c) normalized aerosol MTF_A, MTF_p, derived from the ratio of far target FFT to the near target FFT. Values for f_o, τ, and MTF_A are included. The pixel (a) and FFT (b) data on the left and right corresponds to the near and far target, respectively.

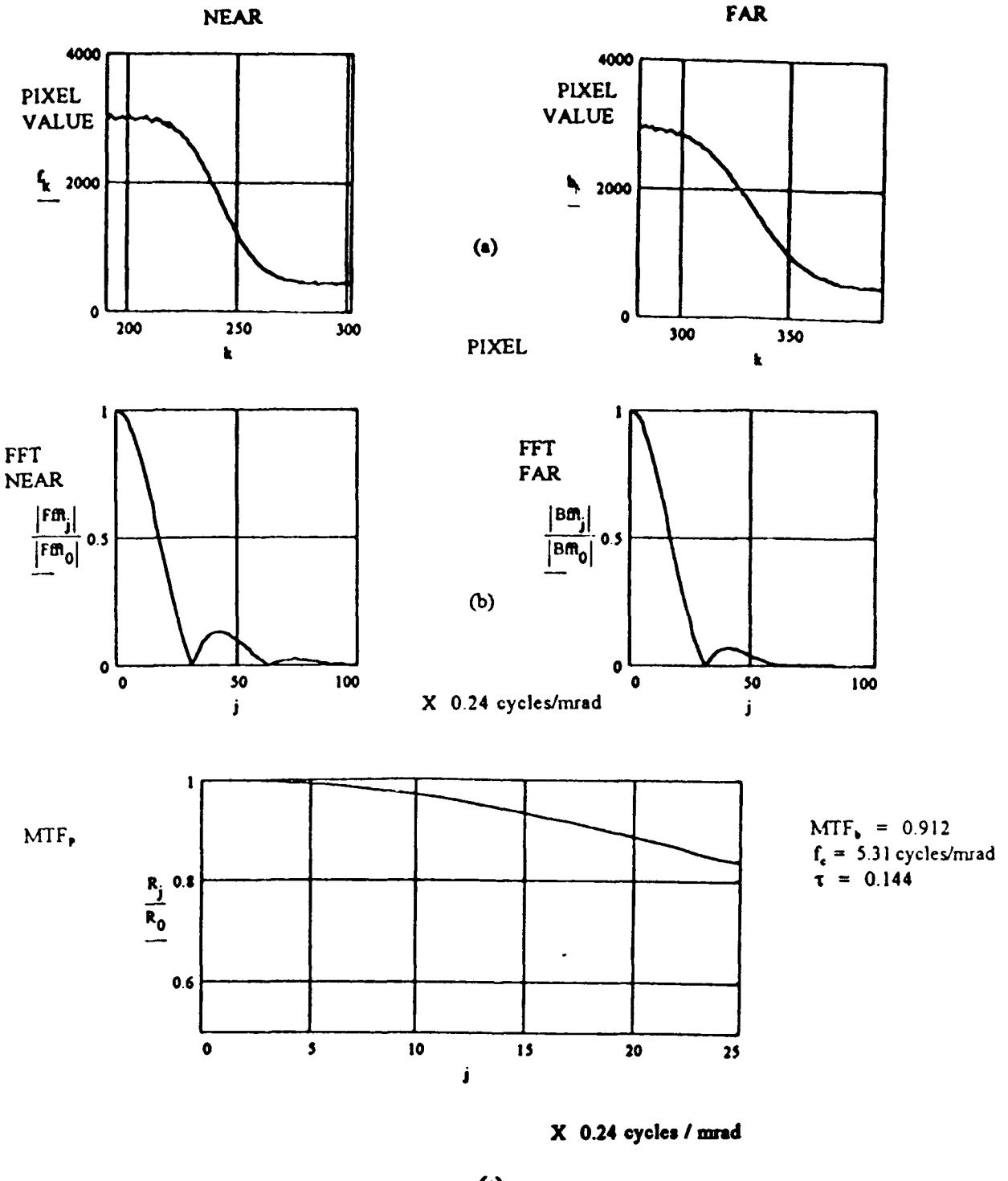

Figure 6. Data from noon of August 21, 1992: (a) line pixel values of the black-white steps for both targets; (b) normalized, line FFTs of both targets based on the corresponding pixel values shown; (c) normalized aerosol MTF_A, MTF_P, derived from the ratio of far target FFT to the near target FFT. Values for f_c, τ, and MTF_A are included. The pixel (a) and FFT (b) data on the left and right corresponds to the near and far target, respectively.

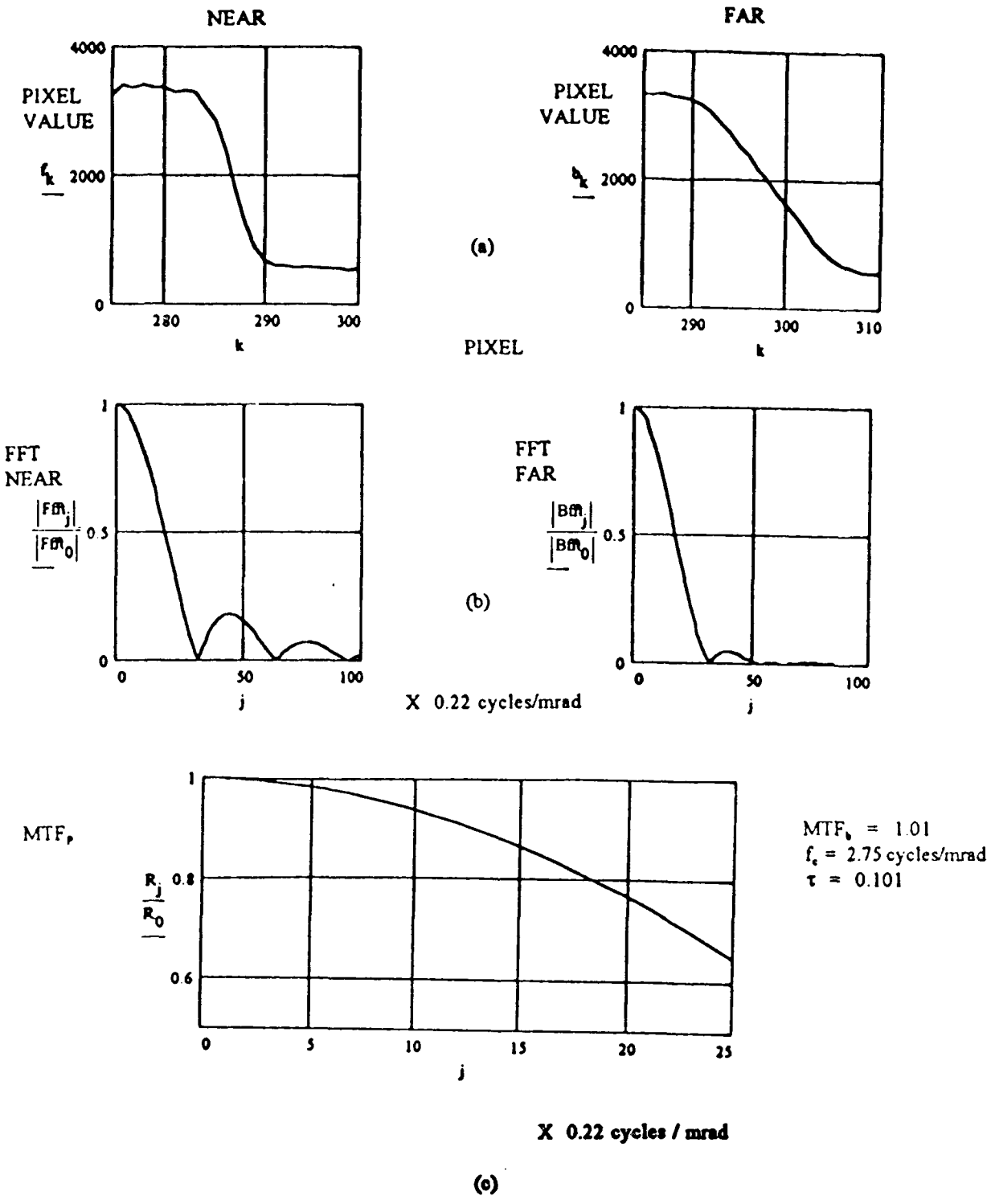

Figure 7. Data from the morning of November 21, 1992: (a) line pixel values of the black-white steps for both targets; (b) normalized, line FFTs of both targets based on the corresponding pixel values shown; (c) normalized aerosol MTF_A, MTF_P, derived from the ratio of far target FFT to the near target FFT. Values for f_c, τ, and MTF_A are included. The pixel (a) and FFT (b) data on the left and right corresponds to the near and far target, respectively.

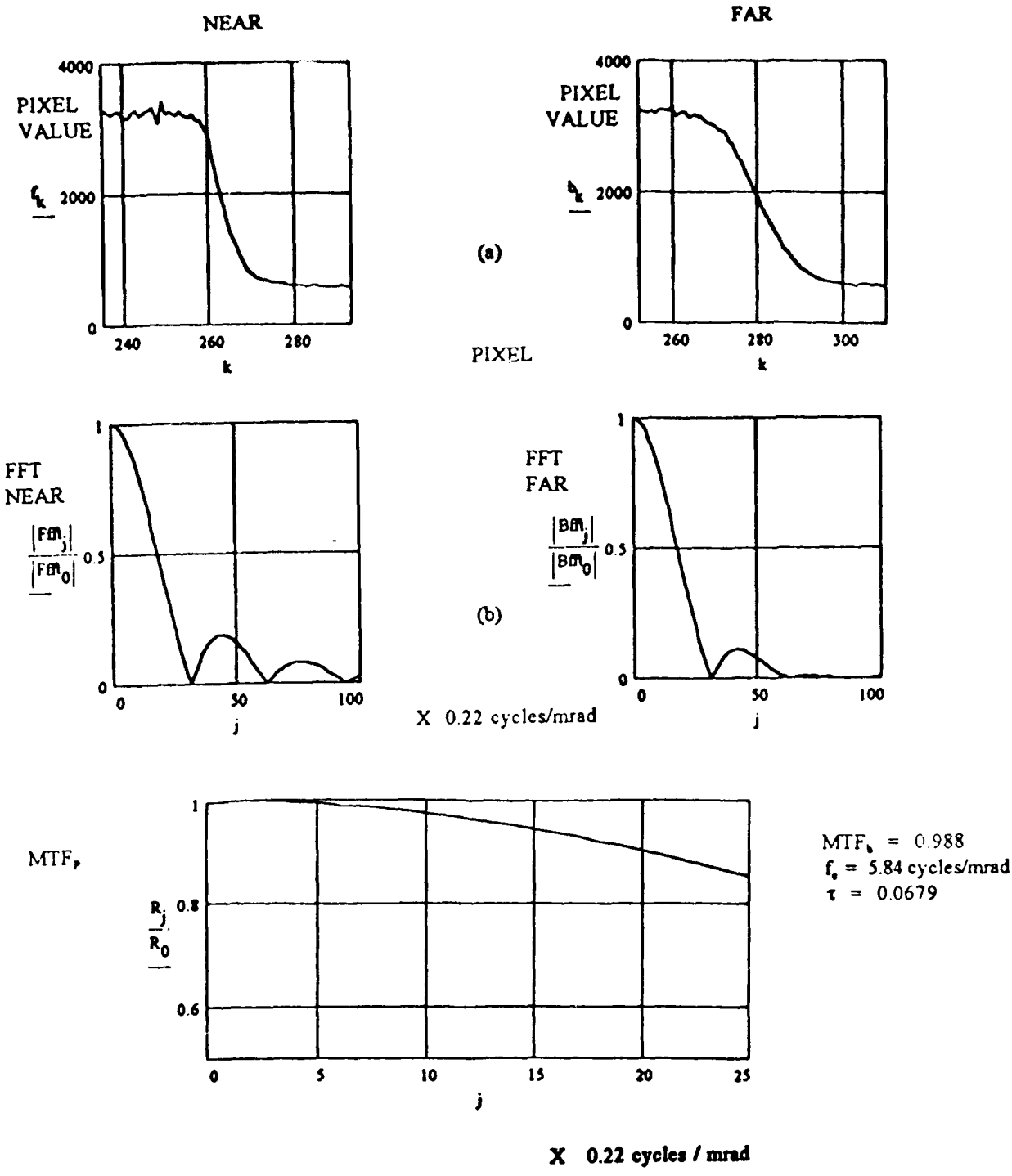

Figure 8. Data from noon of November 21, 1992: (a) line pixel values of the black-white steps for both targets; (b) normalized, line FFTs of both targets based on the corresponding pixel values shown; (c) normalized aerosol MTF_A, MTF_P, derived from the ratio of far target FFT to the near target FFT. Values for f_c, τ, and MTF_A are included. The pixel (a) and FFT (b) data on the left and right corresponds to the near and far target, respectively.

depth based on extinction or scattering coefficient values obtained from contrast, nephelometer and visibility measurements. The DC components of the MTF_A, MTF_b, were estimated from equation (19)using the pixel values of the same black to white steps shown in (a) of Figures 3-6, and calculating the ratio between the far and near target values.

The turbulence MTF_A components are summarized in Figures 9-12. These measurements were based on the amplitude variation of the castellated black and white strips (Figure 2), measured as a function of their spatial frequency. Referring to Figures 9-12, (a) corresponds to the pixel values in the line paths through the the center of the castellated black and white, variable width strips for the near and far targets; (b) corresponds to the normalized, spatial frequency response of the near and far targets as measured from the pixel values shown; and (c) corresponds to the normalized, spatial frequency response of the MTF_A turbulence component, MTF_t, calculated from the ratio of spatial response of the far to near targets, respectively. Estimates of the turbulence cutoff frequencies, f_{ct}, are included in (c). Spatial frequencies ranging from 2.5 to 80 cycles/mrad were observed.

From comparisons between the morning and noon data of the aerosols and turbulence MTF_A components summarized in Figures 5-12, the following observations may be noted:

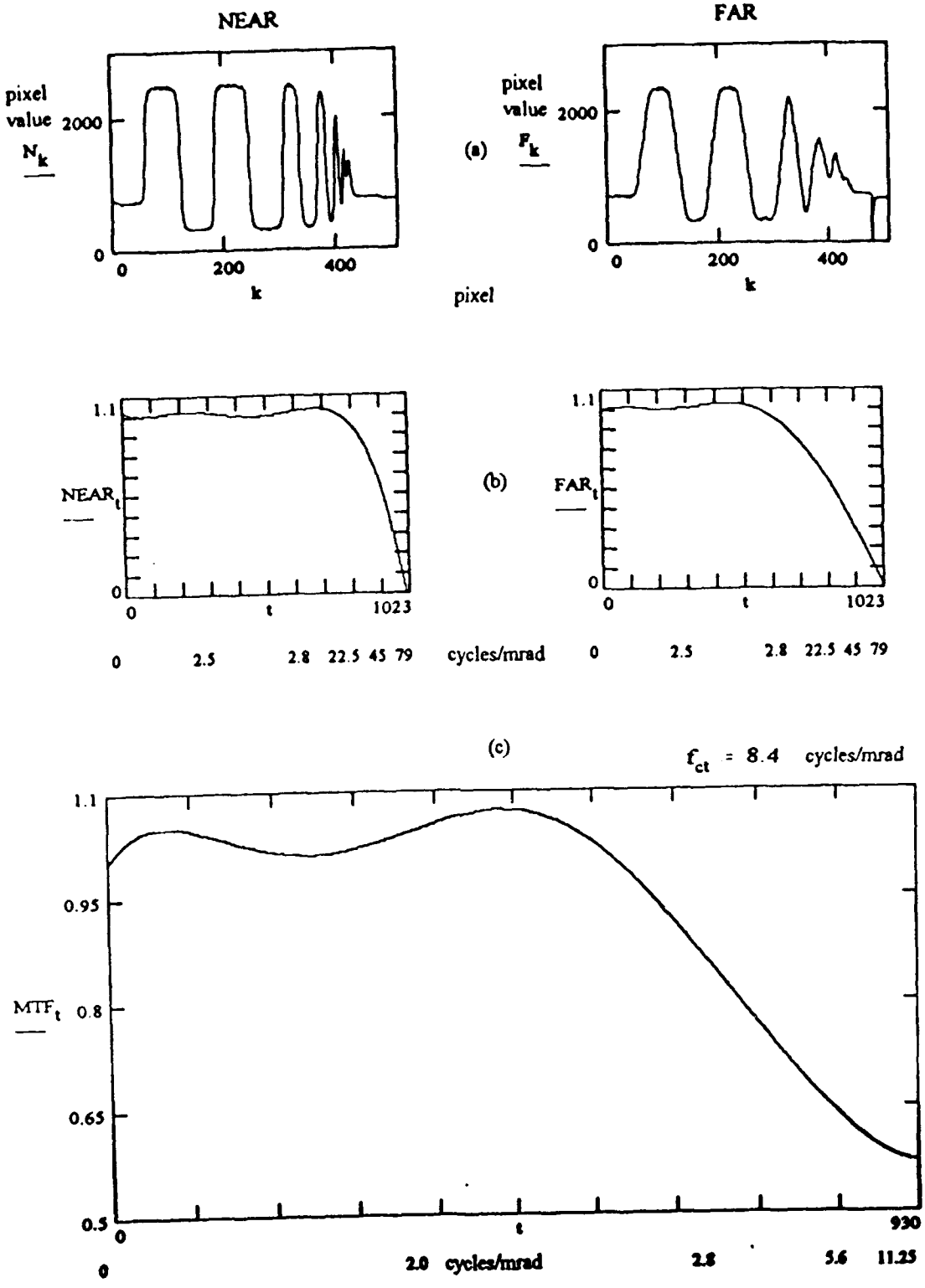

Figure 9 .Data from the morning of August 21, 1992: (a) line pixel values of castellated black/white stripes for both targets; (b) normalized spatial frequency response of both targets based on the corresponding pixel values shown; (c) turbulence MTF_A, MTF_t, derived from the ratio of the far to near target frequeny response. The pixel values (a) and frequency data (b) on the left and right corresponds to the near and far target, respectively.

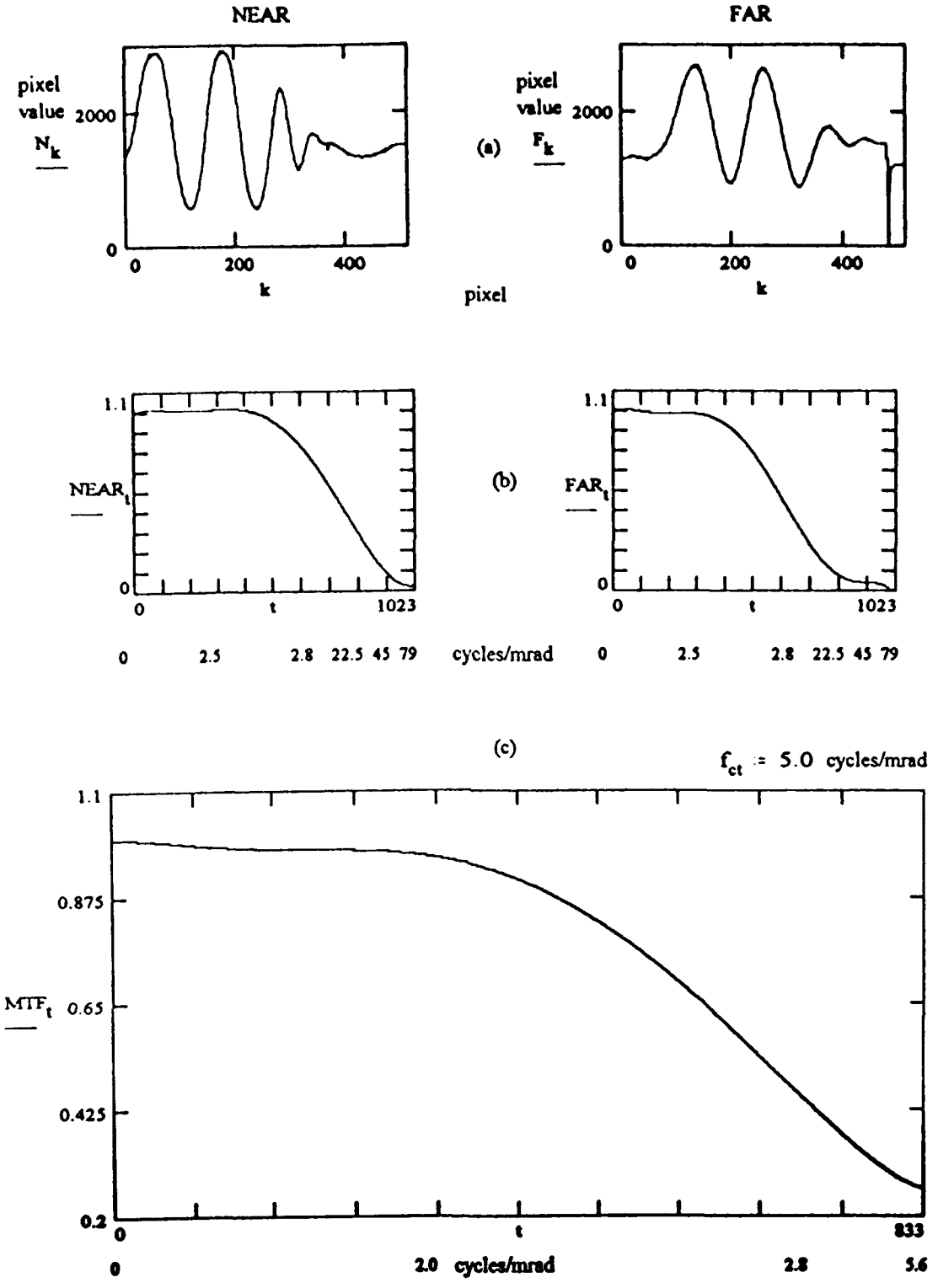

Figure 10. Data from noon of August 21, 1992: (a) line pixel values of castellated black/white stripes for both targets; (b) normalized spatial frequency response of both targets based on the corresponding pixel values shown; (c) turbulence MTF_A. MTF_t, derived from the ratio of the far to near target frequeny response. The pixel values (a) and frequency data (b) on the left and right corresponds to the near and far target, respectively.

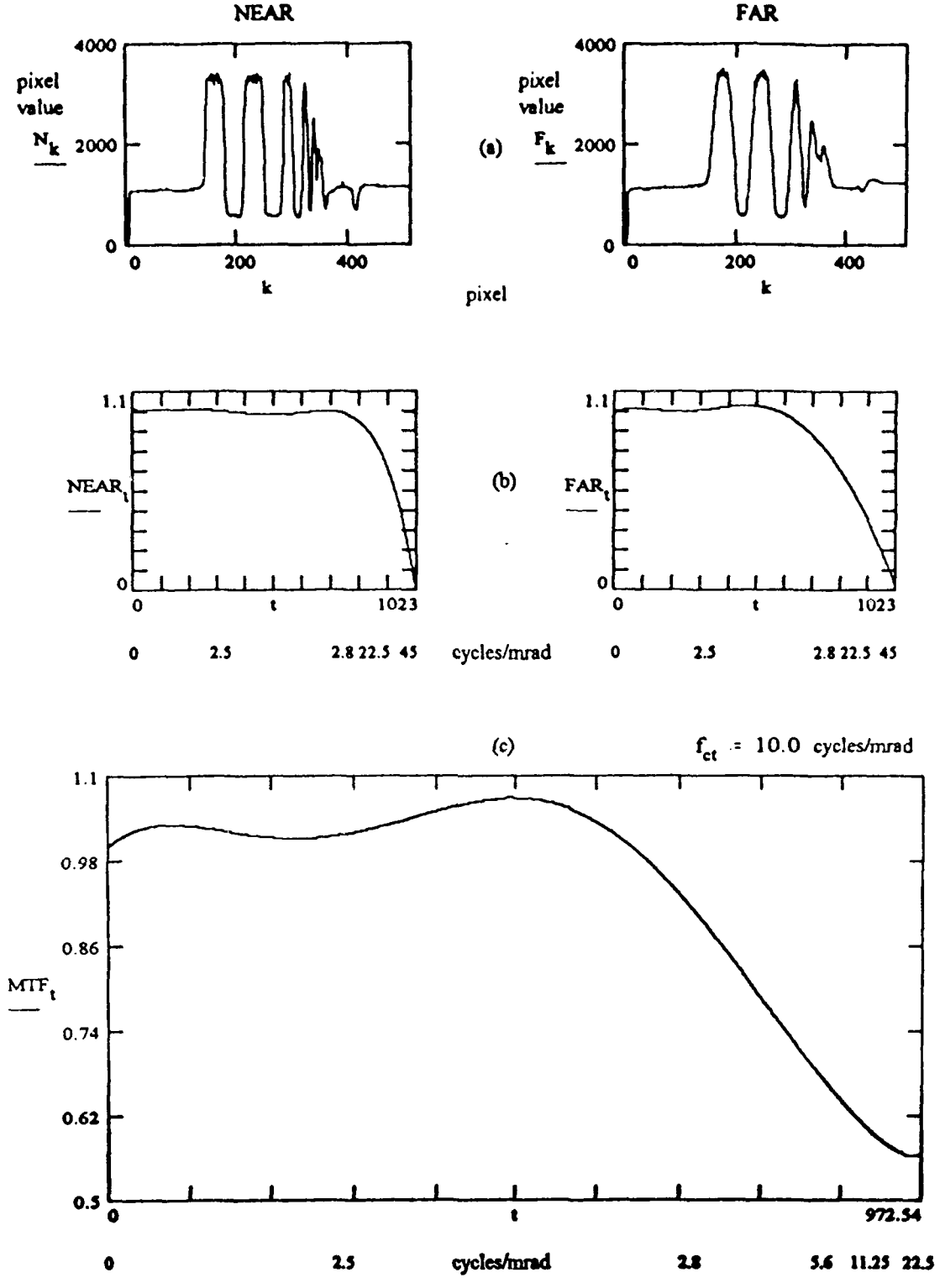

Figure 11. Data from the morning of November 21, 1992: (a) line pixel values of castellated black/white stripes for both targets; (b) normalized spatial frequency response of both targets based on the corresponding pixel values shown; (c) turbulence MTF_A, MTF_t, derived from the ratio of the far to near target frequency response. The pixel values (a) and frequency data (b) on the left and right corresponds to the near and far target, respectively.

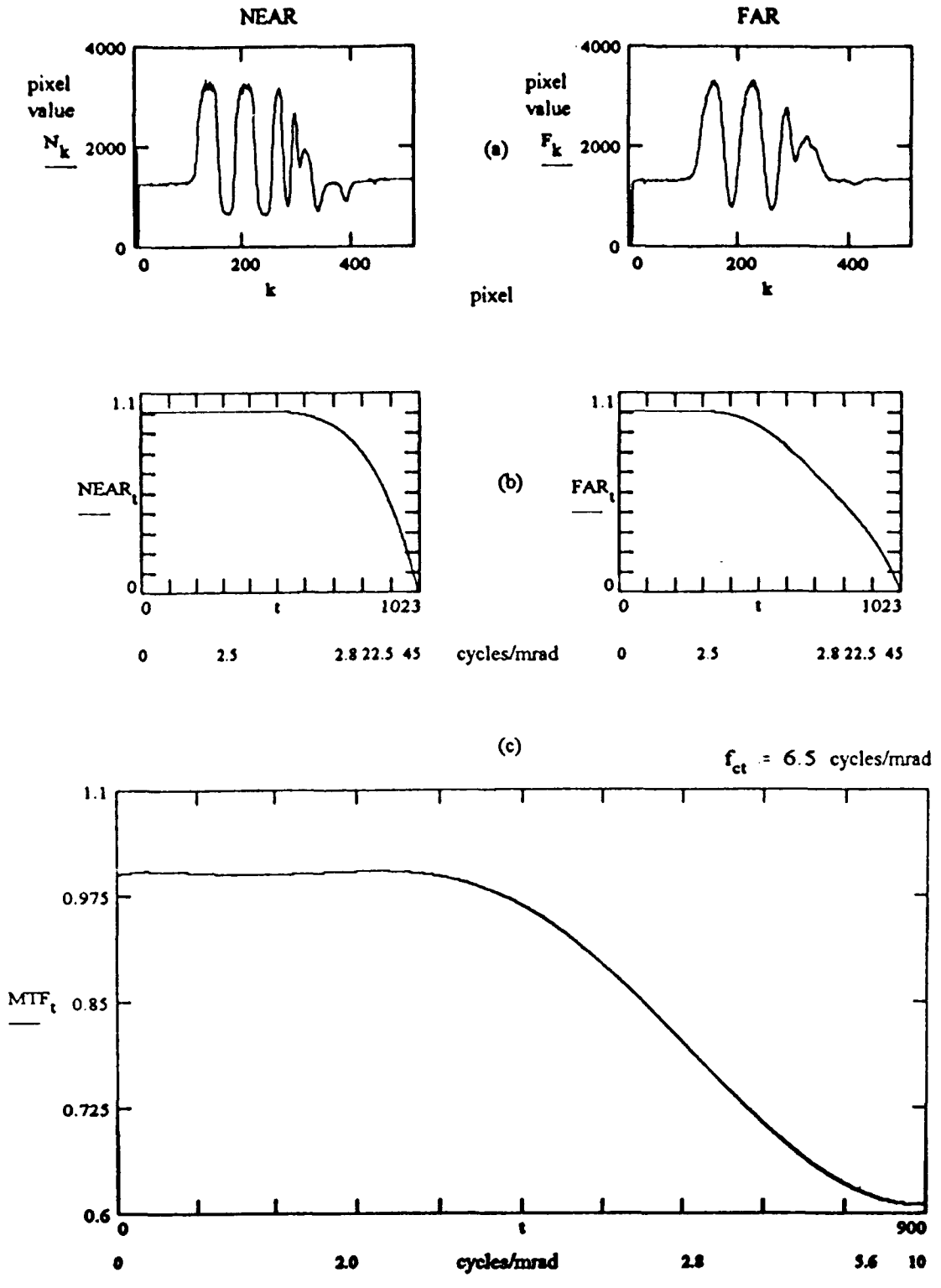

Figure 12 .Data from noon of November 21, 1992: (a) line pixel values of castellated black/white stripes for both targets; (b) normalized spatial frequency response of both targets based on the corresponding pixel values shown; (c) turbulence MTF_A, MTF_t, derived from the ratio of the far to near target frequeny response. The pixel values (a) and frequency data (b) on the left and right corresponds to the near and far target, respectively.

(a) For the aerosol MTF_A components, (Figures 5-8), the cutoff frequencies, f_c, were lower in the morning than at noon, indicting that finer particulates predominated early morning than at noon. This was most likely due to the greater stability of the desert air in the morning.

(b) For the turbulence MTF_A components, (Figures 9-12), the cutoff frequencies, f_{ct}, decrease from morning to noon, indicating a greater turbulence at noon, than in the morning, as expected.

(c) The aerosol MTF_A component agrees closely with equation (6) but not equation (7). This is due to the interaction of turbulence with the aerosols. This is evidenced by the fact that the turbulence cutoff frequencies, f_{ct}, were close to the aerosol cutoff frequencies, f_c, particularly at noon of August 21, 1992.

(d) As indicated in Figure 7(c), the calculated MTF_b, the contrast component of the MTF_A, was greater than one. This is due to the effect of reflection from the flat white paint used on the targets and from the slight non-parallelism between the targets. Use of non-reflective paints should yield more accurate results on the calculation of the MTF_b. Also, positioning of the targets along a line off East-West will minimize reflection. In Addition, precaution has to be taken to insure that both targets have a similar background. However, this does not

affect the FFT analysis since the DC components are removed.

Based on the above analysis procedure, Appendix A, Figures 1-76, summarize the MTF_A component measurements obtained from throughout the year from August 1992 to August 1993. Generally, the results are typical of those described above. Digitized data is available upon request from the Electrical Engineering Department.

Field experiments on the effect of defocusing were found to have a minimal effect on the MTF_A component determination. Extreme defocusing effects can be observed by comparing figures 27 and 28 with Figures 29 and 30, respectively, of Appendix A. The resullts agree with theory, equation (30), which indicates that in determining the MTF_A components by taking ratios of the corresponding MTF_A components between the near and far targets, the effect of the MTF of the imaging system is ideally cancelled.

5. CONCLUSIONS AND RECOMMENDATIONS

The digital video camera/dual target passive optical system described above makes possible the measurement of all MTF_A components. In particular, for the first time, the low frequency component of the optical MTF_A due to the aerosol has been measured, including estimates of the aerosol low frequency cutoff.

Refinement of the FFT analysis should make it possible to increase the aerosol spatial frequency resolution from about 0.12 to less than 0.01 cycles/mrad.

As indicated in (c) of Figures 5-8 and the results shown in Appendix A, measurement of MTF_p, the aerosol component of the MTF_A, provides an accurate technique for characterizing atmospheric aerosols. The basic MTF_p relation, given by equation (6), was verified within 0.5% below f_c , the aerosol cutoff frequency.

Additional studies are suggested to determine the actual relation between the aerosol cutoff frequency, the aerosol distribution, and the interaction between aerosol scattering and turbulence.

6. LIST OF GRANT PUBLICATIONS

The following is a list of publications and technical reports which resulted from this research study.

(1) C. McDonald, "Measurement of the Modulation Transfer Function of Desert Atmospheres," In Proceedings of SPIE Conference on Optical Engineering/Aerospace Sensing, vol. 1487, pp 203-219, "Propagation Engineering: Fourth in Series ," Orlando, Florida, April 1991.

(2) C McDonald, G. Romero, C. Ortiz, J. Carbajal. "Measurement of the aerosol component of the modulation transfer function in the desert atmospheres," In Proceedings of SPIE Conference on Atmosphere Propagation and Remote Sensing, vol 1688, p.p. 86-98, Orlando, Florida, April 1992.

(3) C. McDonald, J. Carbajal, J. Flores, R. Mesta, G. Carrillo, M.A. Nunez, and Luis Carrillo, "Measurement of the overall modulation transfer function of the atmosphere," In Proceedings of SPIE Conference on Atmospheric Propagation and Remote Sensing II, Vol 1968, Orlando Florida, April 1993.

(4) C. McDonald, Gerardo Carrillo, Luis Carrillo, and Miguel Nunez, "Optical and Image Transmission through Desert Atmospheres: Final Report,to the Army Research Office" Grant DAAL03-89-G-0109, Electrical Engineering Department, The University of Texas at El Paso, El Paso, TX, Jan. 15, 1994.

7. LIST OF GRANT PARTICIPANTS

The following is a list of grant participants from the University of Texas at El Paso, including their classification and status.

Staff:

Carlos McDonald, Principal Investigator and Professor of Electrical Engineering

Graduate Students:

Carlos Becera*

Jesus Carbajal

Gonzalo Romero*

Carmen Ortiz*

Undergraduate Students:

Jesus Carbajal*

Gerardo Carrillo*

Luis Carrillo*

Mike Paganini

Jerry Flores

Rick Gamboa

Rick Mesta

Miguel A. Nunez

Gonzalo Romero*

* Completed B.S.E.E.

* Completed M.S.E.E.

BIBLIOGRAPHY

1. N. S. Kopika, "Overview of imaging through the atmosphere," In proceedings of SPIE - The international Society for Optical Engineering, Vol 928, pp. 10-25, Florida, April 1988.

2. C. McDonald, "Measurement of the Modulation Transfer Function of Desert Atmospheres," In Proceedings of SPIE Conference on Optical Engineering/Aerospace Sensing, vol. 1487, pp 203-219, "Propagation Engineering: Fourth in Series ," Orlando, Florida, April 1991.

3. C McDonald, G. Romero, C. Ortiz, J. Carbajal. "Measurement of the aerosol component of the modulation transfer function in the desert atmospheres," In Proceedings of SPIE Conference on Atmosphere Propagation and Remote Sensing, vol 1688, p.p. 86-98, Orlando, Florida, April 1992.

4. M. P. Ekstrom, Digital Image Processing Techniques, Academic Press, New York, 1984.

5. D. Deirmendjian, Electromagnetic Scattering on Spherical Polydispersions, Elsenor, New York, 1969.

6. R.F. Lutomirski, "Atmospheric degradation of electrooptical system performance," Applied Optics, Vol. 17, No 24, pp. 3915-3921, December 1978.

7. N. S. Ekstrom, "Imaging through the atmosphere for airborne reconnaissance," Optical Engineering, Vol. 26, No. 11 pp. 1148-1154, November, 1987.

8. A. Zardecki, A. W. Siegfried, J. F. Embury, "Multiple scattering effects in spatial frequency filter," Applied Optics, Vol. 23, No. 22, November, 1984.

9. Y.Kuga, A. Ishimaru, "Modulation transfer function and image transmission through randomly distributed spherical particles," Journal of the Optical Society of America, Vol.2 No. 12 pp. 2330-2335, December 1985.

10. R.F. Lutomirski and H.T. Yura, "Mutal Coherence of waves in atmosphere," Journal of the Optical Society of America, Vol. 61, p. 482, 1971.

11. R.E. Hufnagel and N. R. Stanley, "Modulation transfer function associated with Image Transmission through turbulent media," Journal of the Optical Society of America, Vol. 54, No. 1, pp. 52-61, 1964.

12. N.S. Kopeika, "Spatial-frequency-and wavelength-dependent effects of aerosols on the atmospheric modulation transfer function," Optical Society of America, Vol. 72, No. 8, pp. 1092-1094, August, 1982.

13. N.S. Kopeika, "Imaging through the atmosphere for Airborne reconnaissance," Optical Engineering, Vol.26, No. 11, pp. 1148-1154, November, 1987.

14. D.L. Walters, and K. E. Kunkel, "Atmospheric modulation transfer function for desert and mountain locations: The atmospheric effects on r_o, "Journal of Optical Society of America, Vol. 71, No. 4, pp. 397-409, 1981.

15. W.E.N. Middleton, Visibility in Meteorology, University of Toronto Press, Toronto, 1941.

16. S.G. Duntley, "The Reduction of Apparent Contrast by the Atmosphere," in Journal of the Optical Society of America, Vol. 38, No. 2, February, 1948.

17. C.McDonald, J. W. Stahoviak, R. Olsen, et al. "Deviation of Transmittance in a Dust Environment Using Imaging Technology," In Proceedings of SPIE - The International Society of Optical Engineering, Optical, Infrared and Millimeter Wave Propagation, Vol. 926, pp. 110-121, Orlando, Florida, April 1988.

18. C. McDonald, J. W. Stahoviak, et al, "Photopic Transmittance, Extinction and Range in Dust Clouds," Report to Atmospheric Sciences Laboratory, White Sands Missile Range, New Mexico, February 1988.

19. R. Bracewell, The Fourier Transform and its Applications, McGraw-Hill, New York, 1965.

20. Luc R. Binsonnete, "Calculation Method of the modulation transfer function in aerosol media," In Proceedings SPIE conference on Propagation Engineering; Third in series, Vol. 1312, Orlando Florida, April 1990.

21. C. McDonald, J. Carbajal, J. Flores, R. Mesta, G. Carrillo, M.A. Nunez, and Luis Carrillo, "Measurement of the overall modulation transfer function of the atmosphere," In Proceedings of SPIE Conference on Atmospheric Propagation and Remote Sensing II, Vol 1968, Orlando Florida, April 1993.

APPENDIX A

SUMMARY OF MTF_A DATA AND

ANALYSIS RESULTS

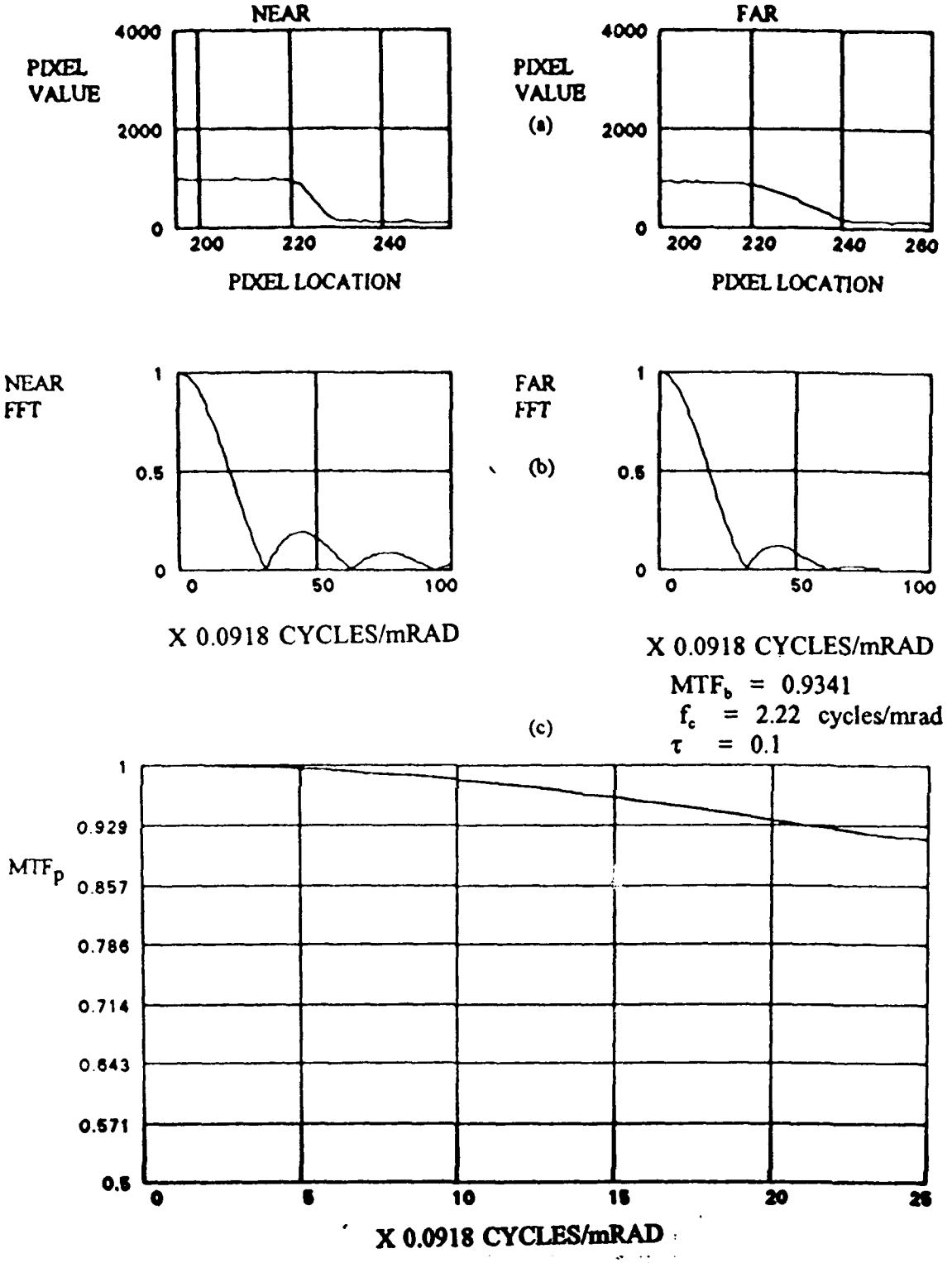

Figure 1. Data from 7:00 AM of August 25, 1993: (a) line pixel values of the black-white steps for both targets; (b) normalized, line FFTs of both targets based on the corresponding pixel values shown; (c) normalized aerosol MTF_p, derived from the ratio of the far target FFT to the near target FFT. Values for f_c, τ, and MTF_b are included.

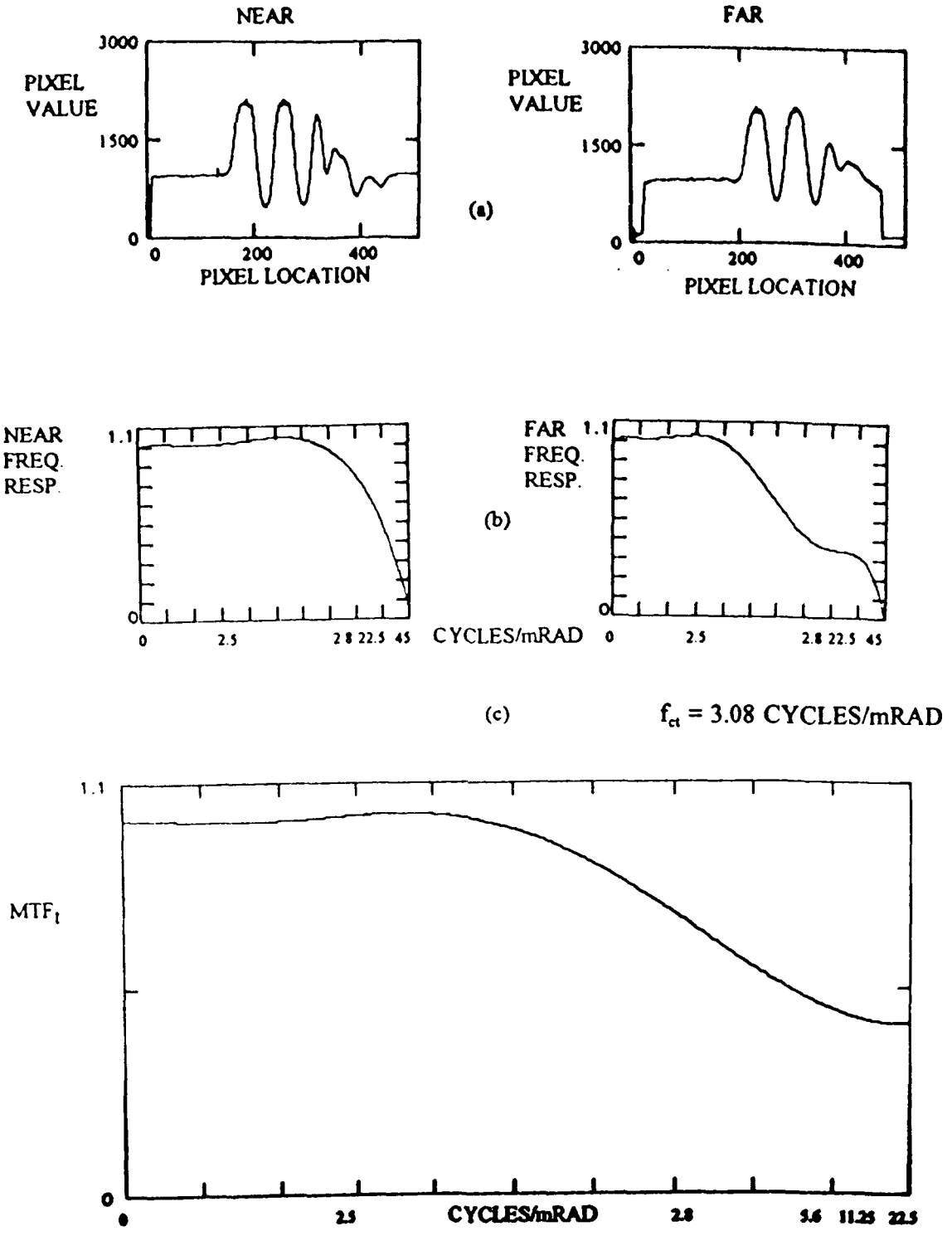

Figure 2. Data from 7:00 A.M.of August 25, 1993: (a) line pixel values of castellated black-white stripes for both targets; (b) normalized spatial frequency response of both targets based on the corresponding pixel values shown; (c) turbulence, MTF_t, derived from the ratio of the far to near target frequency response. Cutoff frequency, f_{ct}, for MTF_t is included.

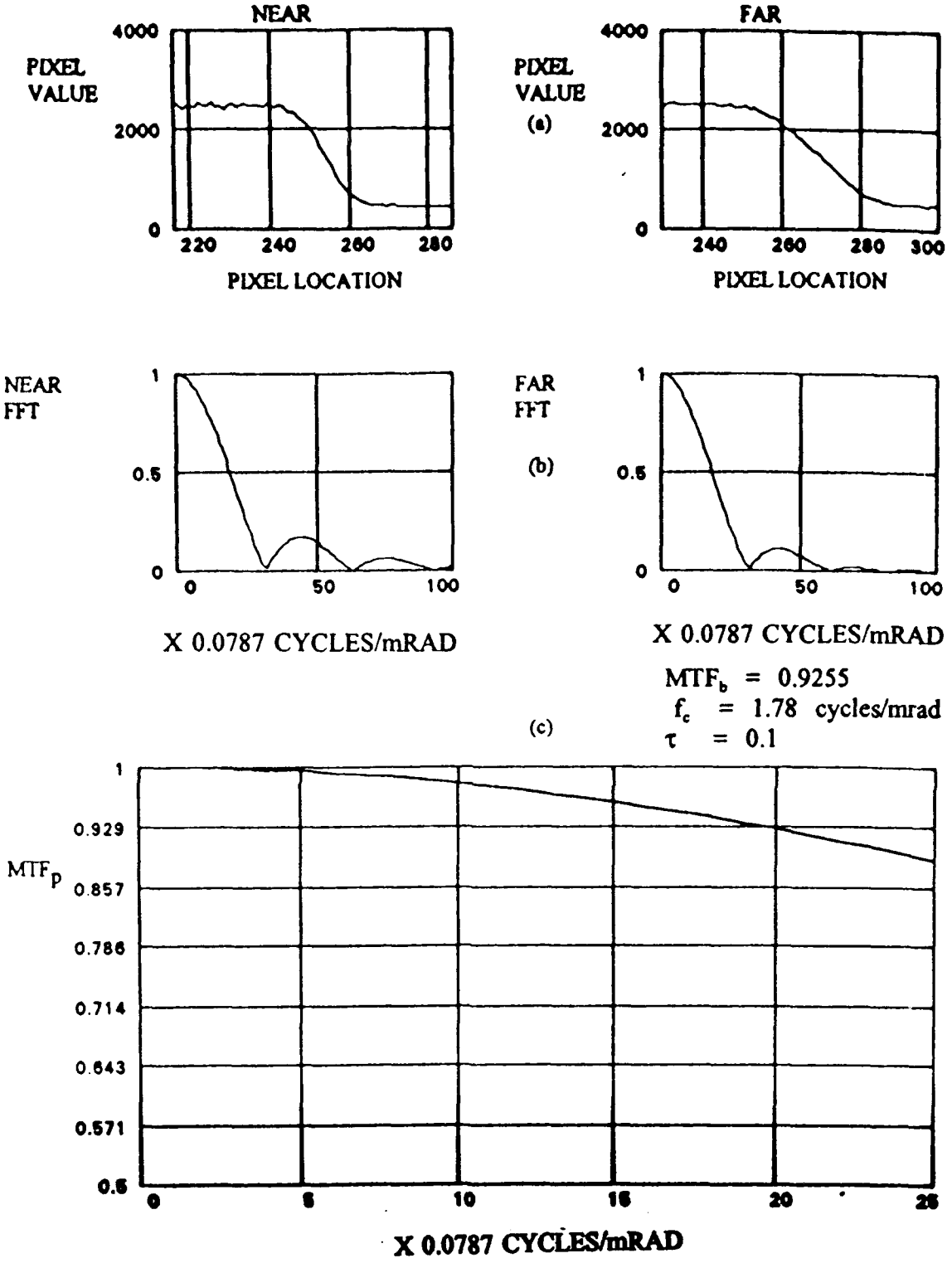

Figure 3. Data from 9:30 AM of August 25, 1993: (a) line pixel values of the black-white steps for both targets; (b) normalized, line FFTs of both targets based on the corresponding pixel values shown; (c) normalized aerosol MTF_p, derived from the ratio of the far target FFT to the near target FFT. Values for f_c, τ, and MTF_b are included.

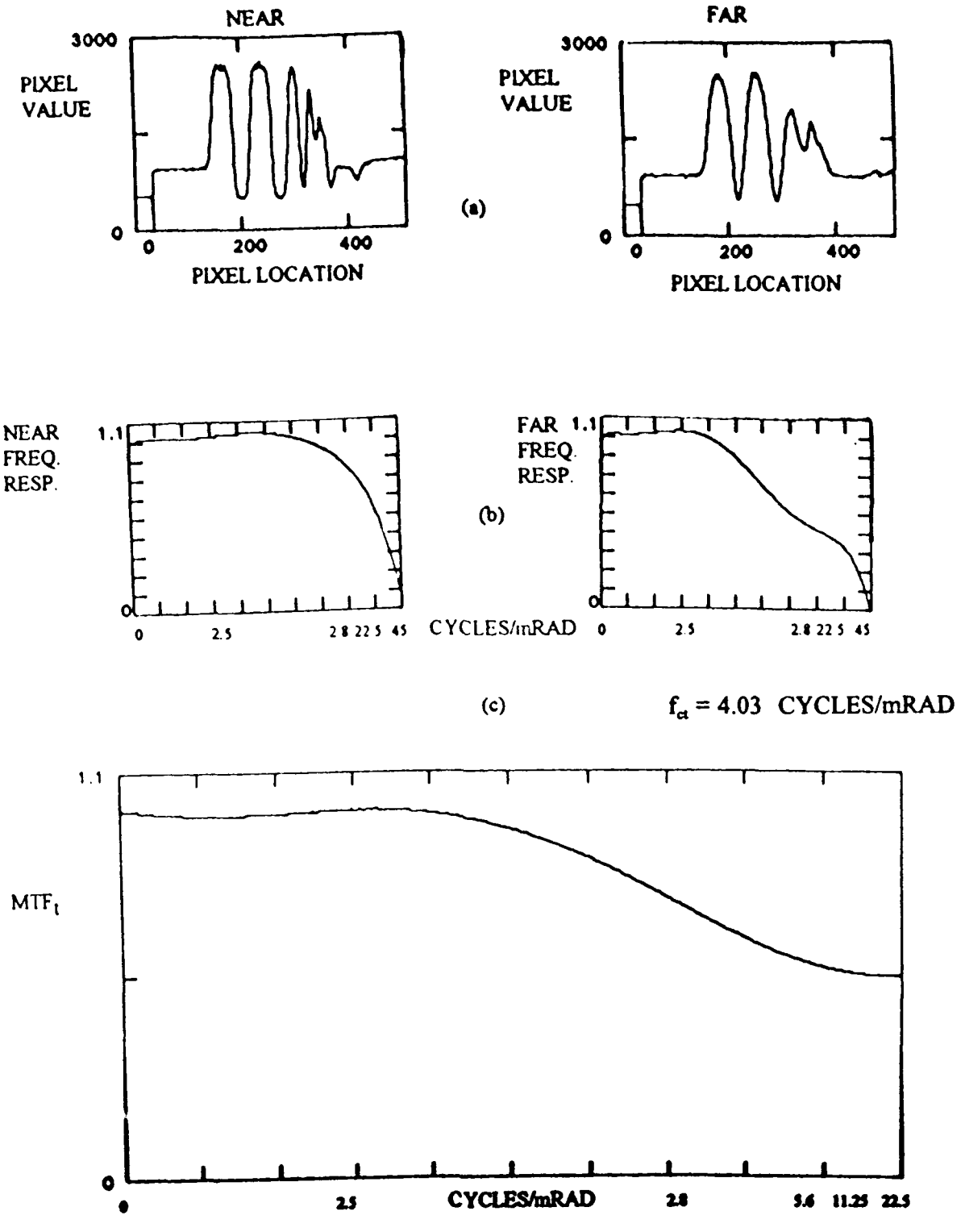

Figure 4. Data from 9:30 A.M. of August 25, 1993: (a) line pixel values of castellated black-white stripes for both targets; (b) normalized spatial frequency response of both targets based on the corresponding pixel values shown; (c) turbulence, MTF_t, derived from the ratio of the far to near target frequency response. Cutoff frequency, f_{ct}, for MTF_t is included.

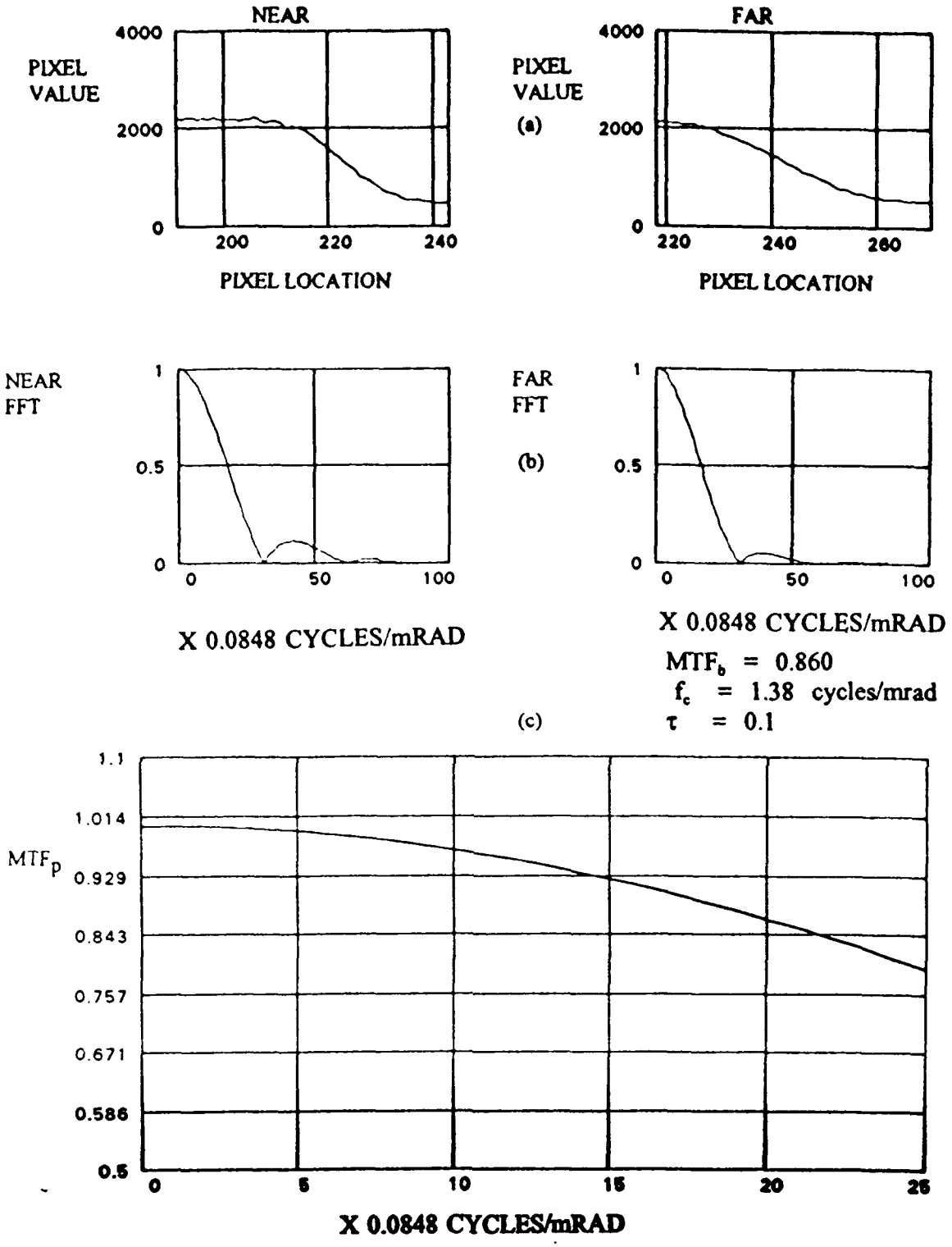

Figure 5. Data from 12:00 PM of August 25 , 1993: (a) line pixel values of the black-white steps for both targets; (b) normalized, line FFTs of both targets based on the corresponding pixel values shown; (c) normalized aerosol MTF_p , derived from the ratio of the far target FFT to the near target FFT. Values for f_c, τ, and MTF_b are included.

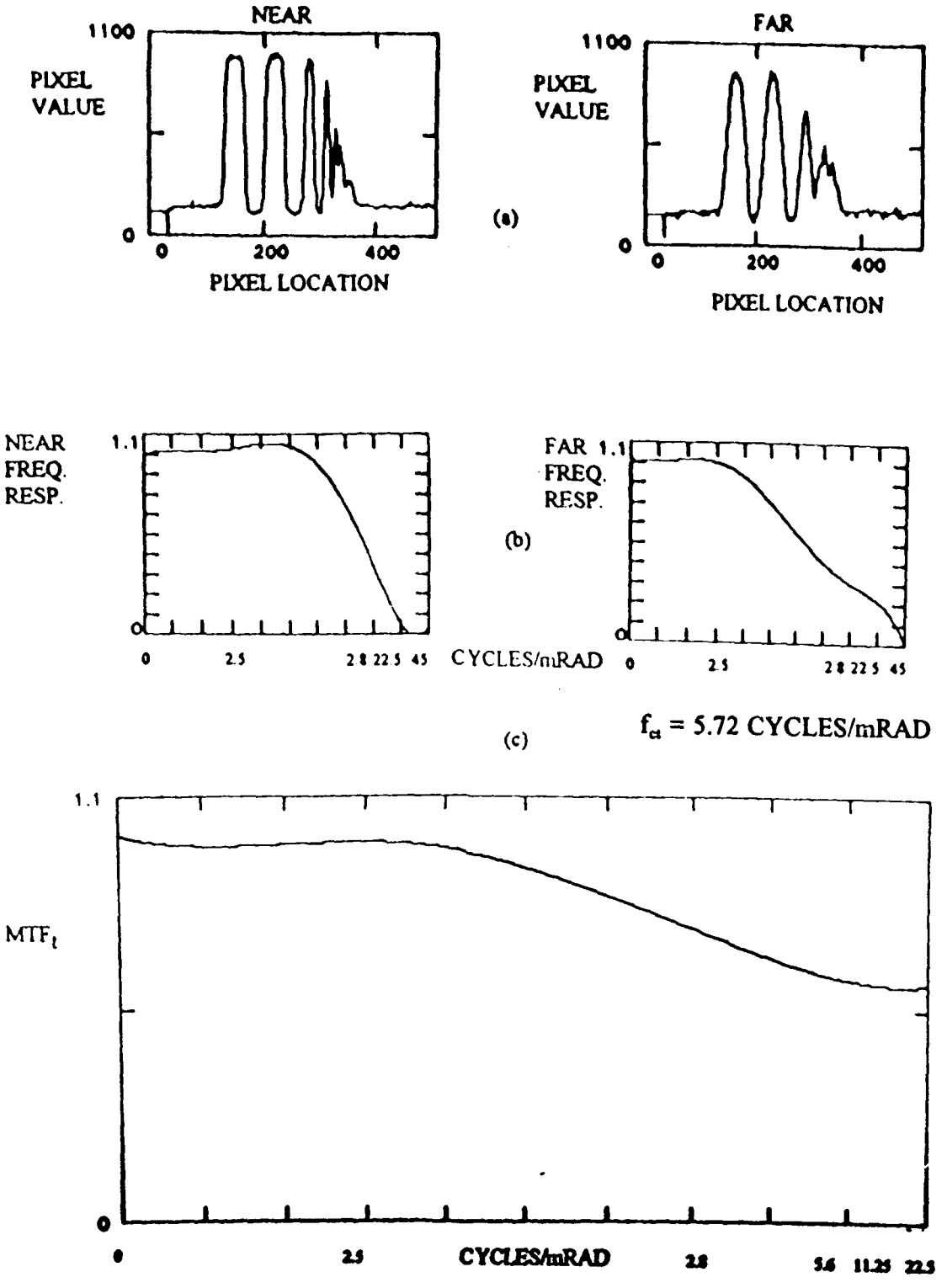

Figure 6. Data from 12:00 P.M. of August 25, 1993: (a) line pixel values of castellated black-white stripes for both targets; (b) normalized spatial frequency response of both targets based on the corresponding pixel values shown; (c) turbulence, MTF_t, derived from the ratio of the far to near target frequency response. Cutoff frequency, f_{ct}, for MTF_t is included.

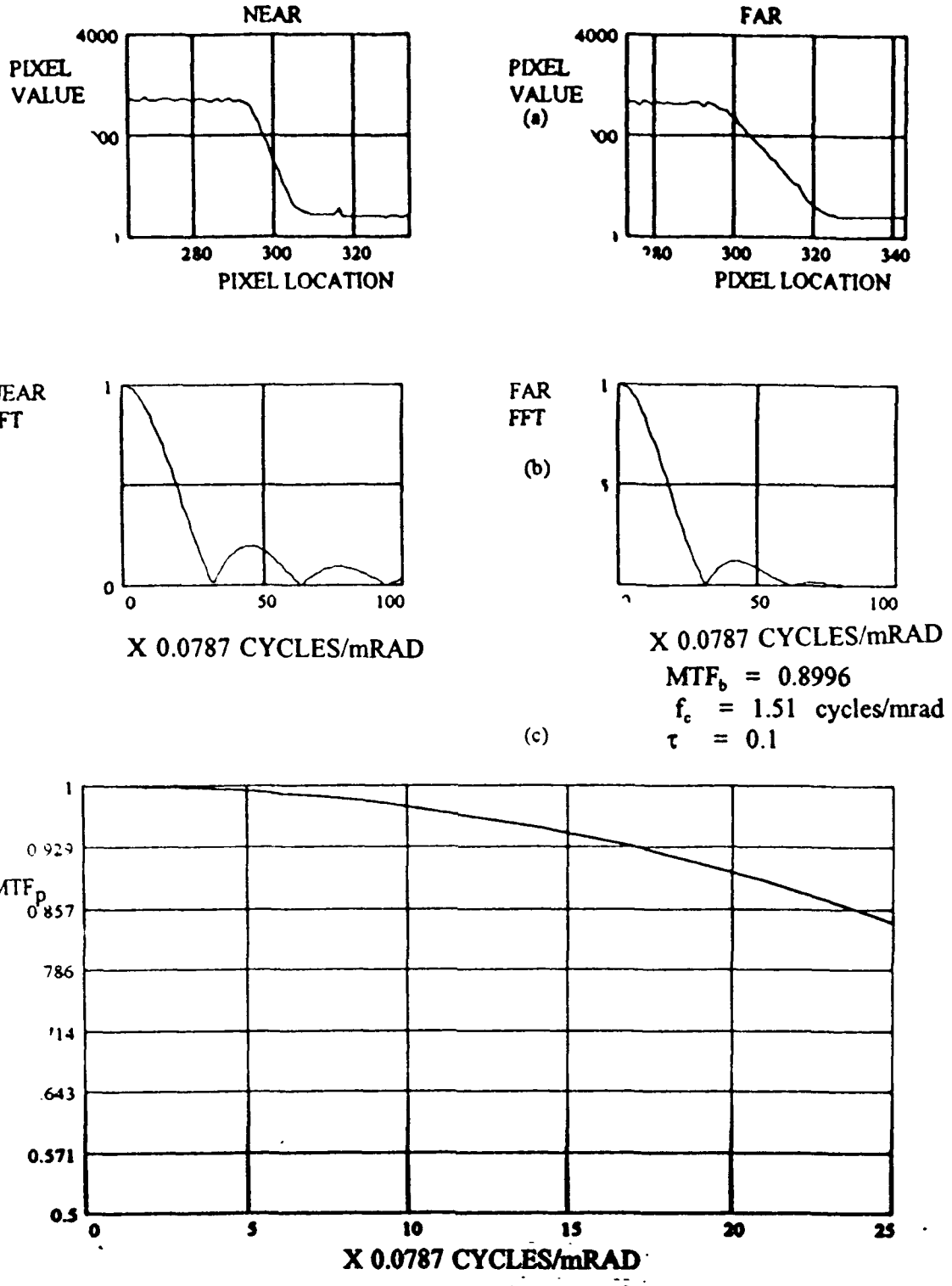

Figure 7. Data from 7:50 AM of July 10, 1993: (a) line pixel values of the black-white steps for both targets; (b) normalized, line FFTs of both targets based on the corresponding pixel values shown; (c) normalized aerosol MTF_p, derived from the ratio of the far target FFT to the near target FFT. Values for f_c, τ, and MTF_b are included.

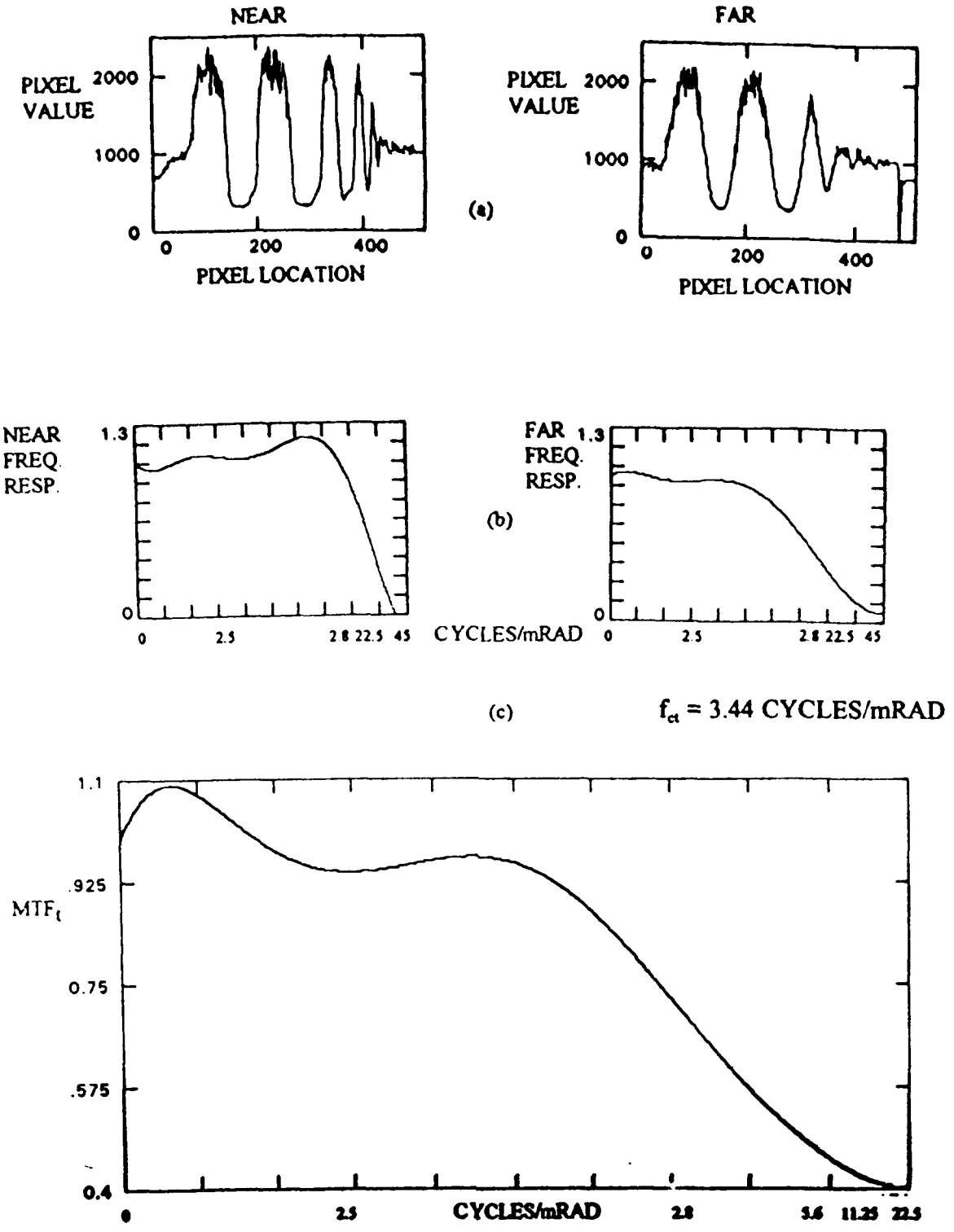

Figure 8. Data from 7:50 A.M. of July 10, 1993: (a) line pixel values of castellated black-white stripes for both targets; (b) normalized spatial frequency response of both targets based on the corresponding pixel values shown; (c) turbulence, MTF_t, derived from the ratio of the far to near target frequency response. Cutoff frequency, f_{ct}, for MTF_t is included.

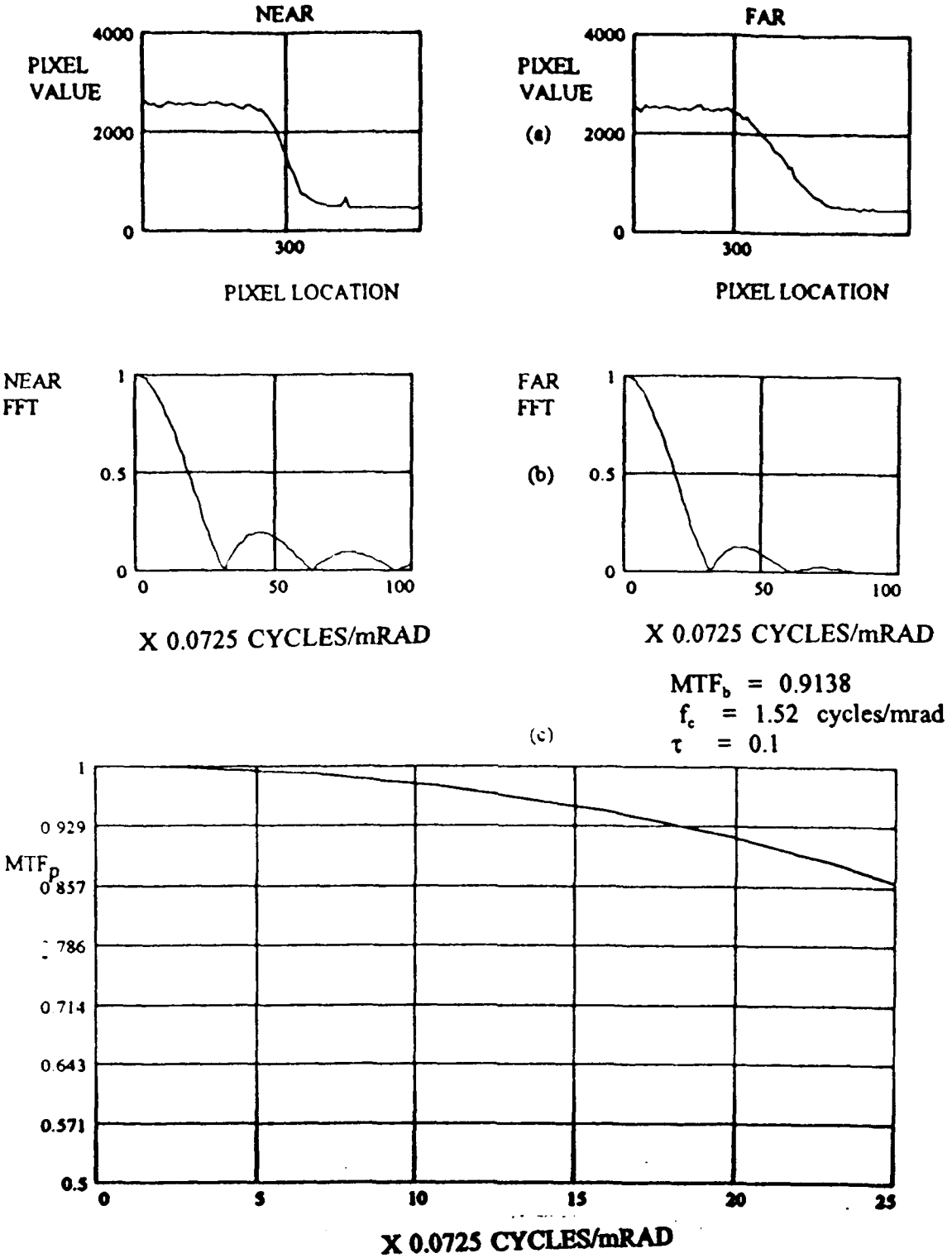

Figure 9. Data from 8:30 AM of July 10, 1993: (a) line pixel values of the black-white steps for both targets; (b) normalized, line FFTs of both targets based on the corresponding pixel values shown; (c) normalized aerosol MTF_p, derived from the ratio of the far target FFT to the near target FFT. Values for f_c, τ, and MTF_b are included.

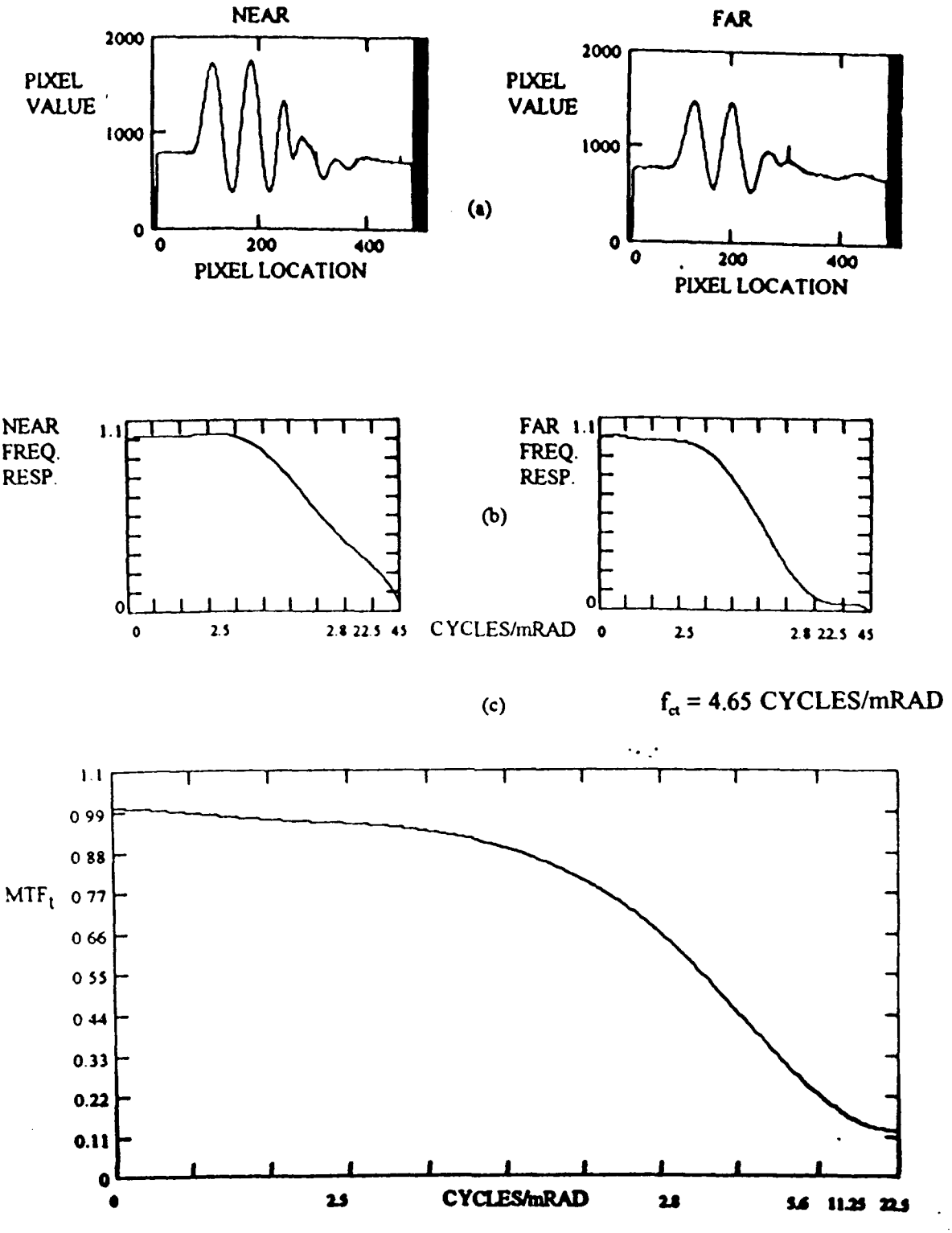

Figure 10. Data from 8:30 A.M. of July 10, 1993: (a) line pixel values of castellated black-white stripes for both targets; (b) normalized spatial frequency response of both targets based on the corresponding pixel values shown; (c) turbulence, MTF_t, derived from the ratio of the far to near target frequency response. Cutoff frequency, f_{ct}, for MTF_t is included.

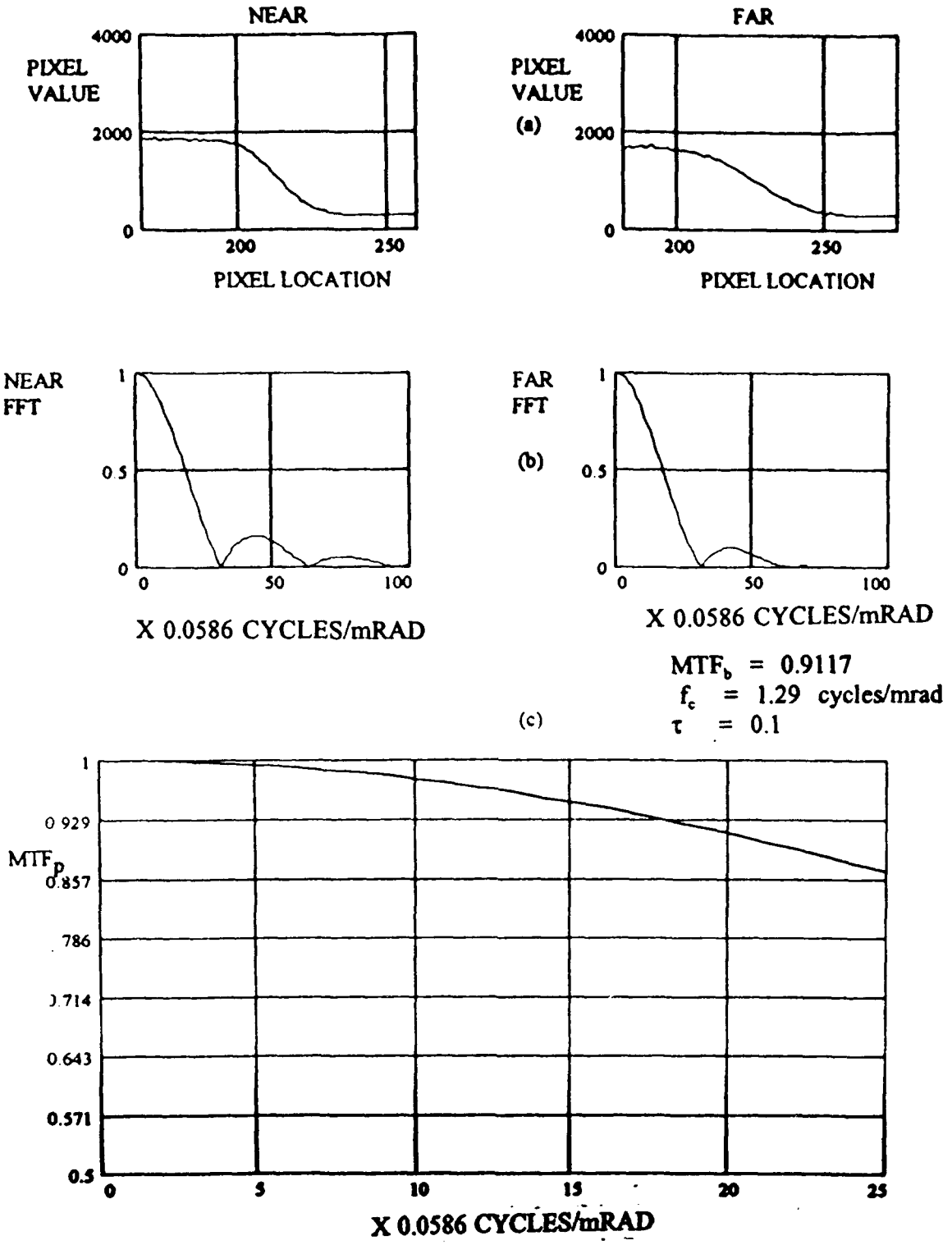

Figure 11. Data from 11:30 AM of July 10, 1993: (a) line pixel values of the black-white steps for both targets; (b) normalized, line FFTs of both targets based on the corresponding pixel values shown; (c) normalized aerosol MTF_p, derived from the ratio of the far target FFT to the near target FFT. Values for f_c, τ, and MTF_b are included.

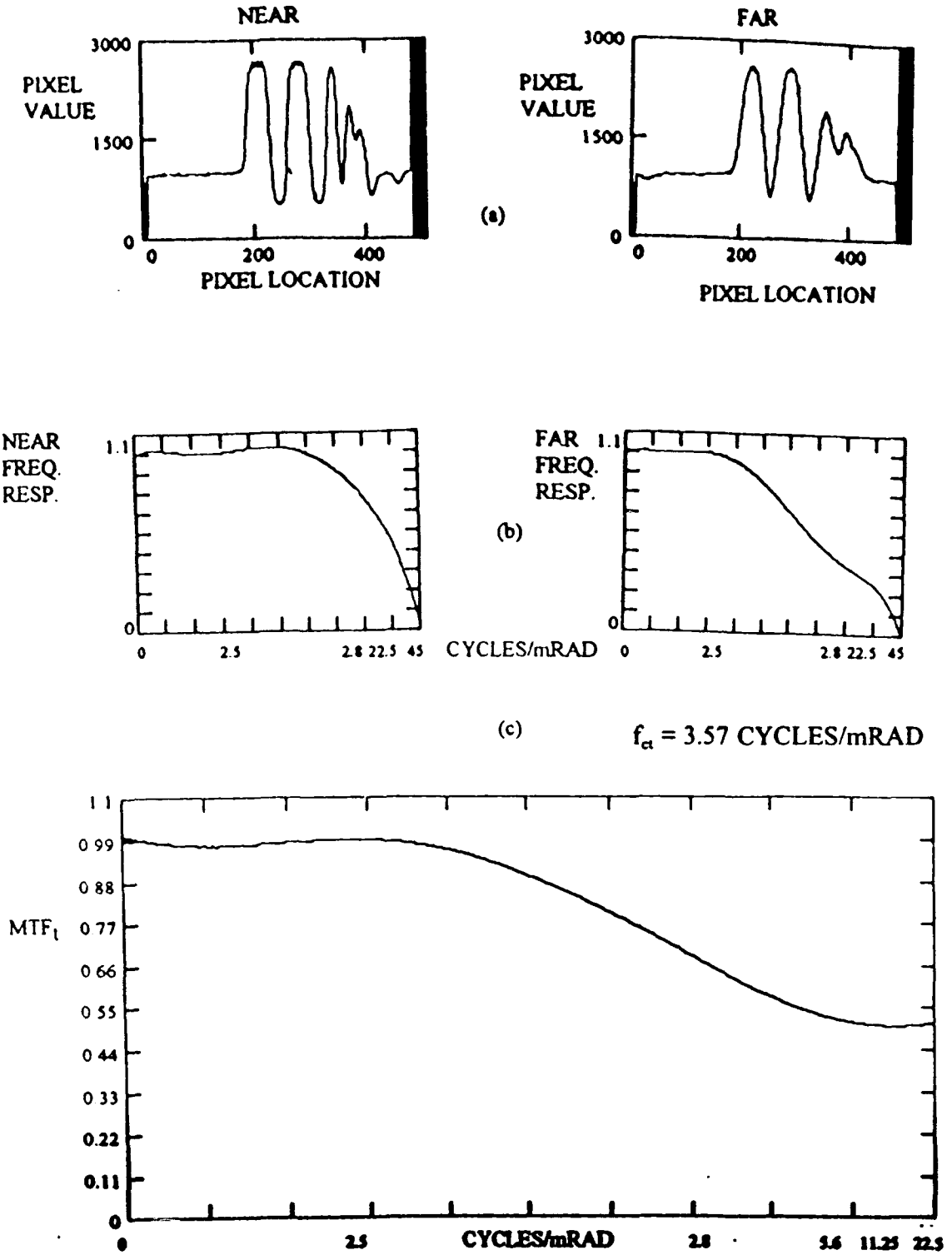

Figure 12. Data from 11:30 A.M. of July 10, 1993: (a) line pixel values of castellated black-white stripes for both targets; (b) normalized spatial frequency response of both targets based on the corresponding pixel values shown; (c) turbulence, MTF_t, derived from the ratio of the far to near target frequency response. Cutoff frequency, f_{ct}, for MTF_t is included.

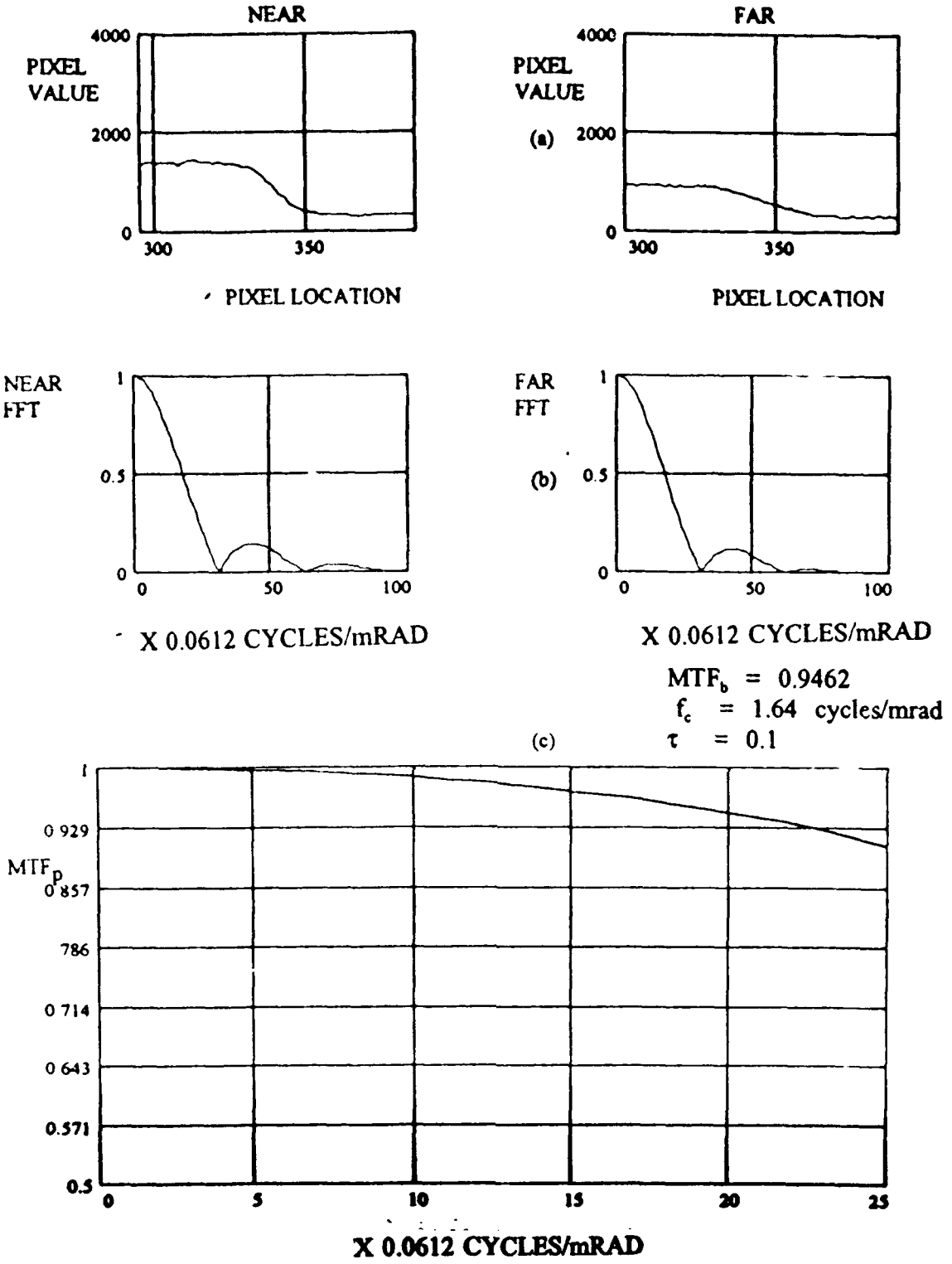

Figure 13. Data from 7:35 AM of June 26 , 1993: (a) line pixel values of the black-white steps for both targets; (b) normalized, line FFTs of both targets based on the corresponding pixel values shown; (c) normalized aerosol MTF_p , derived from the ratio of the far target FFT to the near target FFT. Values for f_c, τ, and MTF_b are included.

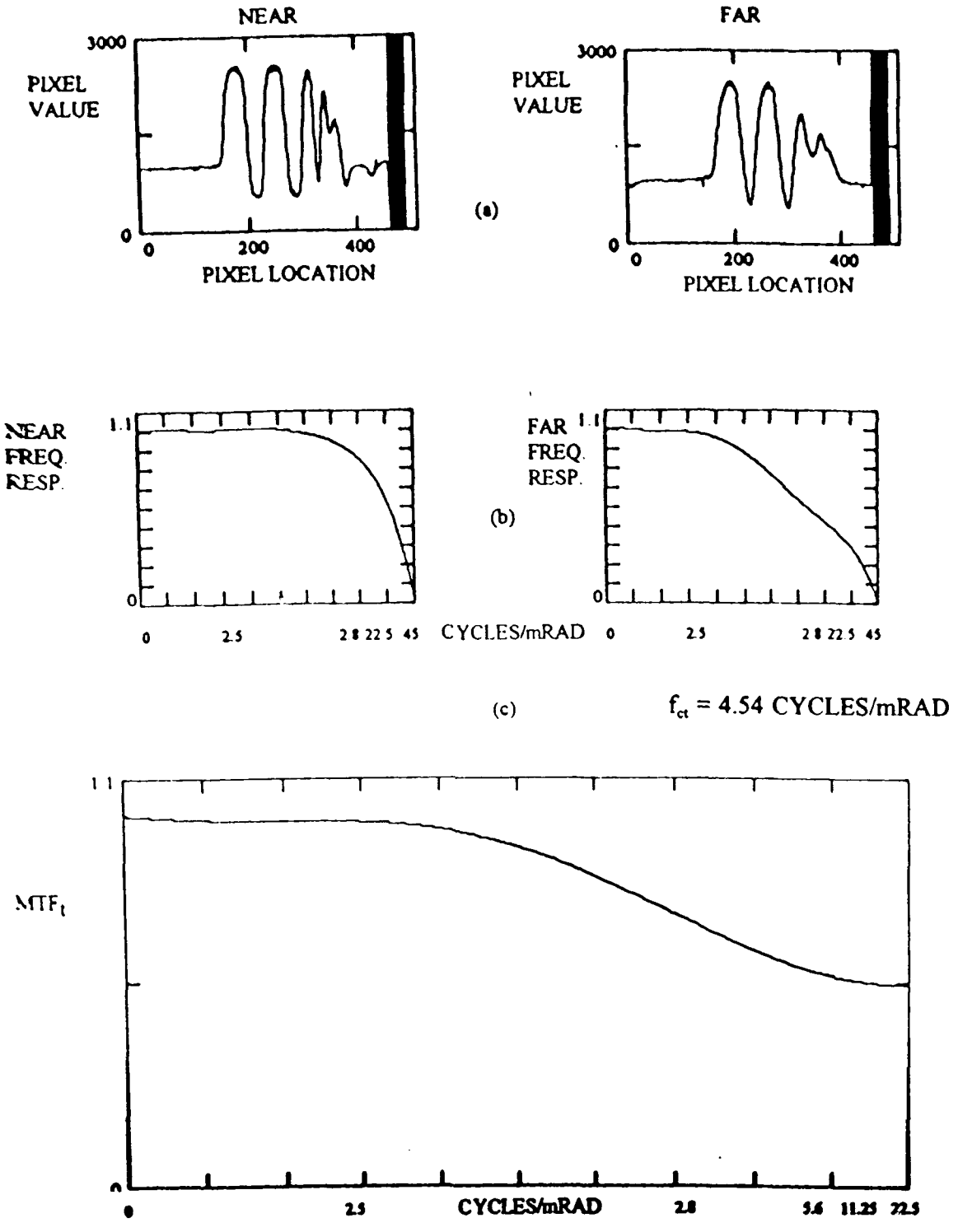

Figure 14. Data from 7:35 A.M. of June 26, 1993: (a) line pixel values of castellated black-white stripes for both targets; (b) normalized spatial frequency response of both targets based on the corresponding pixel values shown; (c) turbulence, MTF_t, derived from the ratio of the far to near target frequency response. Cutoff frequency, f_{ct}, for MTF_t is included.

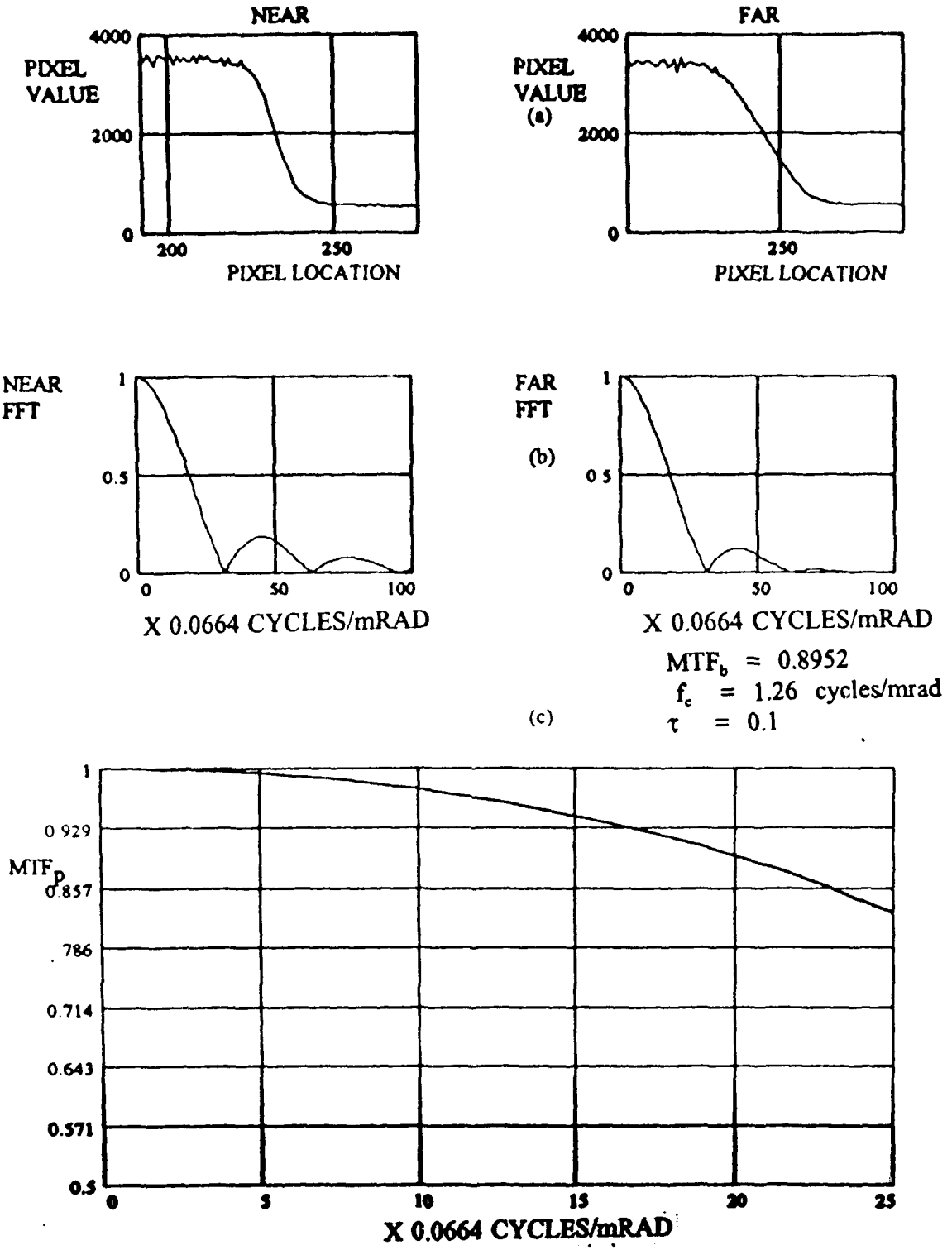

Figure 15. *Data from 8:45 AM of June 26, 1993:* (a) line pixel values of the black-white steps for both targets; (b) normalized, line FFTs of both targets based on the corresponding pixel values shown; (c) normalized aerosol MTF_p, derived from the ratio of the far target FFT to the near target FFT. Values for f_c, τ, and MTF_b are included.

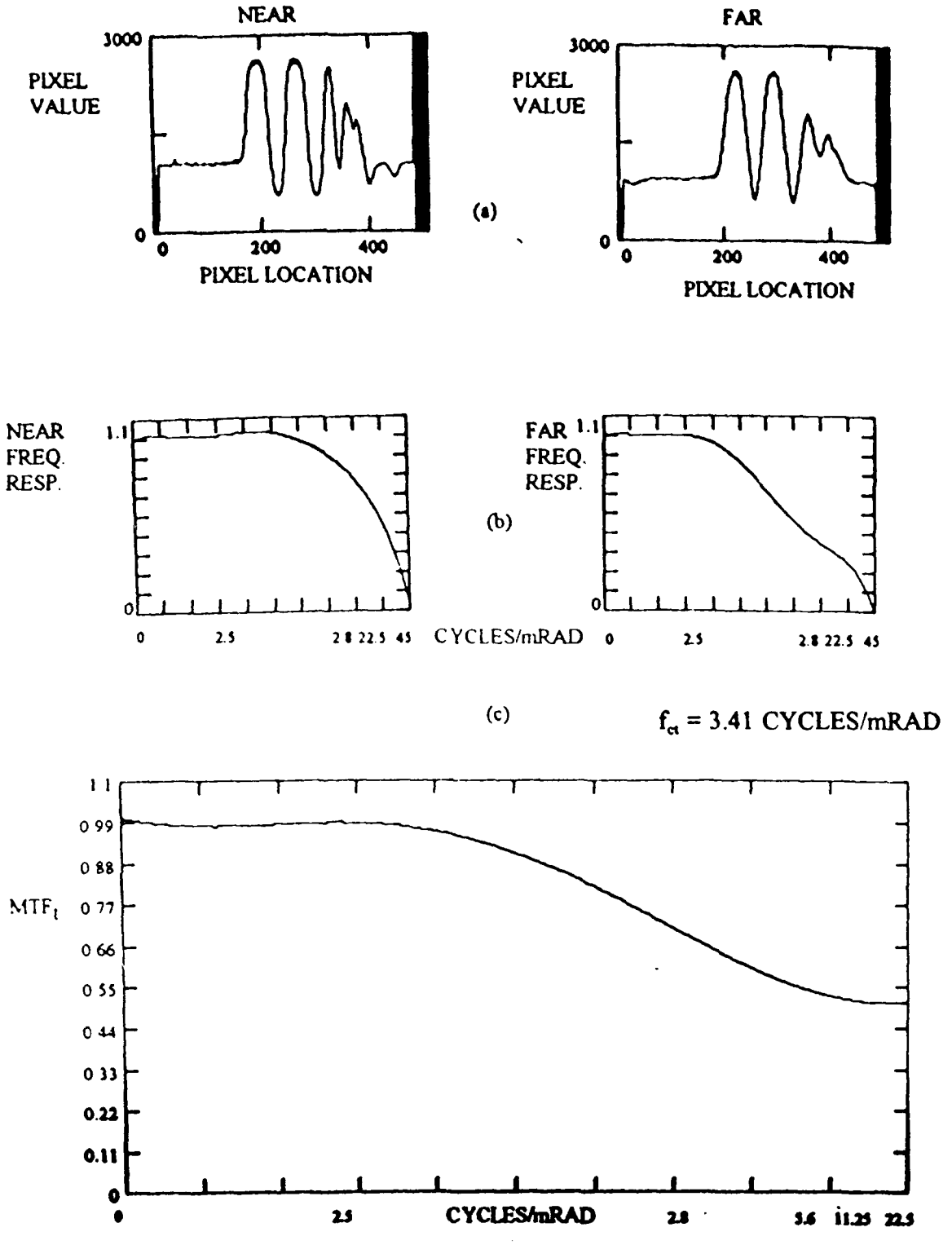

Figure 16. Data from 8:45 A.M. of June 26, 1993: (a) line pixel values of castellated black-white stripes for both targets; (b) normalized spatial frequency response of both targets based on the corresponding pixel values shown; (c) turbulence, MTF_t, derived from the ratio of the far to near target frequency response. Cutoff frequency, f_{ct}, for MTF_t is included.

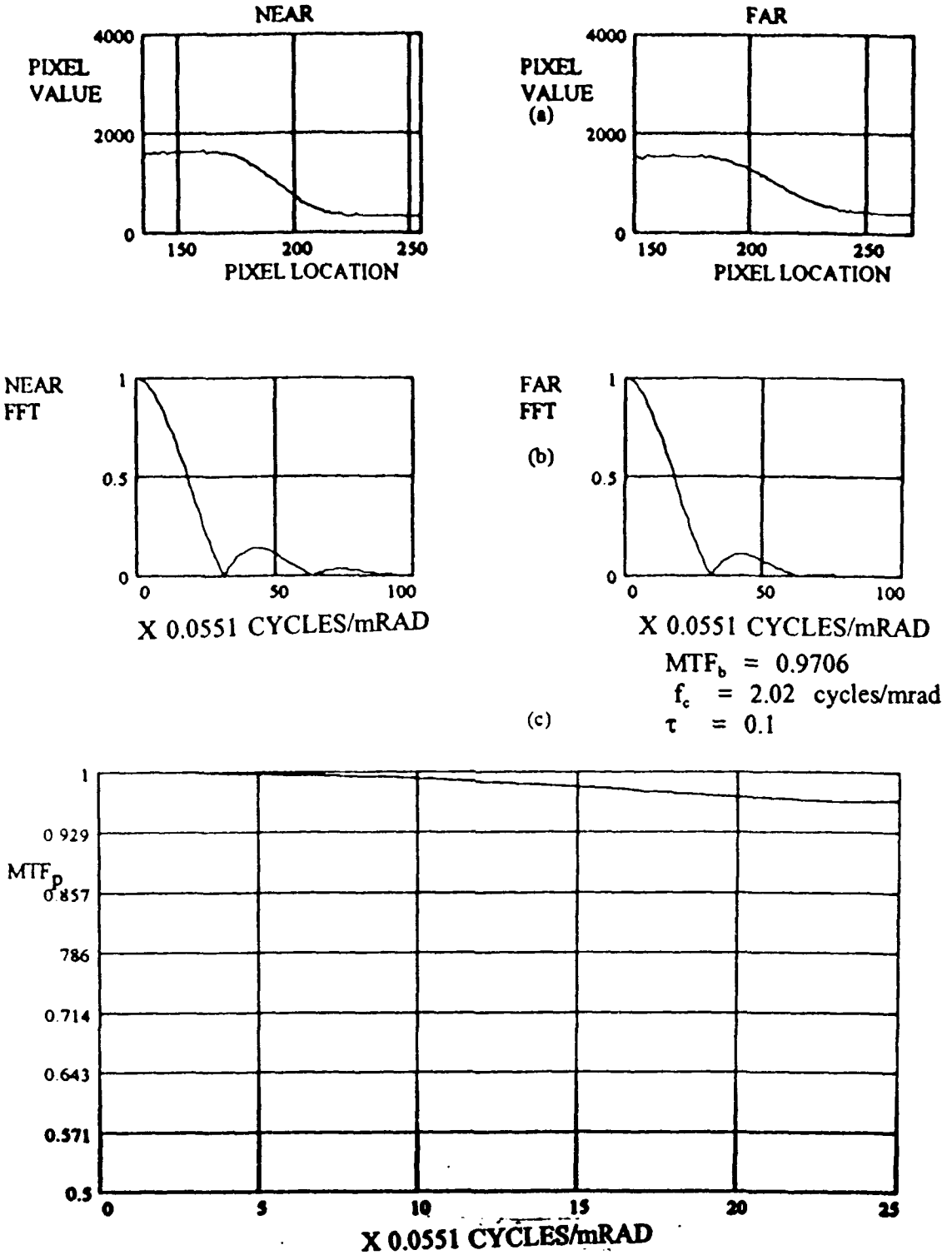

Figure 17. Data from 12:00 PM of June 26 , 1993: (a) line pixel values of the black-white steps for both targets; (b) normalized, line FFTs of both targets based on the corresponding pixel values shown; (c) normalized aerosol MTF_p , derived from the ratio of the far target FFT to the near target FFT. Values for f_c, τ, and MTF_b are included.

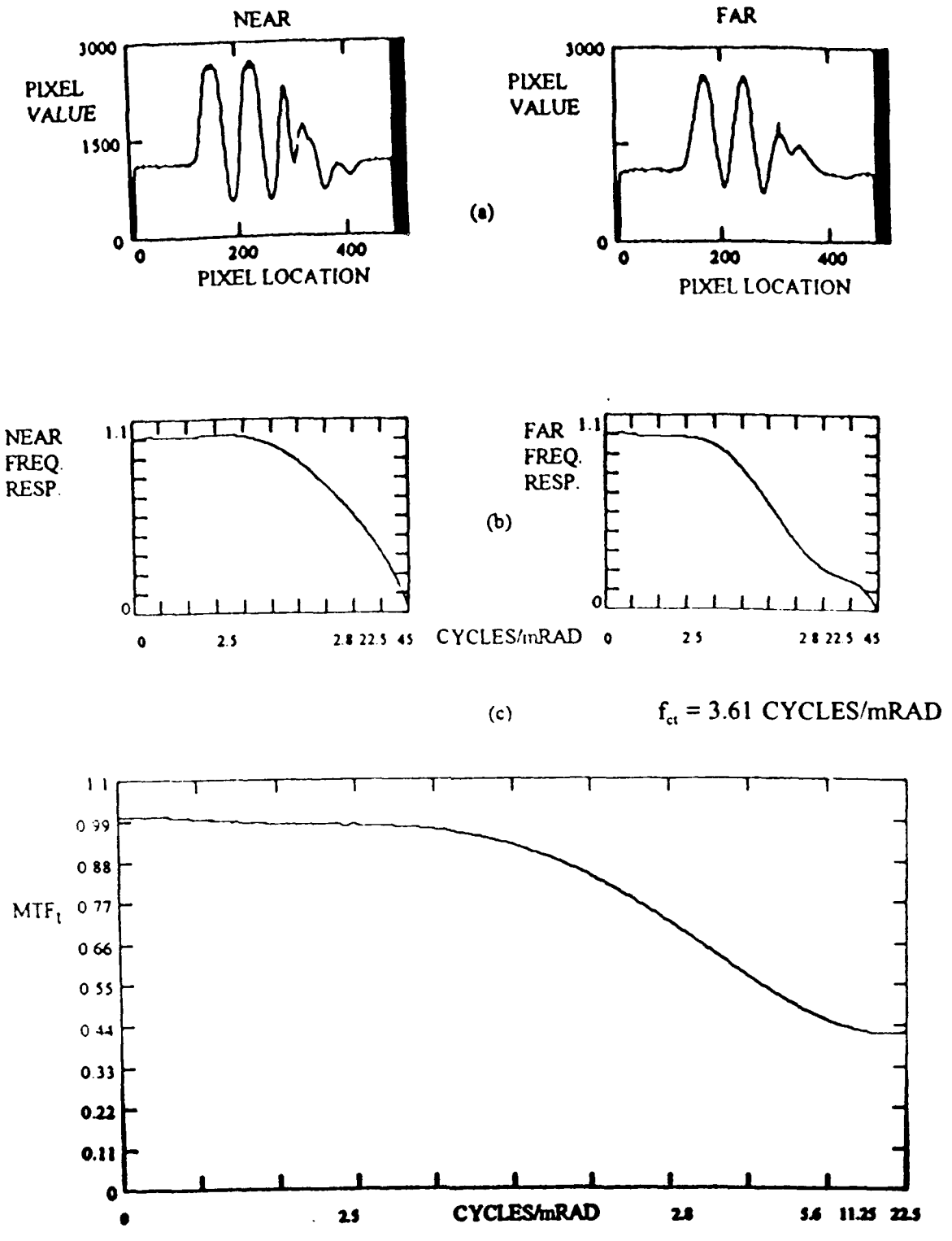

Figure 18. Data from 12:00 P.M. of June 26, 1993: (a) line pixel values of castellated black-white stripes for both targets; (b) normalized spatial frequency response of both targets based on the corresponding pixel values shown; (c) turbulence, MTF_t, derived from the ratio of the far to near target frequency response. Cutoff frequency, f_{ct}, for MTF_t is included.

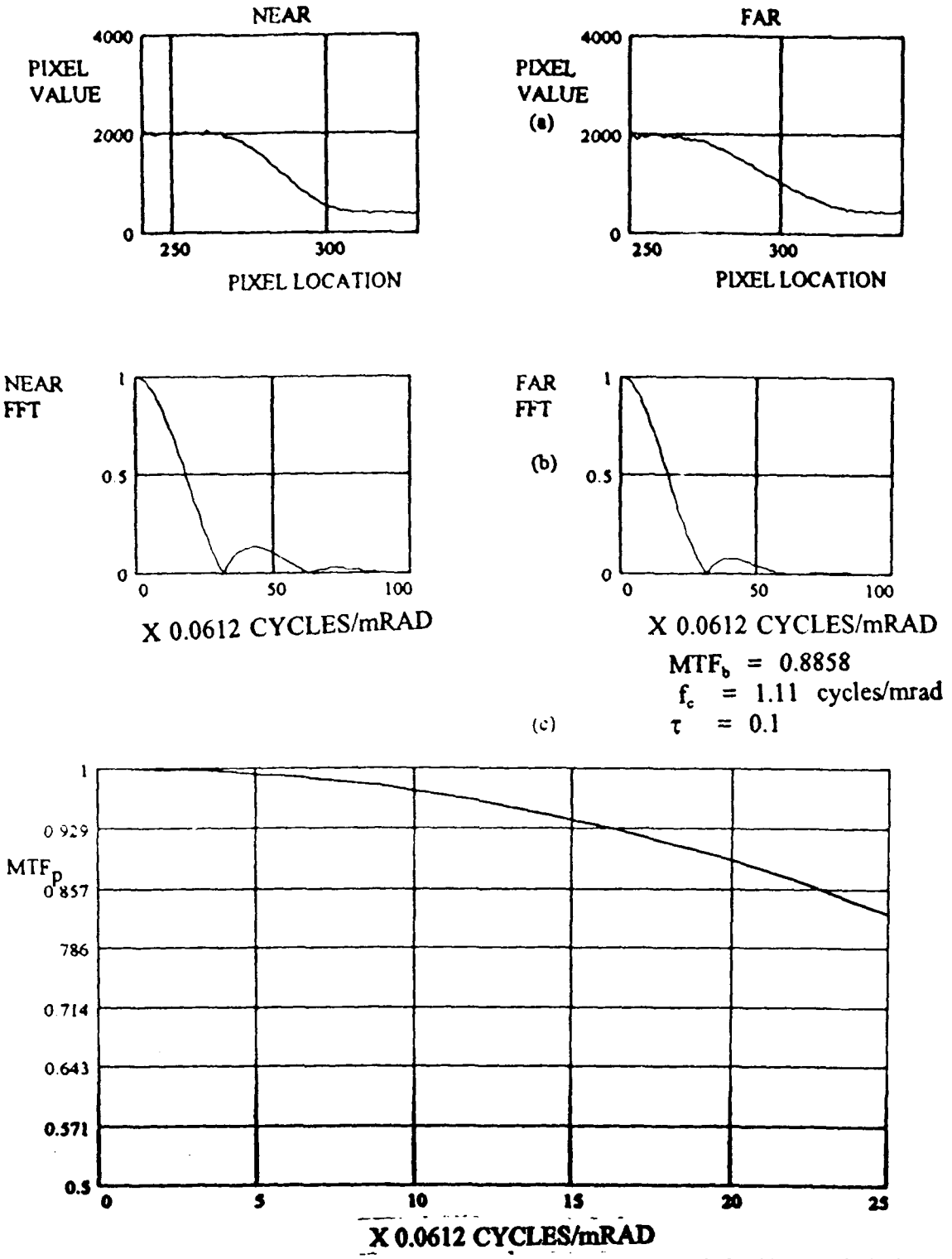

Figure 19. Data from 10:30 AM of June 12, 1993: (a) line pixel values of the black-white steps for both targets; (b) normalized, line FFTs of both targets based on the corresponding pixel values shown; (c) normalized aerosol MTF_p, derived from the ratio of the far target FFT to the near target FFT. Values for f_c, τ, and MTF_b are included.

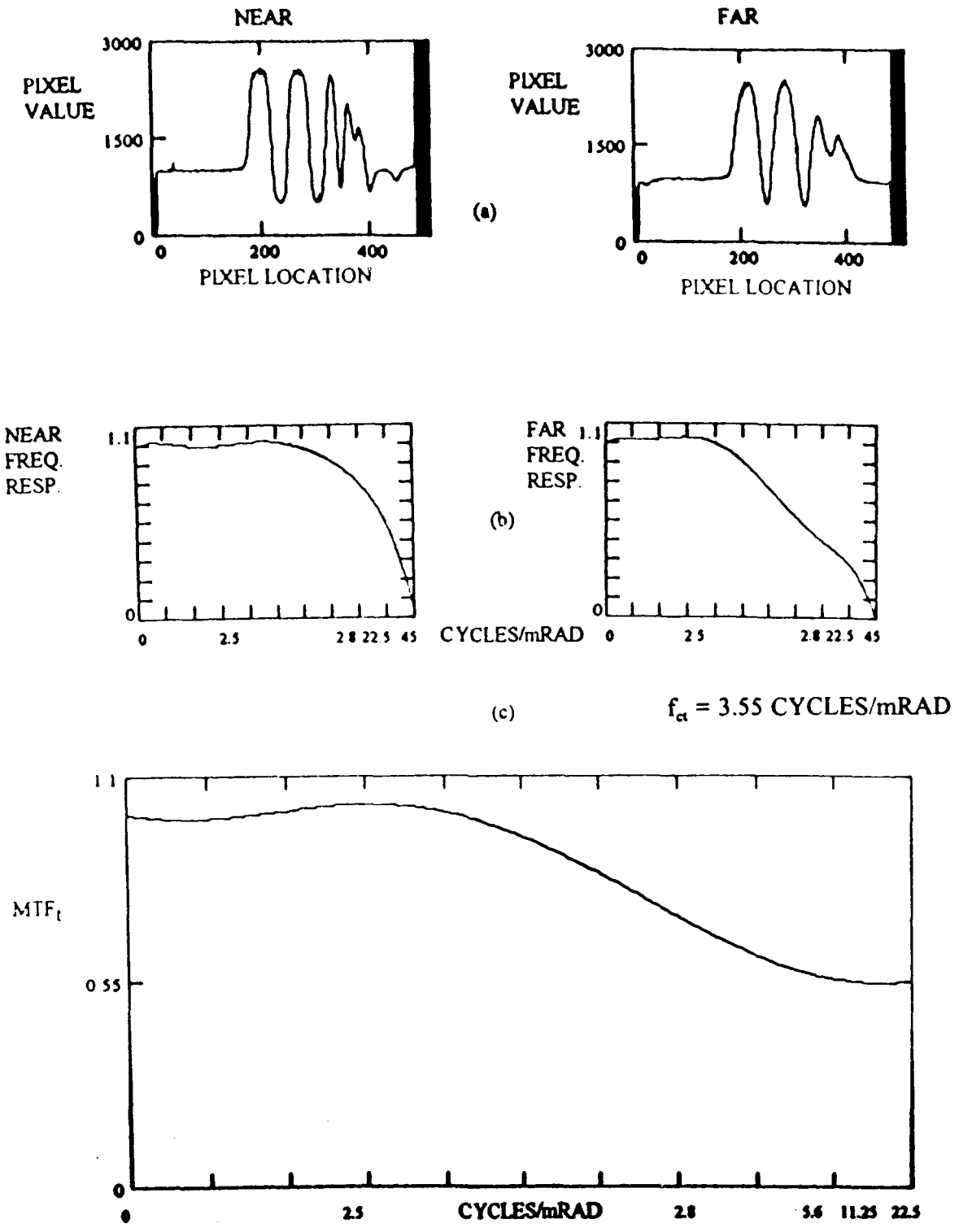

Figure 20. Data from 10:30 A.M. of June 12, 1993: (a) line pixel values of castellated black-white stripes for both targets; (b) normalized spatial frequency response of both targets based on the corresponding pixel values shown; (c) turbulence, MTF_t, derived from the ratio of the far to near target frequency response. Cutoff frequency, f_{ct}, for MTF_t is included.

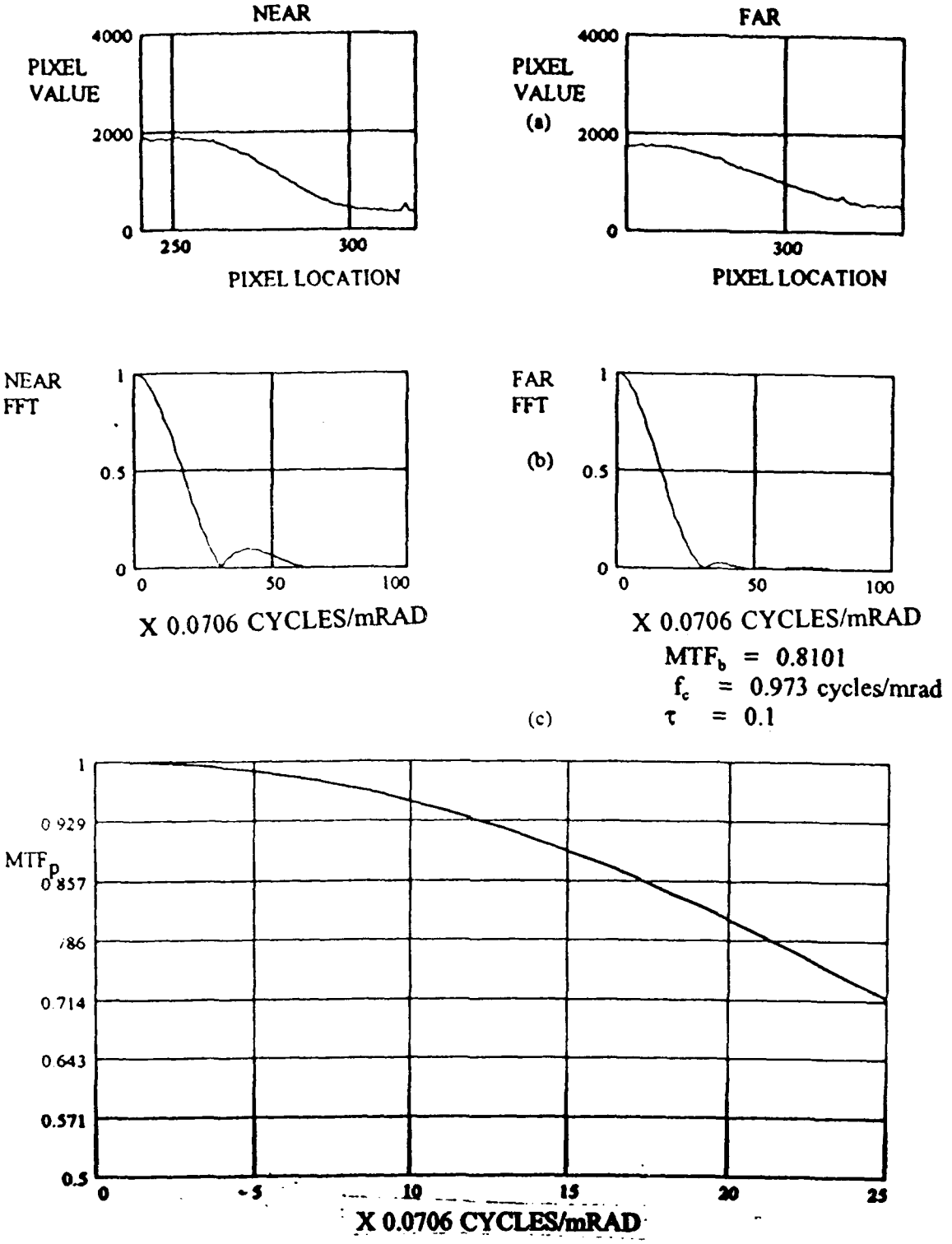

Figure 21. Data from 11:27 AM of June 12, 1993: (a) line pixel values of the black-white steps for both targets; (b) normalized, line FFTs of both targets based on the corresponding pixel values shown; (c) normalized aerosol MTF_p, derived from the ratio of the far target FFT to the near target FFT. Values for f_c, τ, and MTF_b are included.

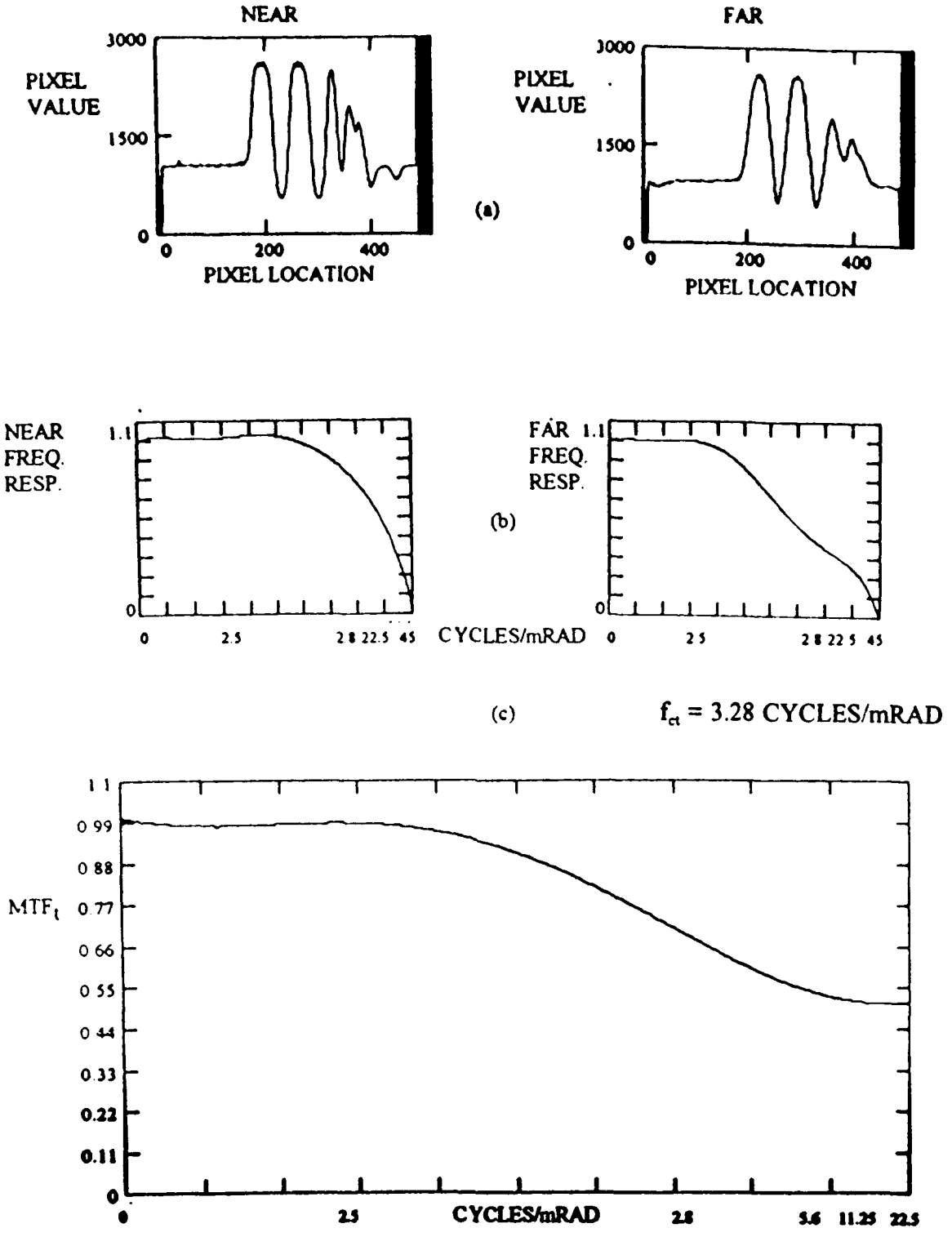

Figure 22. Data from 11:27 A.M. of June 12, 1993: (a) line pixel values of castellated black-white stripes for both targets; (b) normalized spatial frequency response of both targets based on the corresponding pixel values shown; (c) turbulence, MTF_t, derived from the ratio of the far to near target frequency response. Cutoff frequency, f_{ct}, for MTF_t is included.

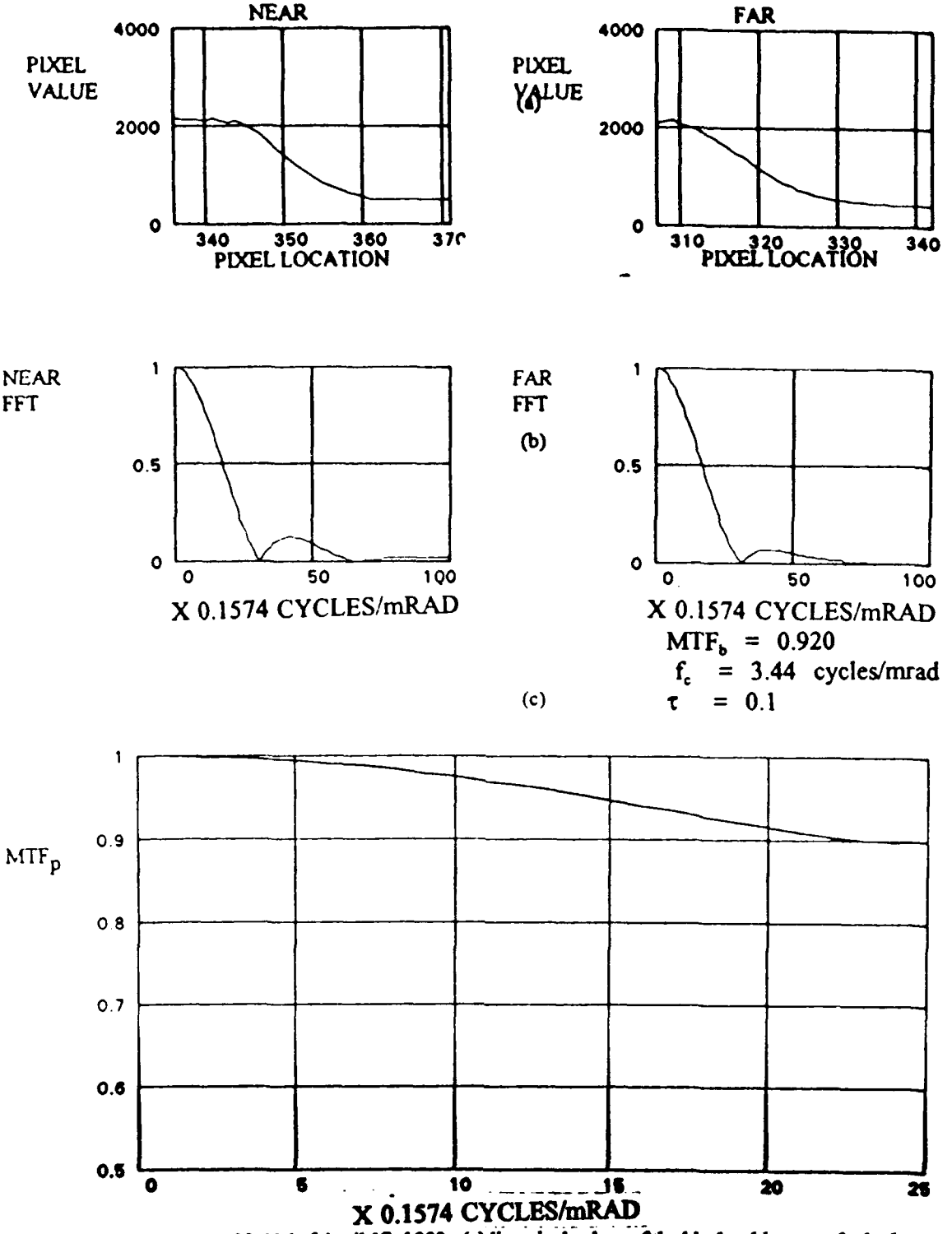

Figure 23. Data from 10:00 AM of April 17, 1993: (a) line pixel values of the black-white steps for both targets; (b) normalized, line FFTs of both targets based on the corresponding pixel values shown; (c) normalized aerosol MTF_p, derived from the ratio of the far target FFT to the near target FFT. Values for f_c, τ, and MTF_b are included.

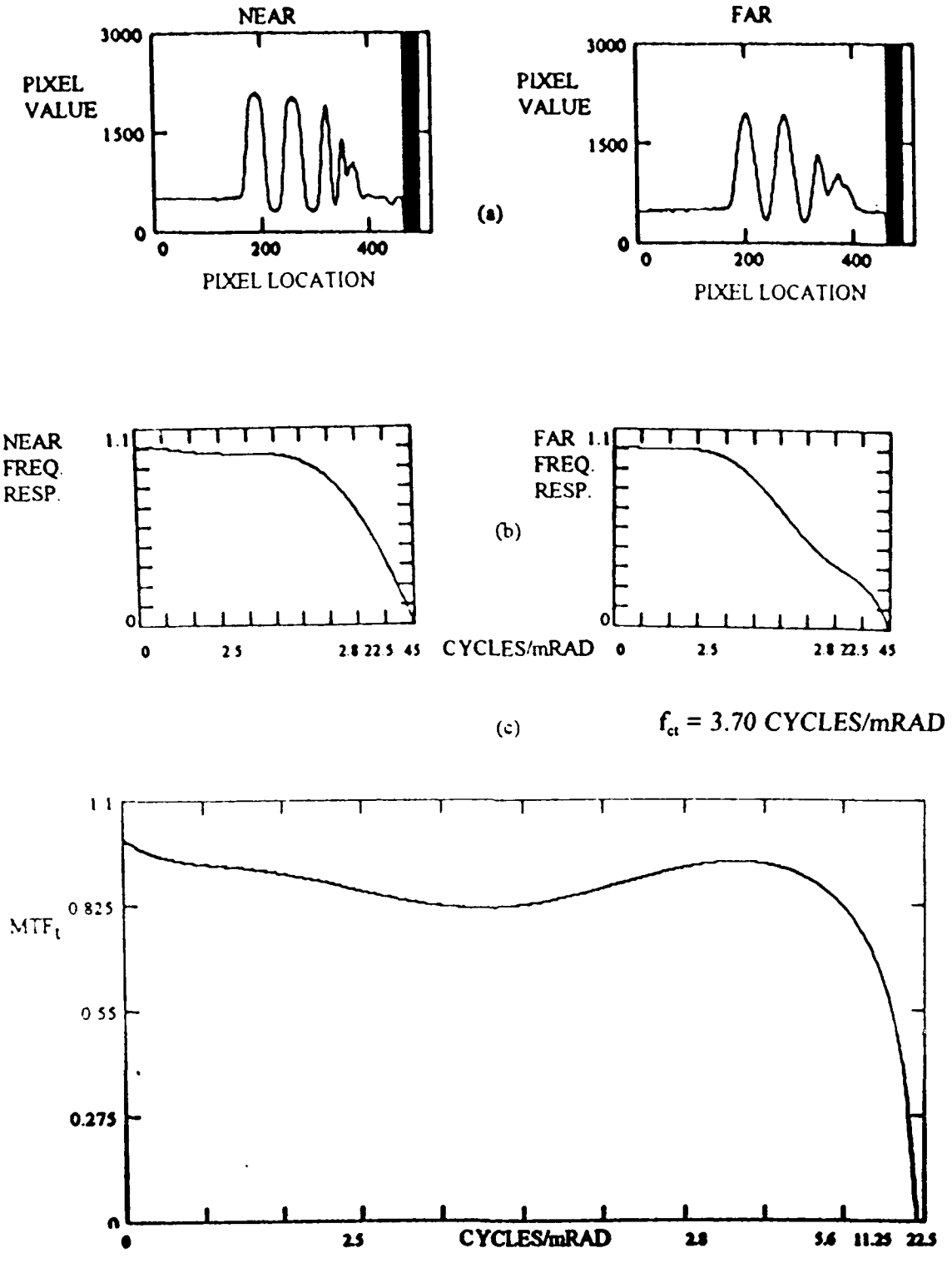

Figure 24. Data from 10:00 A.M. of April 17, 1993: (a) line pixel values of castellated black-white stripes for both targets; (b) normalized spatial frequency response of both targets based on the corresponding pixel values shown; (c) turbulence, MTF_t, derived from the ratio of the far to near target frequency response. Cutoff frequency, f_{ct}, for MTF_t is included.

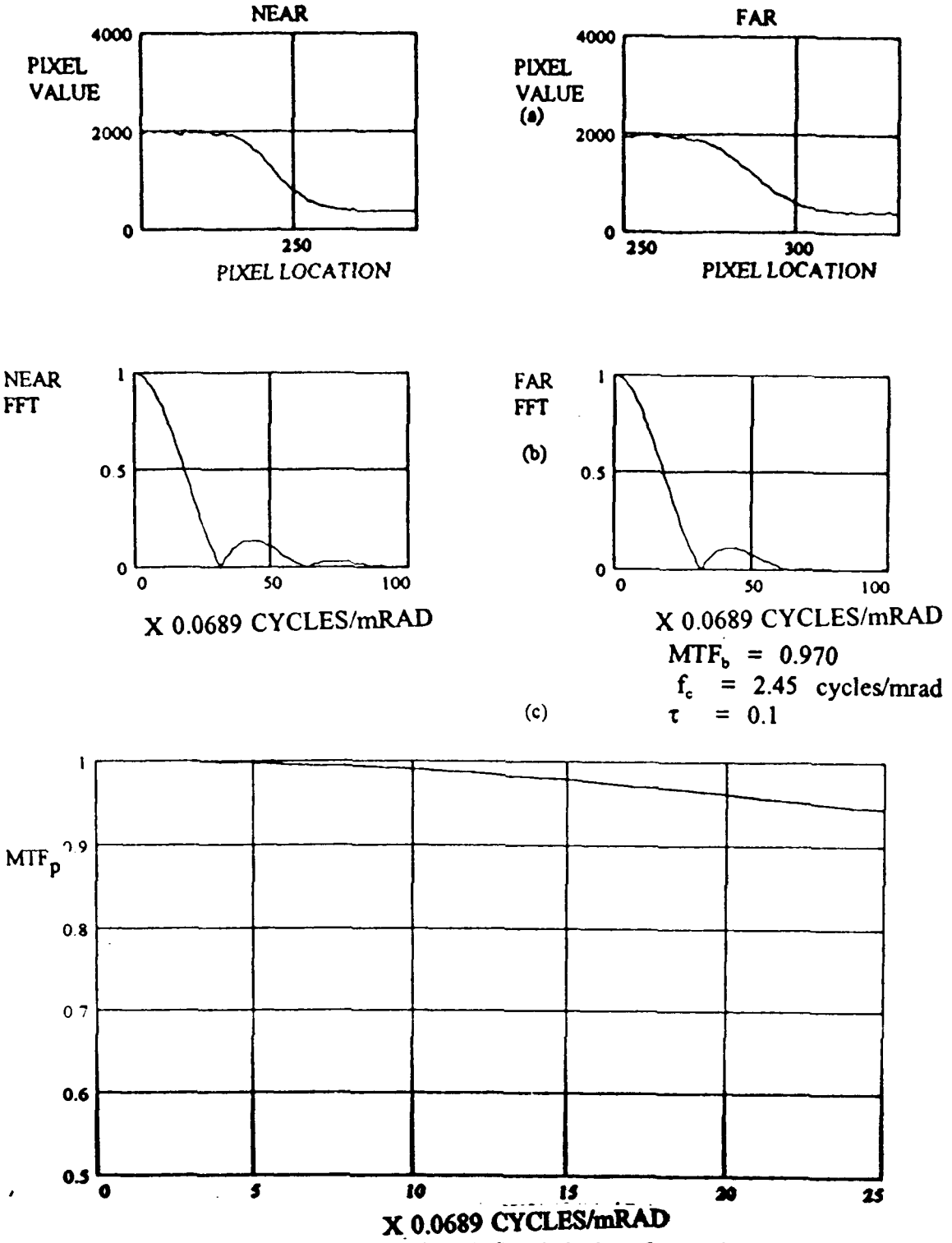

Figure 25. Data from 12:00 PM of April 17, 1993: (a) line pixel values of the black-white steps for both targets; (b) normalized, line FFTs of both targets based on the corresponding pixel values shown; (c) normalized aerosol MTF_p, derived from the ratio of the far target FFT to the near target FFT. Values for f_c, τ, and MTF_b are included.

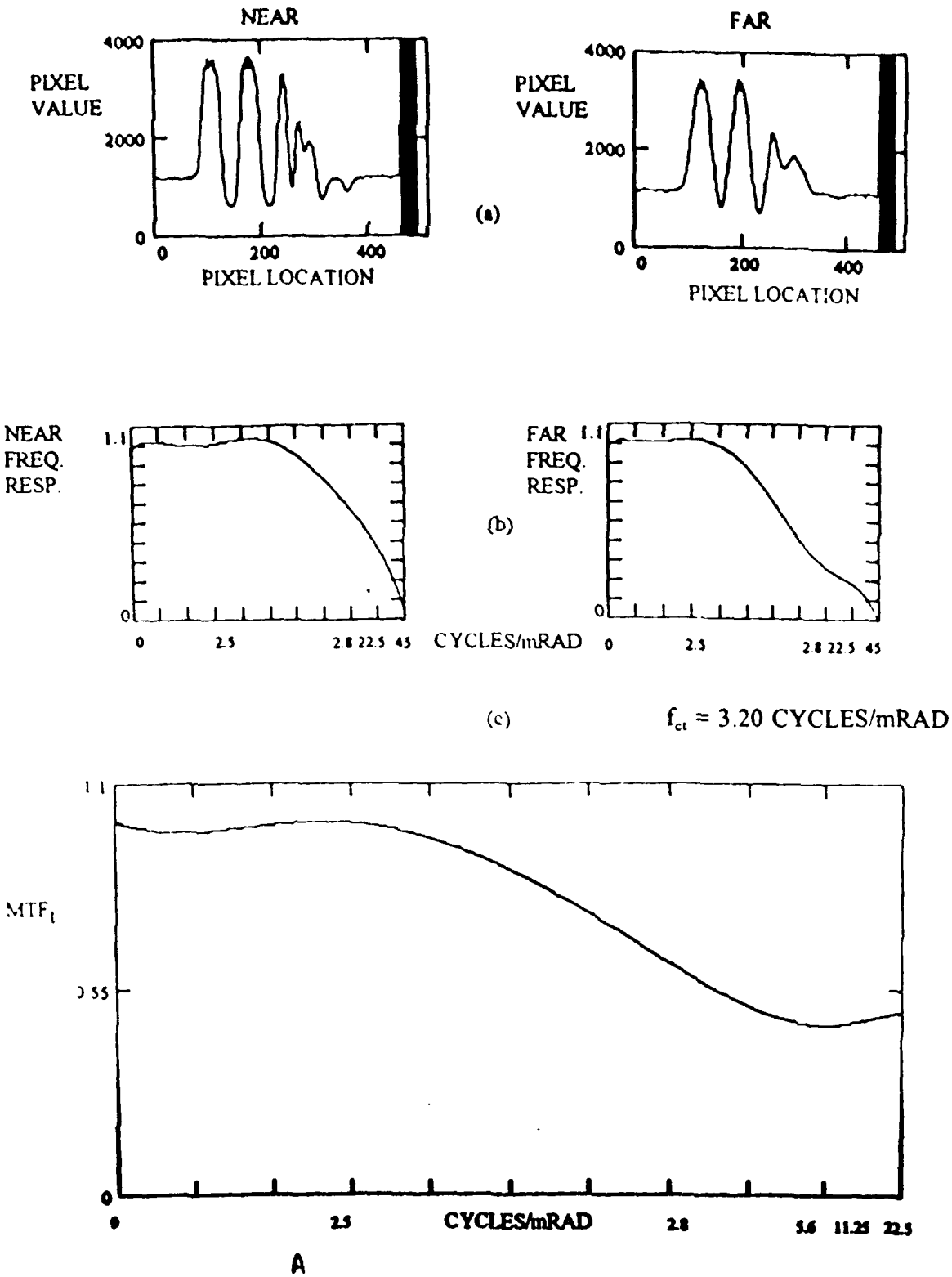

Figure 26. Data from 11:30 P.M. of April 17, 1993: (a) line pixel values of castellated black-white stripes for both targets; (b) normalized spatial frequency response of both targets based on the corresponding pixel values shown; (c) turbulence, MTF_t, derived from the ratio of the far to near target frequency response. Cutoff frequency, f_{ct}, for MTF_t is included.

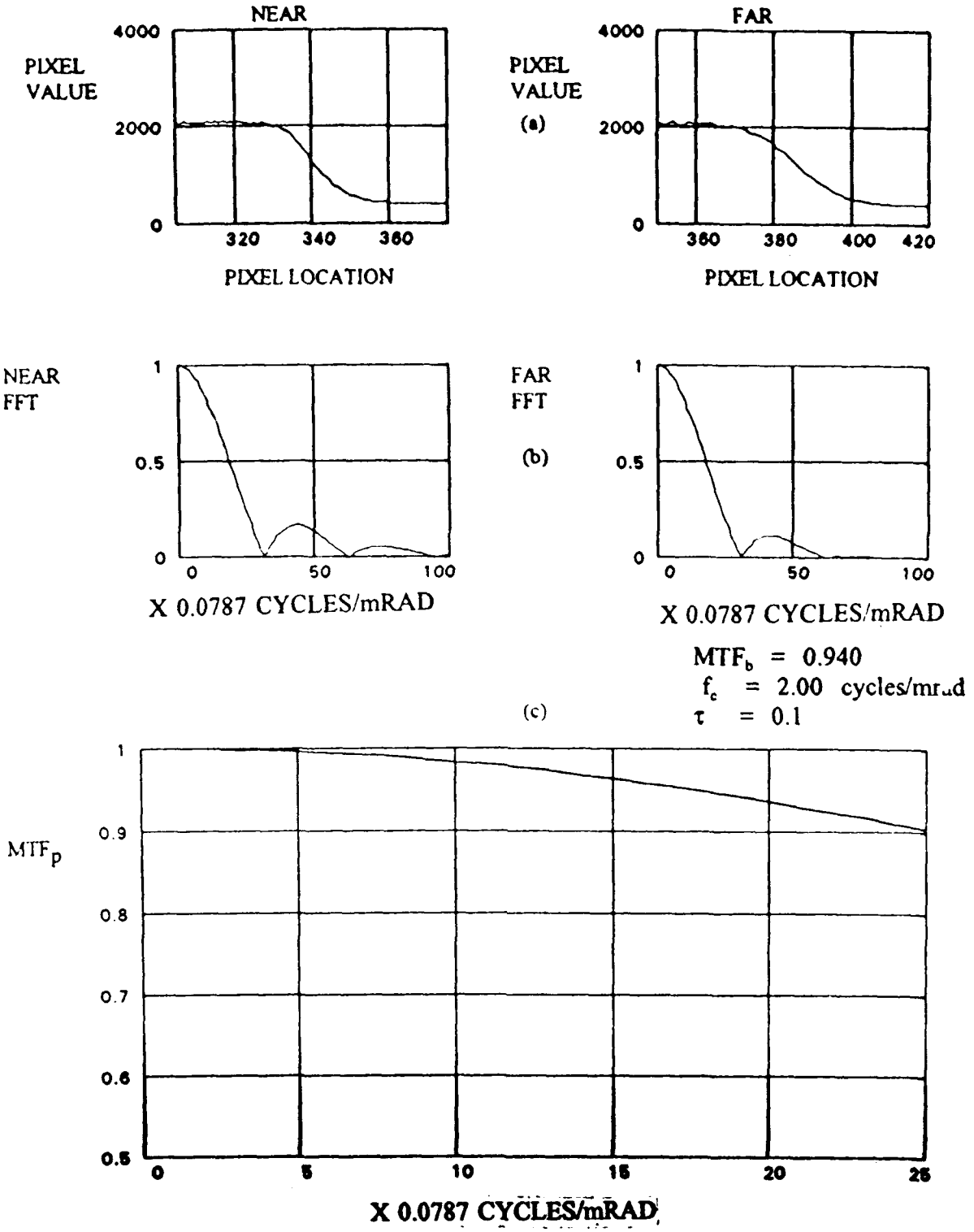

Figure 27. Data from 11:15 AM of April 17, 1993: (a) line pixel values of the black-white steps for both targets; (b) normalized, line FFTs of both targets based on the corresponding pixel values shown; (c) normalized aerosol MTF_p, derived from the ratio of the far target FFT to the near target FFT. Values for f_c, τ, and MTF_b are included. Focus on near target.

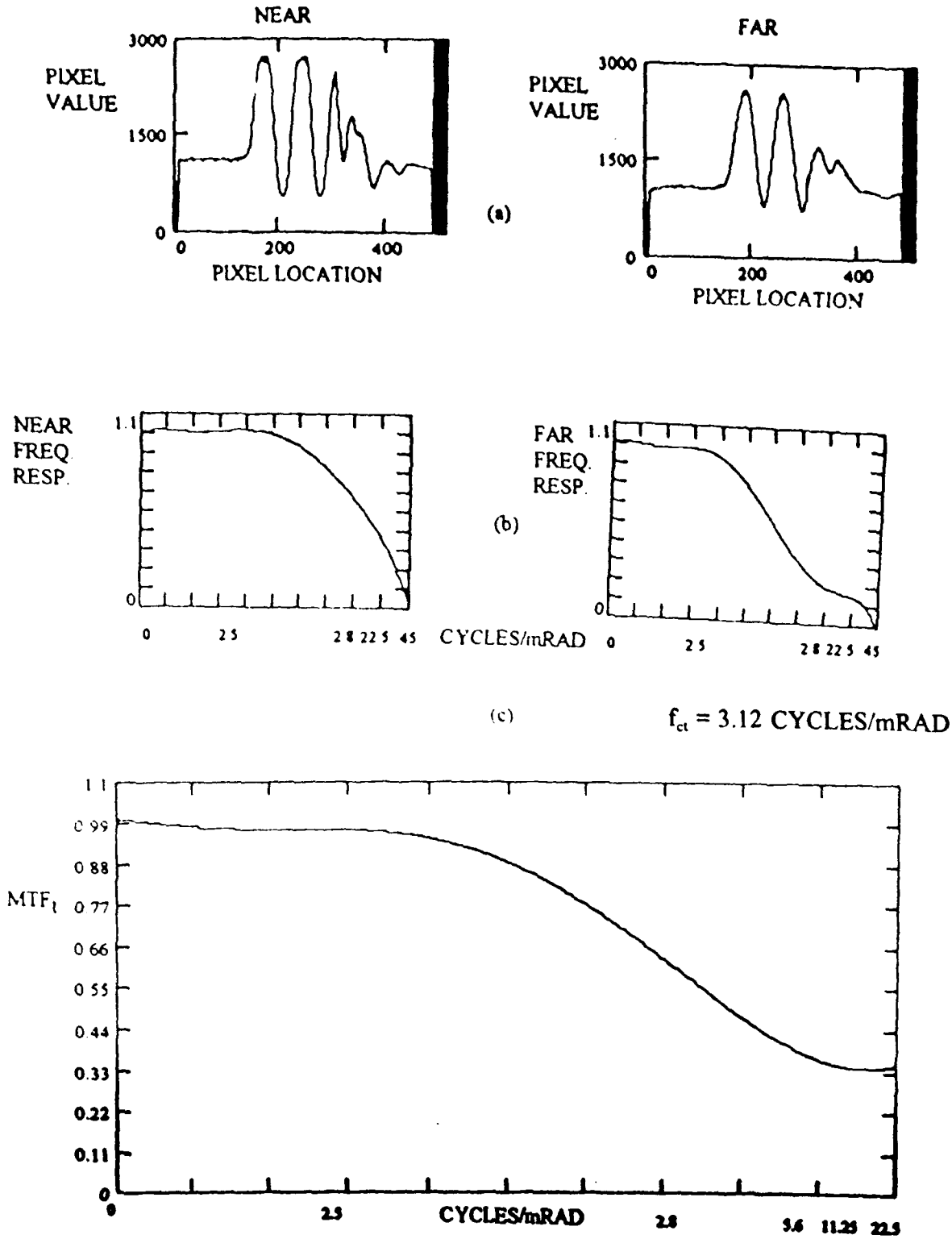

Figure 28. Data from 11:15 A.M. of April 27, 1993: (a) line pixel values of castellated black-white stripes for both targets; (b) normalized spatial frequency response of both targets based on the corresponding pixel values shown; (c) turbulence, MTF_t, derived from the ratio of the far to near target frequency response. Cutoff frequency, f_{ct}, for MTF_t is included. Focus on near target.

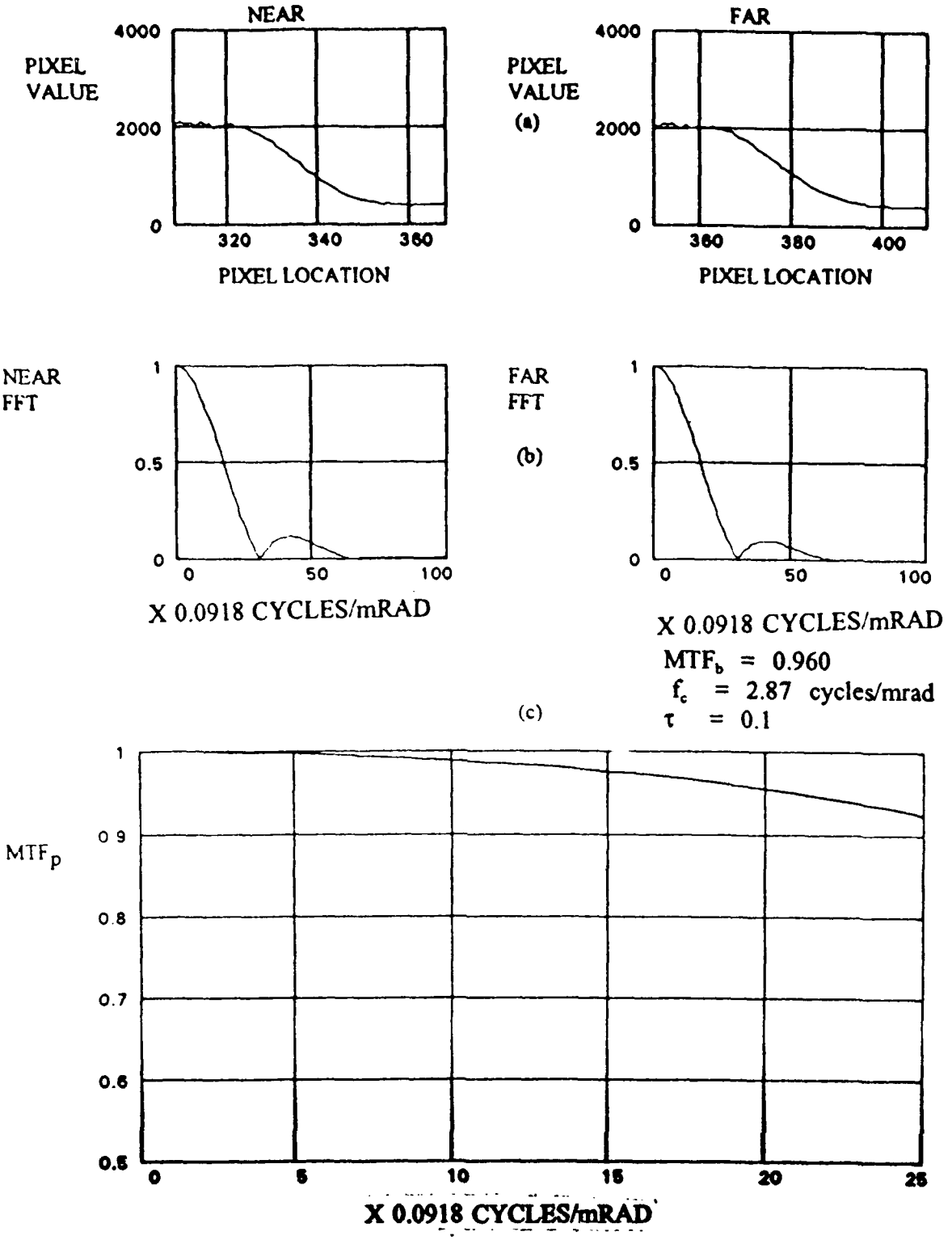

Figure 29. Data from 11:20 AM of April 17, 1993: (a) line pixel values of the black-white steps for both targets; (b) normalized, line FFTs of both targets based on the corresponding pixel values shown; (c) normalized aerosol MTF_p, derived from the ratio of the far target FFT to the near target FFT. Values for f_c, τ, and MTF_b are included. Focus beyond near target.

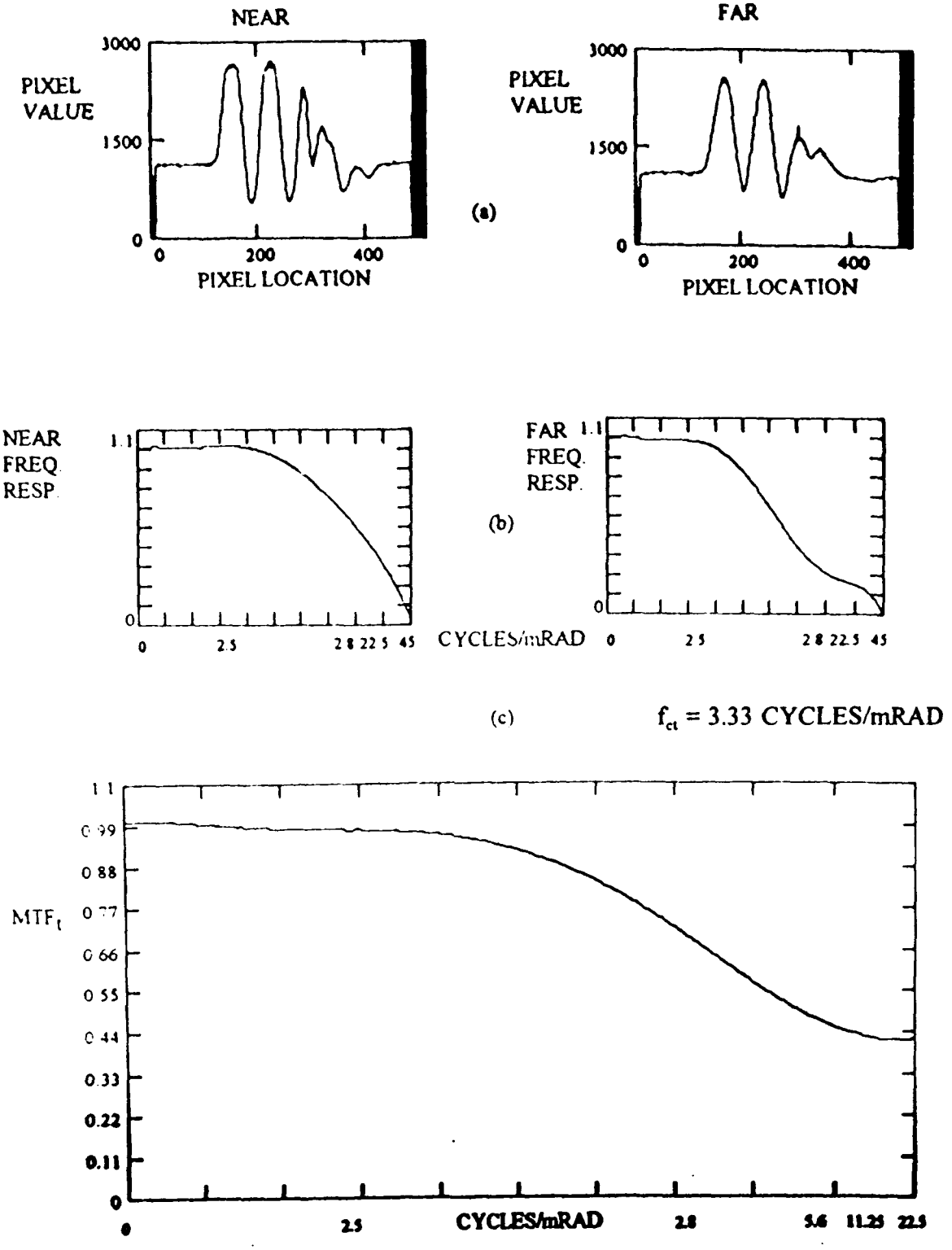

Figure 30. Data from 11:20 A.M. of April 17, 1993: (a) line pixel values of castellated black-white stripes for both targets; (b) normalized spatial frequency response of both targets based on the corresponding pixel values shown; (c) turbulence, MTF_t, derived from the ratio of the far to near target frequency response. Cutoff frequency, f_{ct}, for MTF_t is included. Focus beyond near target.

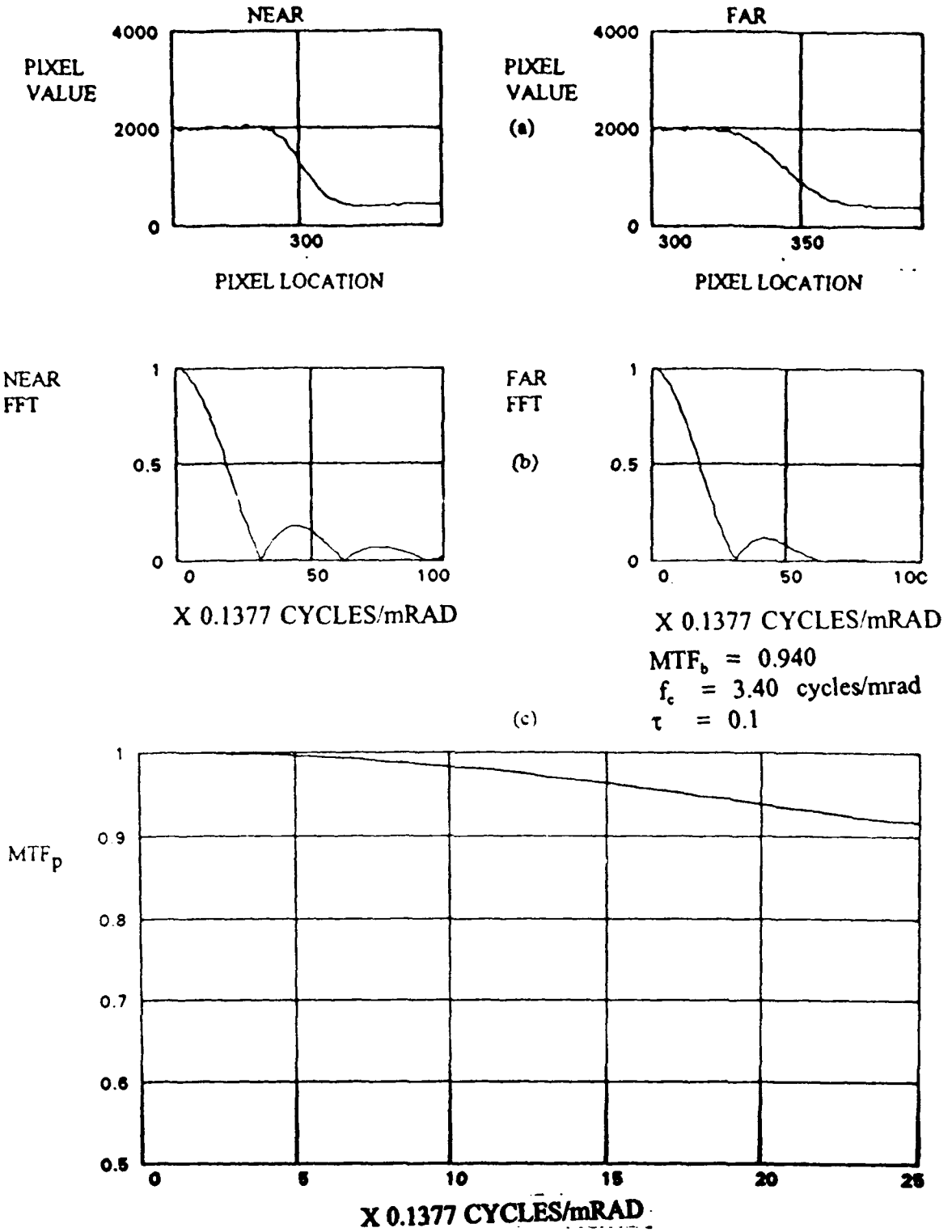

Figure 31. Data from 11:40 AM of April 17, 1993: (a) line pixel values of the black-white steps for both targets; (b) normalized, line FFTs of both targets based on the corresponding pixel values shown; (c) normalized aerosol MTF_p, derived from the ratio of the far target FFT to the near target FFT. Values for f_c, τ, and MTF_b are included. Focus closer than near target.

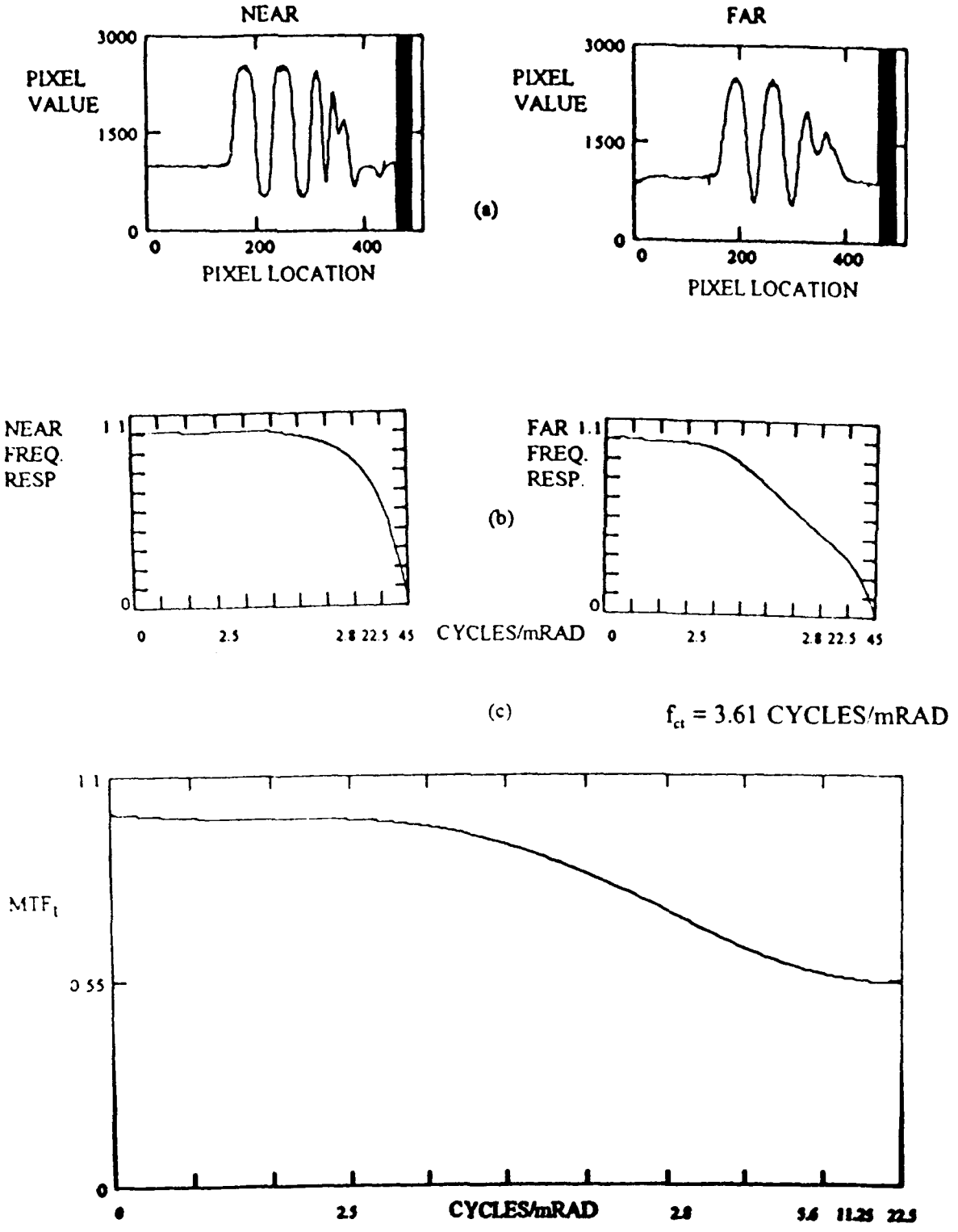

Figure 32. Data from 11:40 A.M. of April 17, 1993: (a) line pixel values of castellated black-white stripes for both targets; (b) normalized spatial frequency response of both targets based on the corresponding pixel values shown; (c) turbulence, MTF_t, derived from the ratio of the far to near target frequency response. Cutoff frequency, f_{ct}, for MTF_t is included. Focused closer than near target.

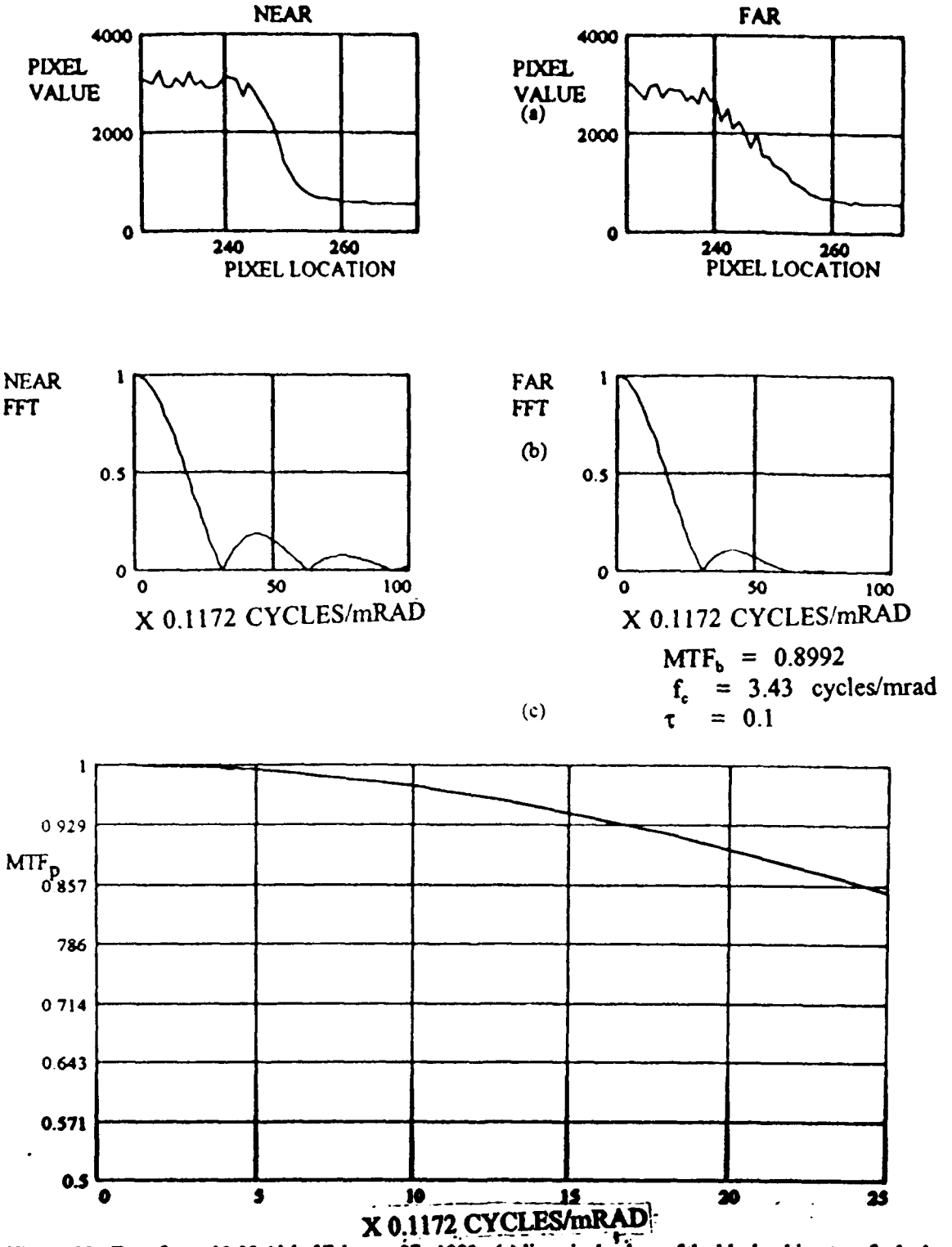

Figure 33. Data from 10:00 AM of February 27 , 1993: (a) line pixel values of the black-white steps for both targets; (b) normalized, line FFTs of both targets based on the corresponding pixel values shown; (c) normalized aerosol MTF_p , derived from the ratio of the far target FFT to the near target FFT. Values for f_c, τ, and MTF_b are included.

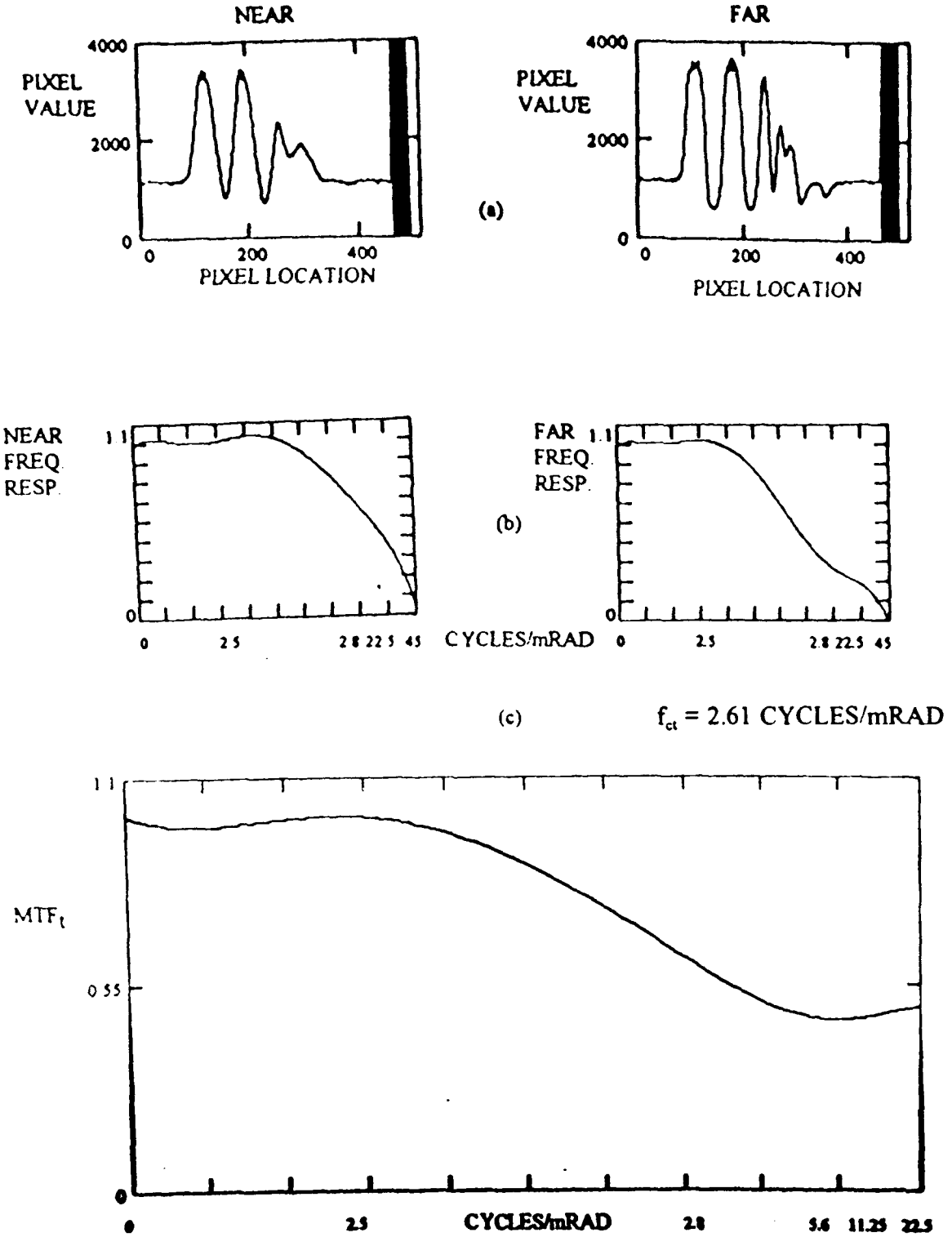

Figure 34. Data from 10:00 A.M. of February 27, 1993: (a) line pixel values of castellated black-white stripes for both targets; (b) normalized spatial frequency response of both targets based on the corresponding pixel values shown; (c) turbulence, MTF_t, derived from the ratio of the far to near target frequency response. Cutoff frequency, f_{ct}, for MTF_t is included.

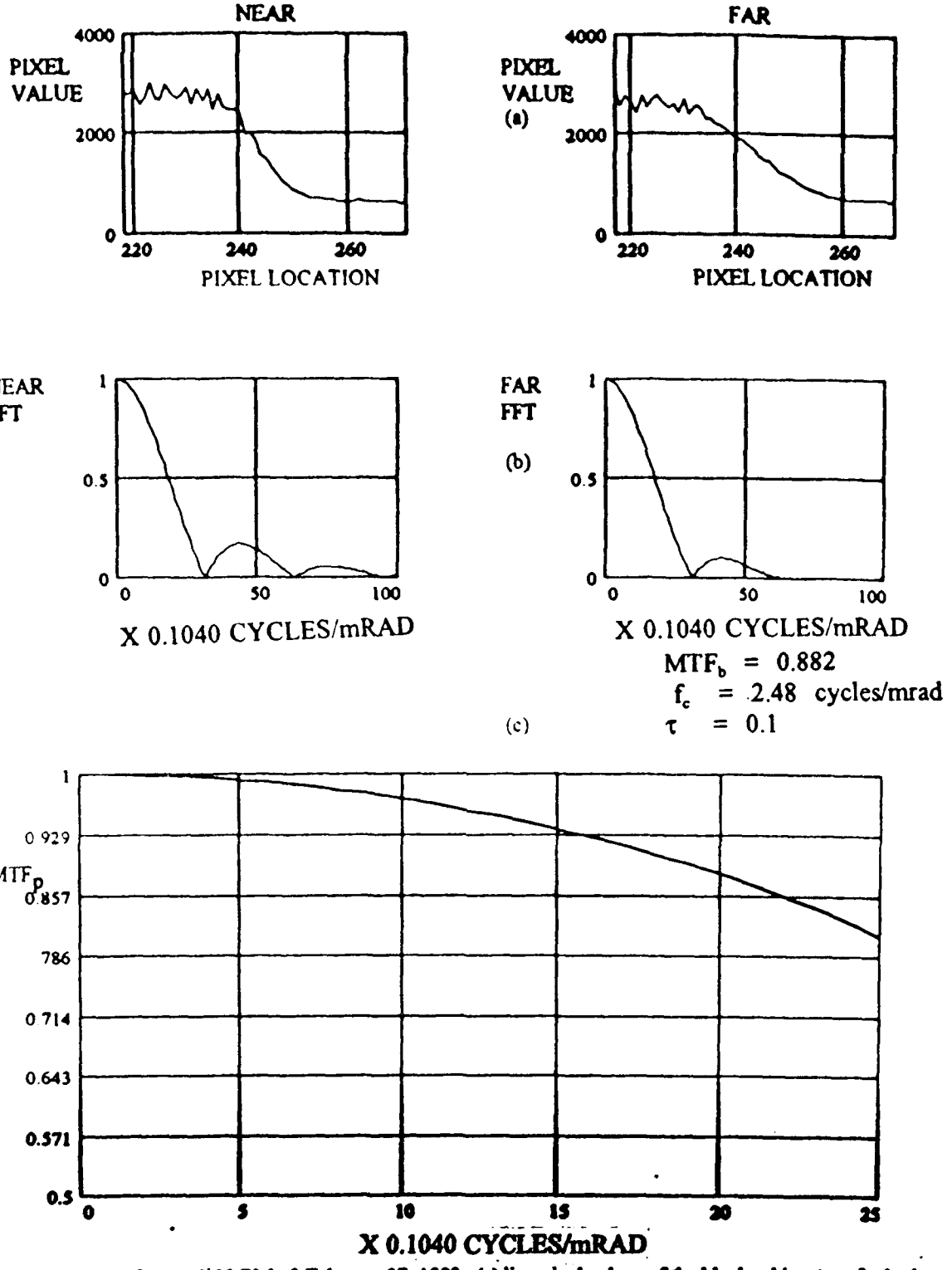

Figure 35. Data from 12:00 PM of February 27, 1993: (a) line pixel values of the black-white steps for both targets; (b) normalized, line FFTs of both targets based on the corresponding pixel values shown; (c) normalized aerosol MTF_p, derived from the ratio of the far target FFT to the near target FFT. Values for f_c, τ, and MTF_b are included.

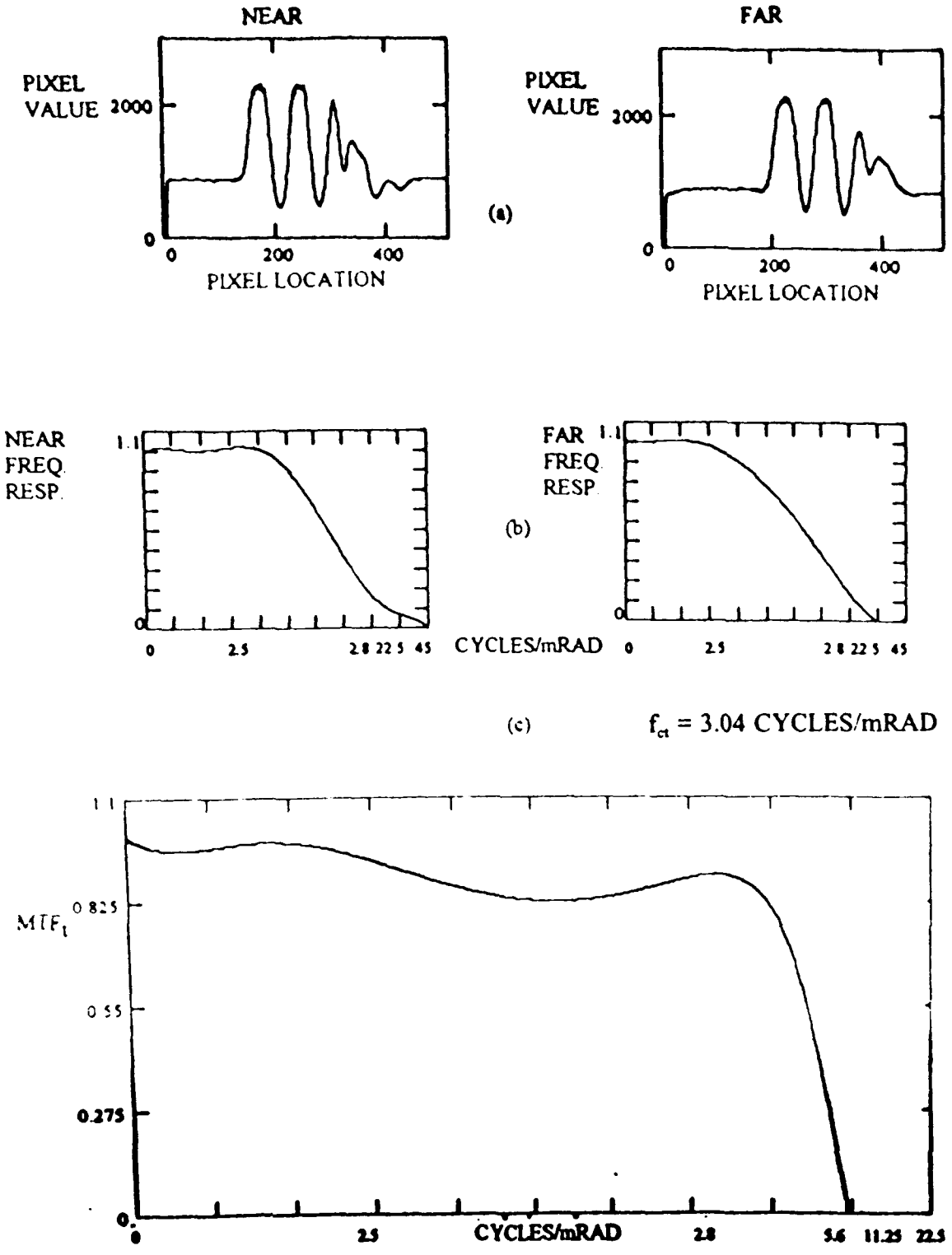

Figure 36. Data from 12:00 P.M. of February 27, 1993: (a) line pixel values of castellated black-white stripes for both targets; (b) normalized spatial frequency response of both targets based on the corresponding pixel values shown; (c) turbulence, MTF_t, derived from the ratio of the far to near target frequency response. Cutoff frequency, f_{ct}, for MTF_t is included.

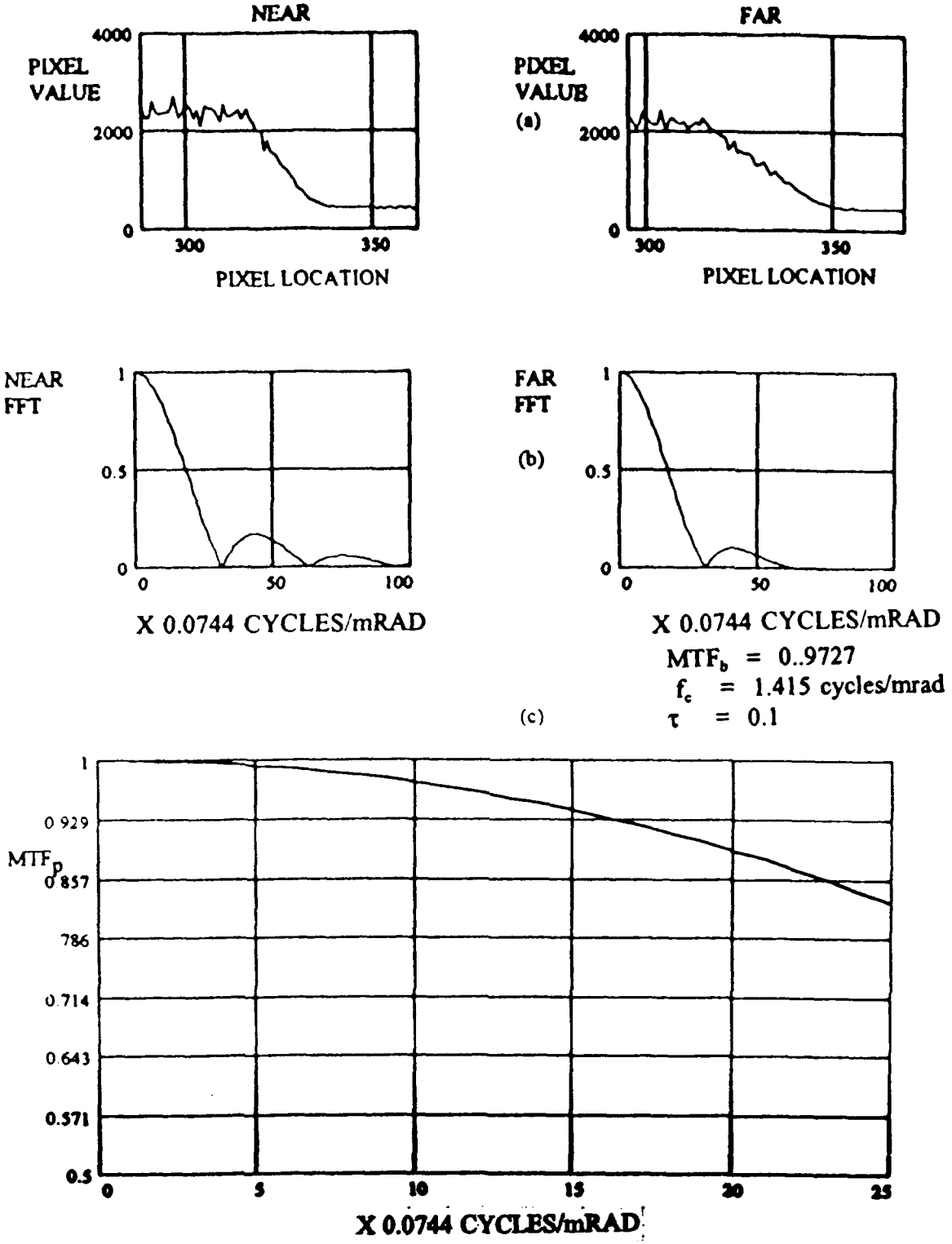

Figure 37. Data from 9:00 AM of December 22, 1992: (a) line pixel values of the black-white steps for both targets; (b) normalized, line FFTs of both targets based on the corresponding pixel values shown; (c) normalized aerosol MTF_p, derived from the ratio of the far target FFT to the near target FFT. Values for f_c, τ, and MTF_b are included.

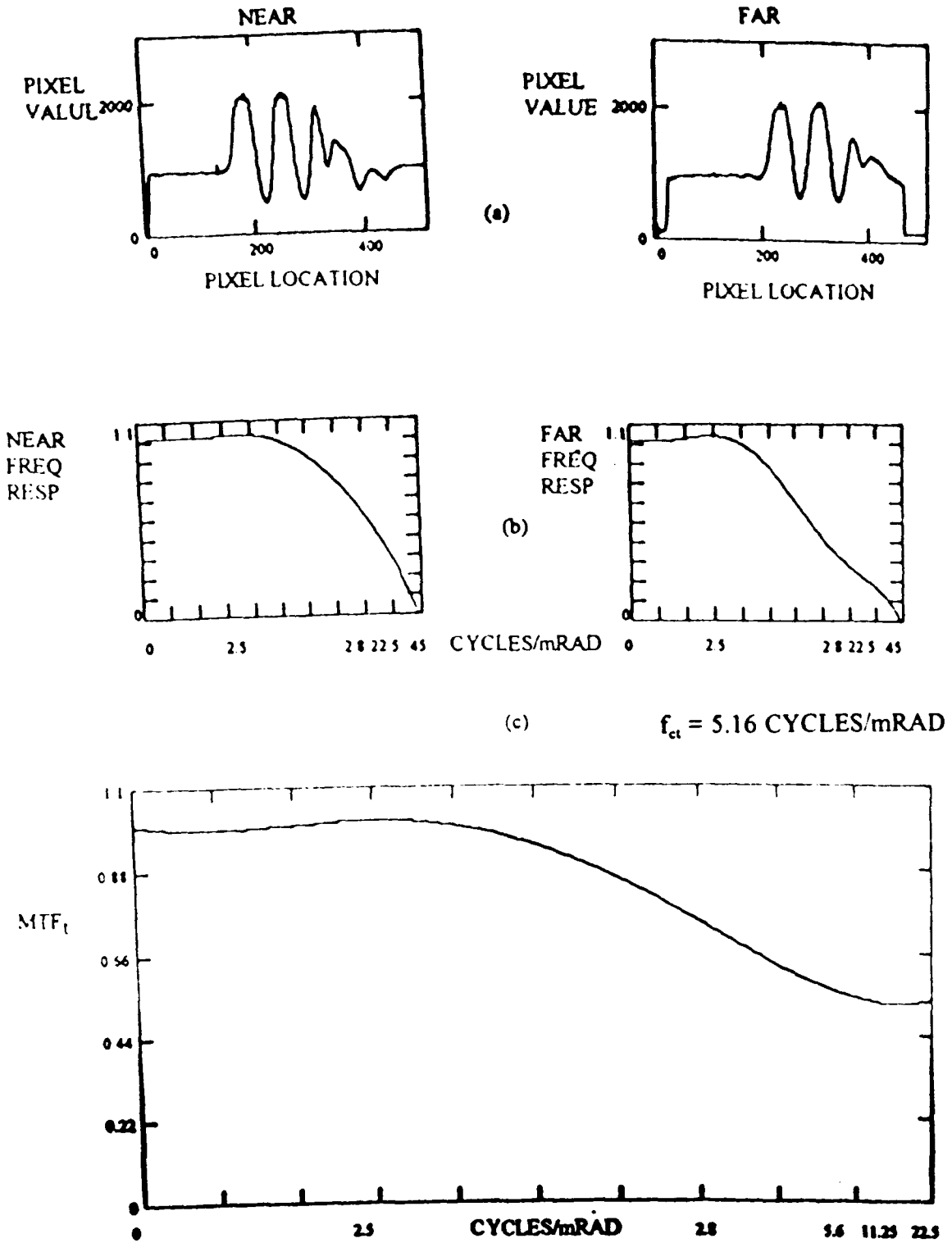

Figure 38. Data from 9:00 A.M. of December 22, 1992: (a) line pixel values of castellated black-white stripes for both targets; (b) normalized spatial frequency response of both targets based on the corresponding pixel values shown; (c) turbulence, MTF_t, derived from the ratio of the far to near target frequency response. Cutoff frequency, f_{ct}, for MTF_t is included.

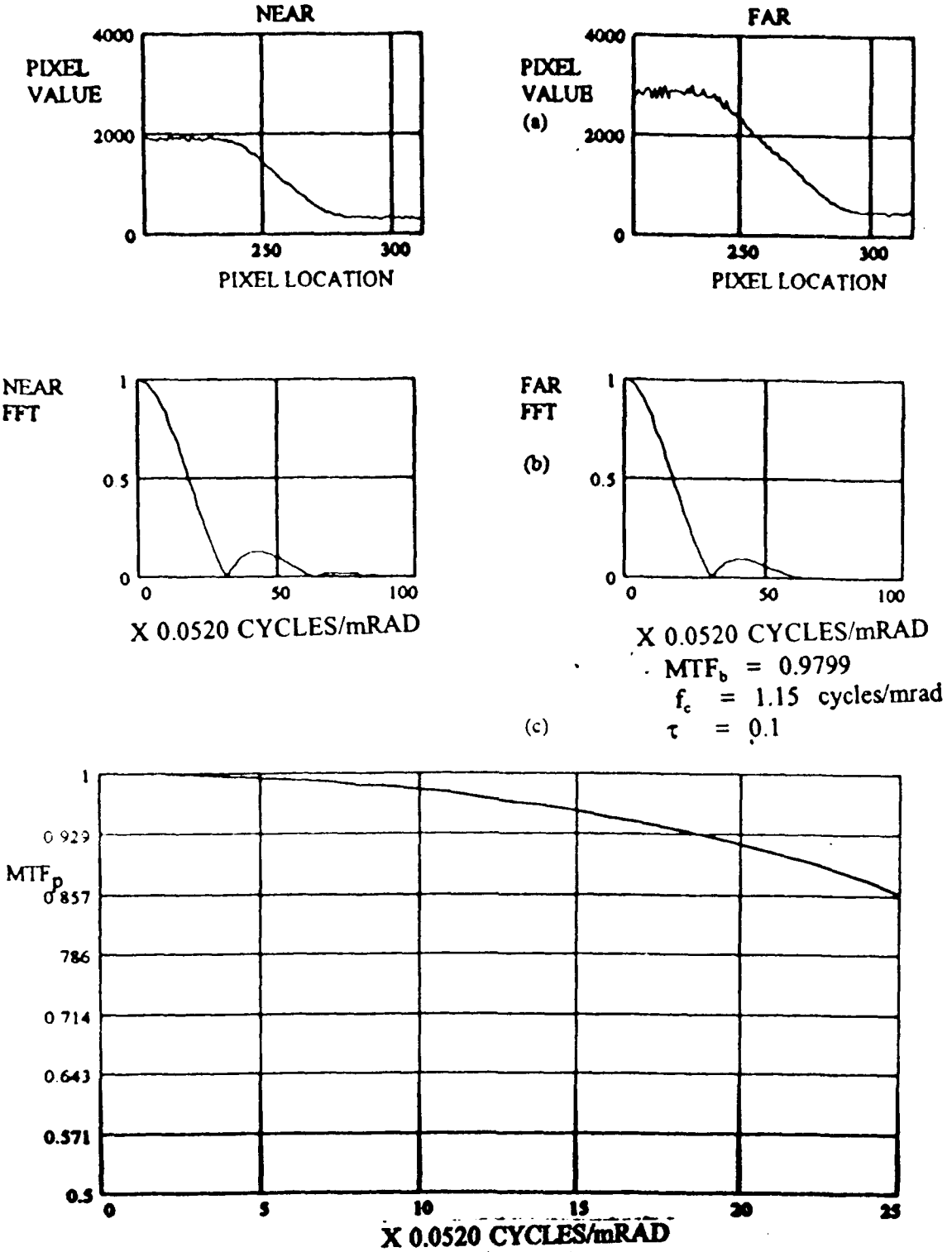

Figure 39. Data from 9:57 AM of December 22, 1992: (a) line pixel values of the black-white steps for both targets; (b) normalized, line FFTs of both targets based on the corresponding pixel values shown; (c) normalized aerosol MTF_p, derived from the ratio of the far target FFT to the near target FFT. Values for f_c, τ, and MTF_b are included.

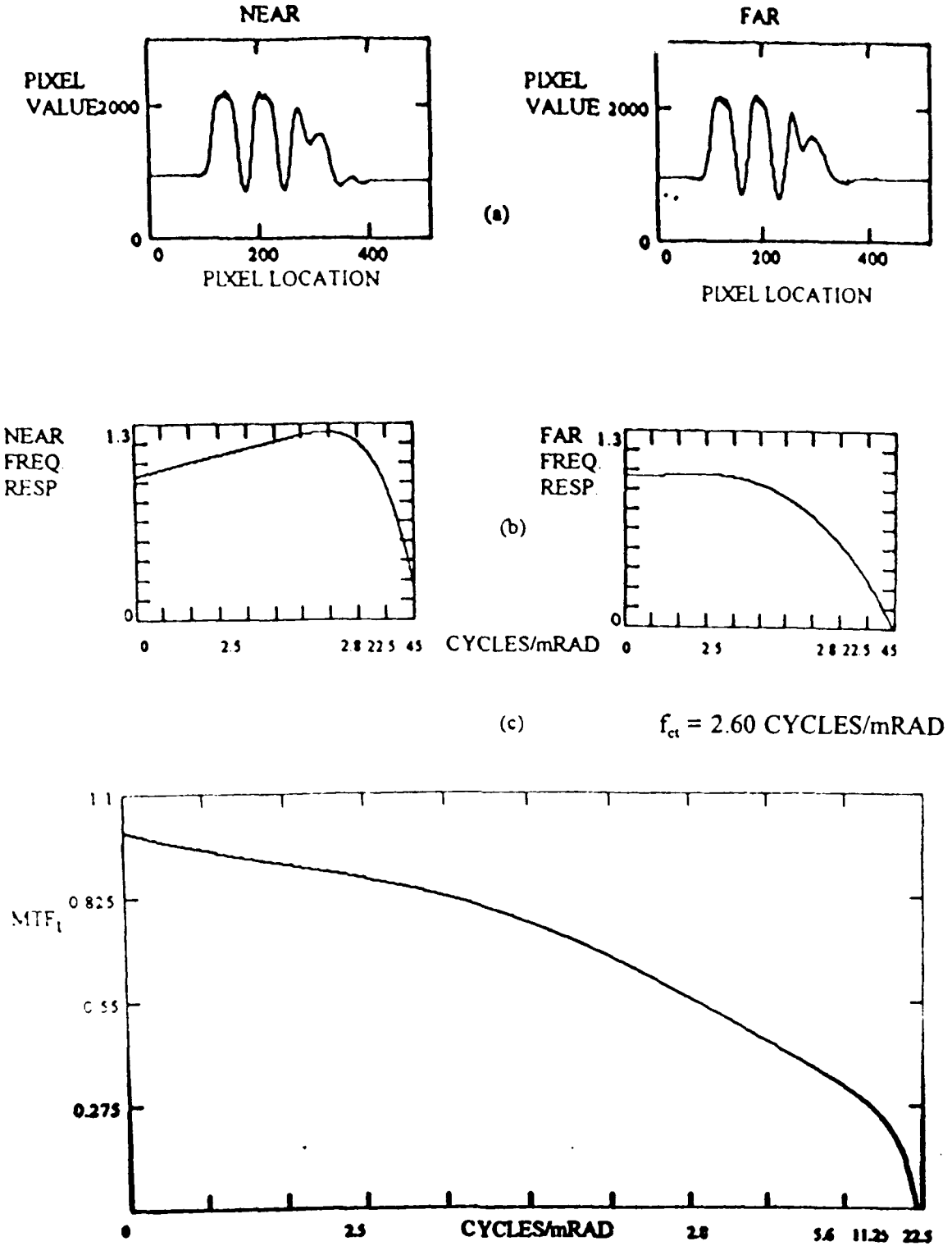

Figure 40. Data from 9:57 A.M. of December 22, 1992: (a) line pixel values of castellated black-white stripes for both targets; (b) normalized spatial frequency response of both targets based on the corresponding pixel values shown; (c) turbulence, MTF_t, derived from the ratio of the far to near target frequency response. Cutoff frequency, f_{ct}, for MTF_t is included.

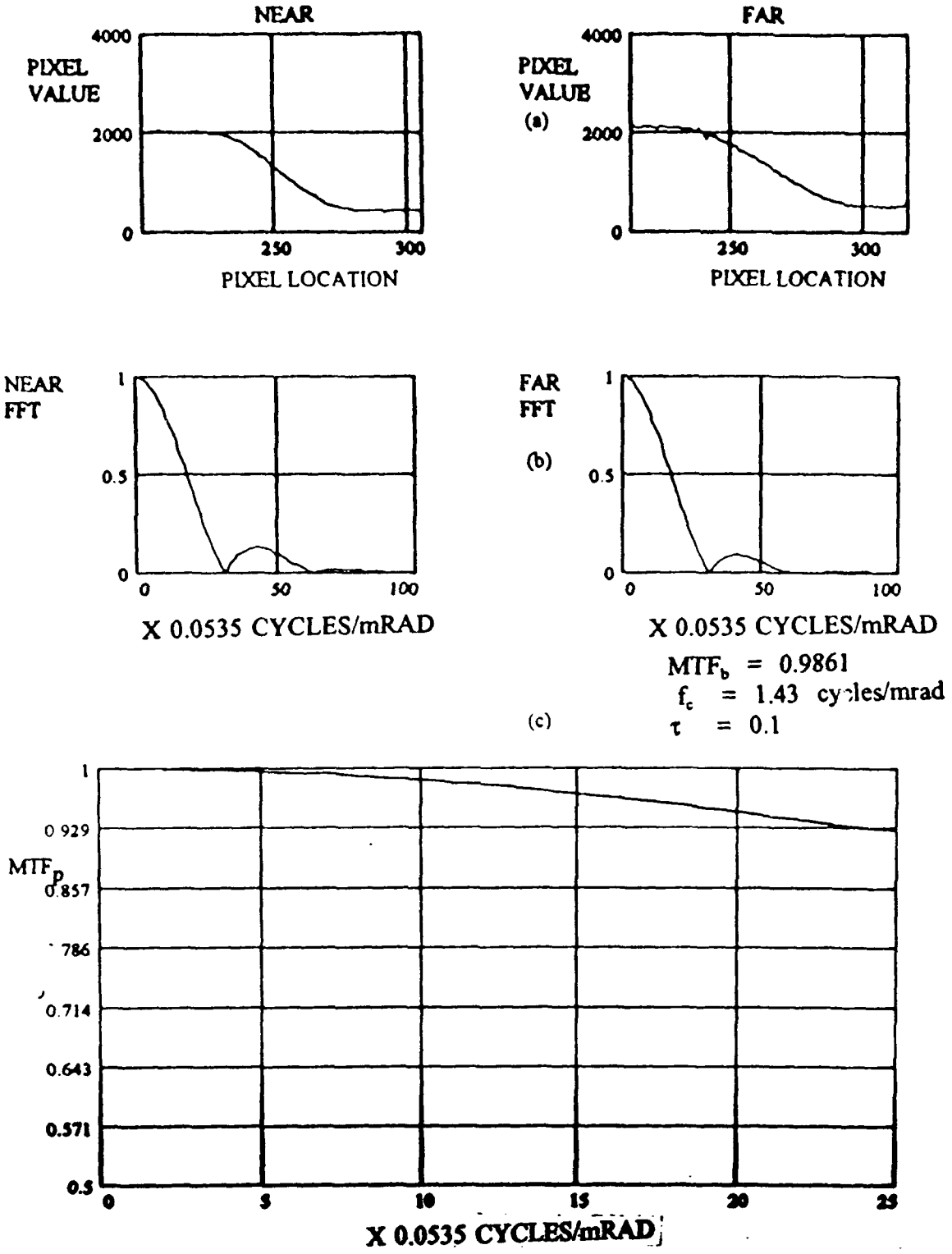

Figure 41. Data from 11:00 AM of December 22, 1992: (a) line pixel values of the black-white steps for both targets; (b) normalized, line FFTs of both targets based on the corresponding pixel values shown; (c) normalized aerosol MTF_p, derived from the ratio of the far target FFT to the near target FFT. Values for f_c, τ, and MTF_b are included.

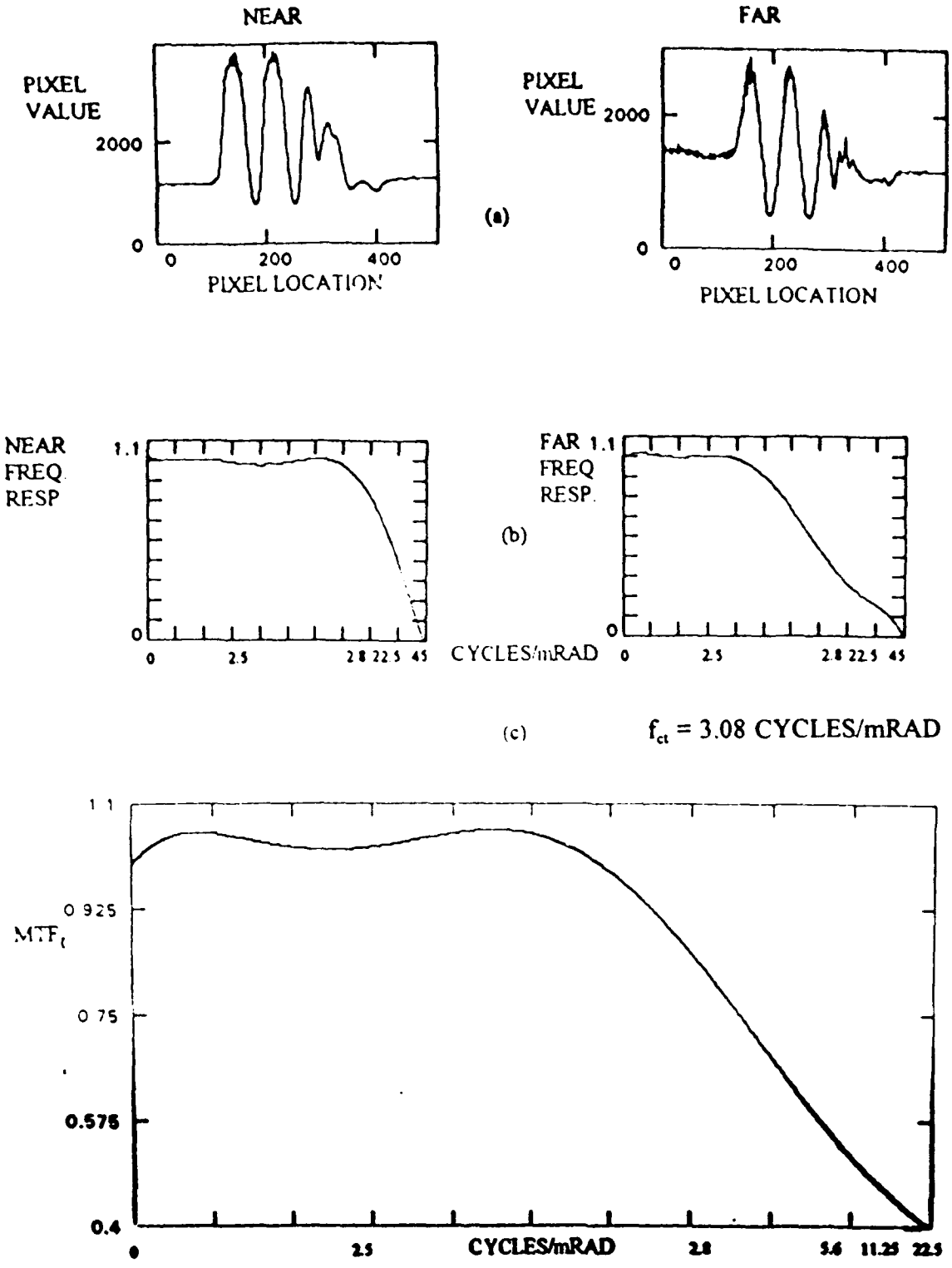

Figure 42. Data from 11:00 A.M. of December 22, 1992: (a) line pixel values of castellated black-white stripes for both targets; (b) normalized spatial frequency response of both targets based on the corresponding pixel values shown; (c) turbulence, MTF_t, derived from the ratio of the far to near target frequency response. Cutoff frequency, f_{ct}, for MTF_t is included.

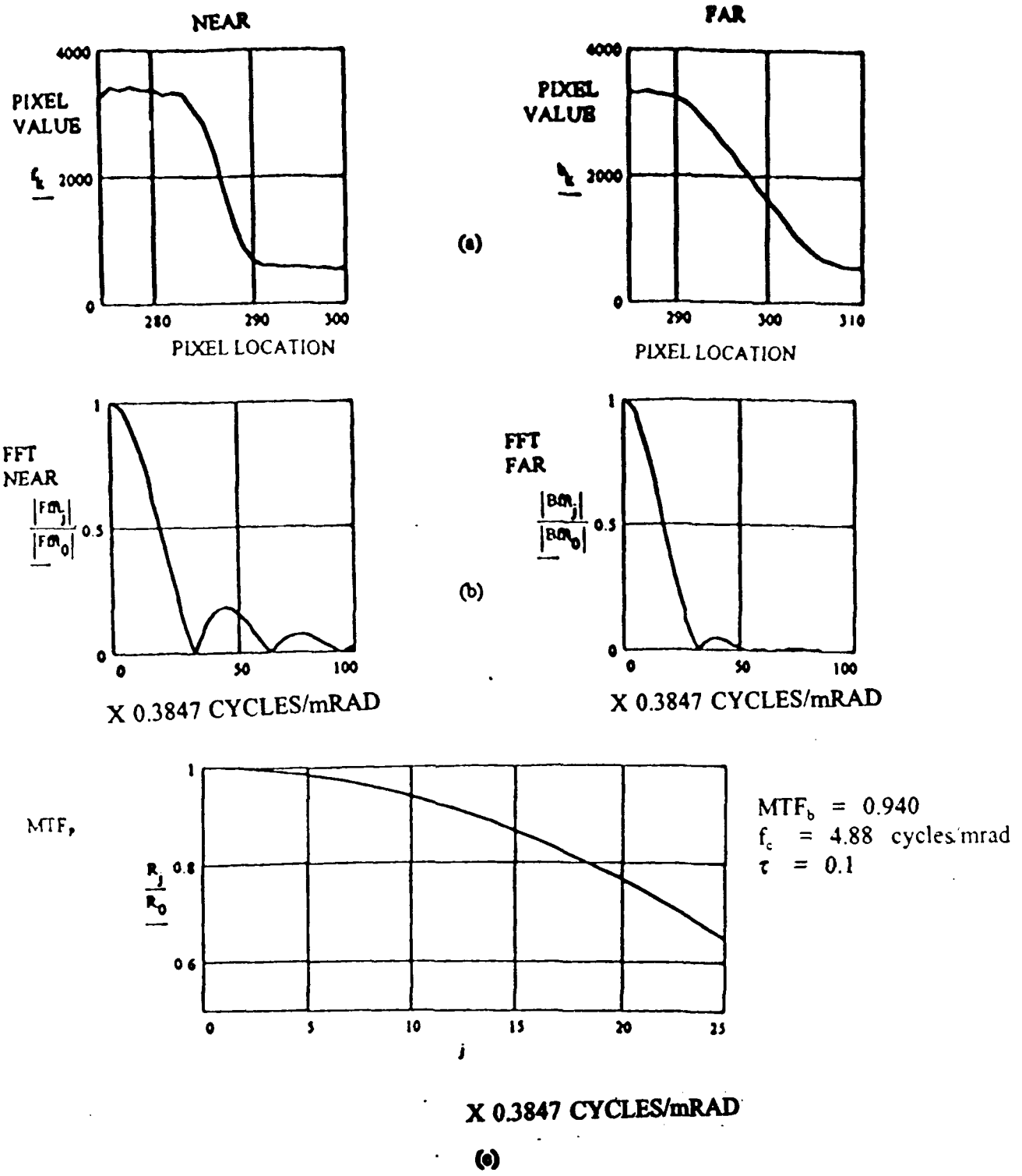

Figure 43. Data from 7:00 AM of November 21, 1992: (a) line pixel values of the black-white steps for both targets; (b) normalized, line FFTs of both targets based on the corresponding pixel values shown; (c) normalized aerosol MTF_p, derived from the ratio of the far target FFT to the near target FFT. Values for f_c, τ, and MTF_b are included.

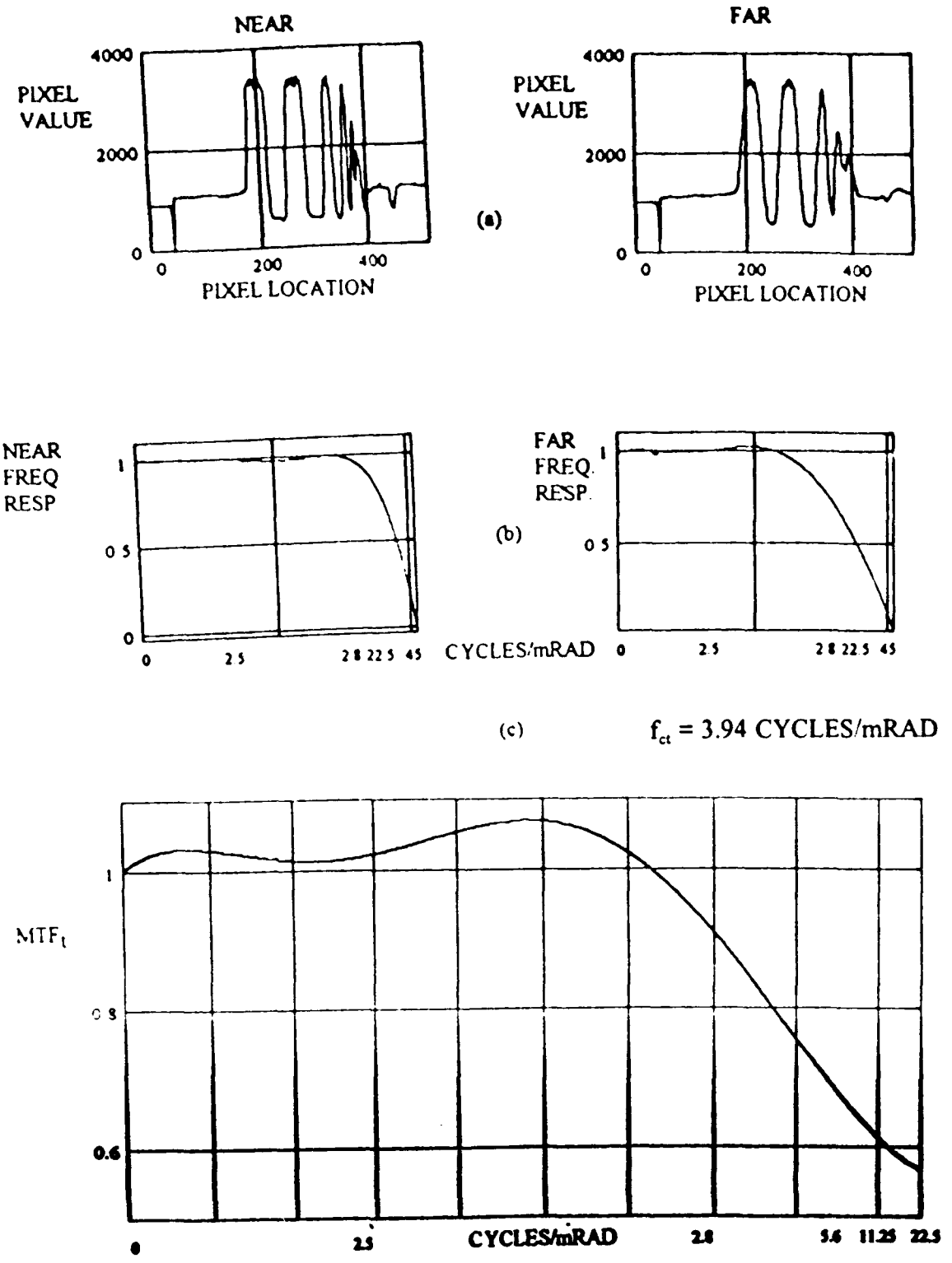

Figure 44. Data from 7:00 A.M. of November 21, 1992: (a) line pixel values of castellated black-white stripes for both targets; (b) normalized spatial frequency response of both targets based on the corresponding pixel values shown; (c) turbulence, MTF_t, derived from the ratio of the far to near target frequency response. Cutoff frequency, f_{ct}, for MTF_t is included.

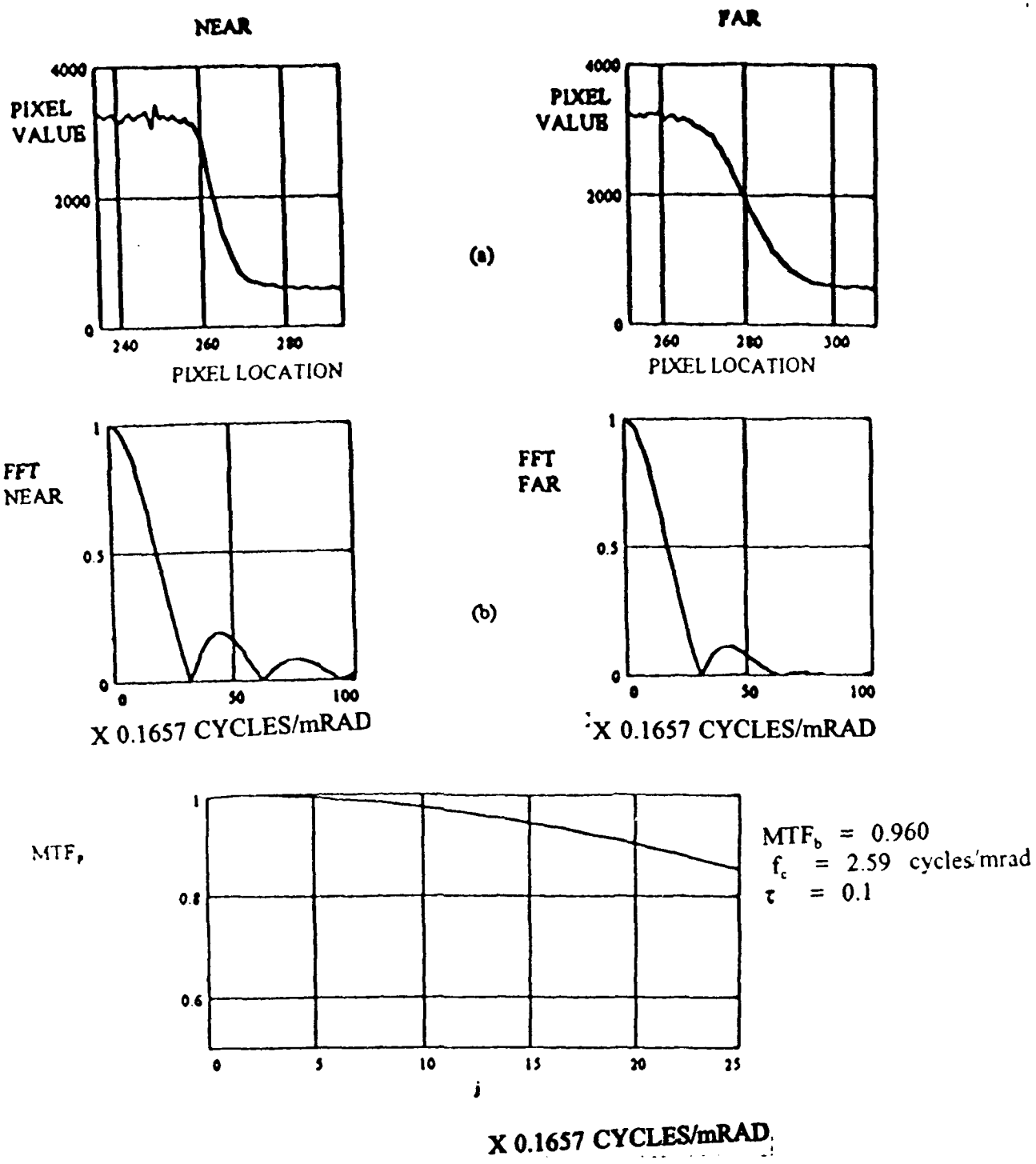

Figure 45. Data from 12:00 PM of November 21, 1992: (a) line pixel values of the black-white steps for both targets; (b) normalized, line FFTs of both targets based on the corresponding pixel values shown; (c) normalized aerosol MTF_p, derived from the ratio of the far target FFT to the near target FFT. Values for f_c, τ, and MTF_b are included.

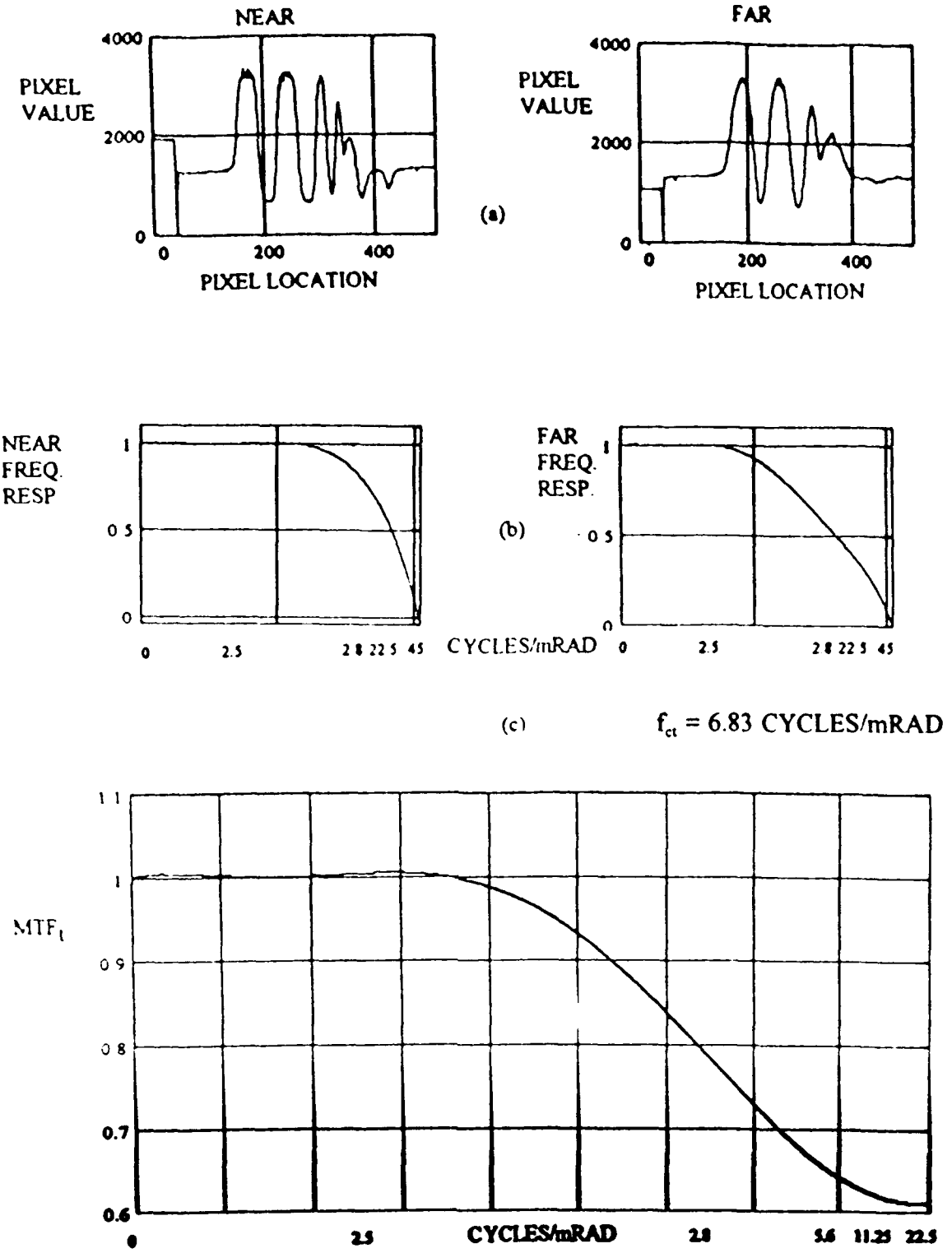

Figure 46. Data from 12:00 P.M. of November 21, 1992: (a) line pixel values of castellated black-white stripes for both targets; (b) normalized spatial frequency response of both targets based on the corresponding pixel values shown; (c) turbulence, MTF_t, derived from the ratio of the far to near target frequency response. Cutoff frequency, f_{ct}, for MTF_t is included.

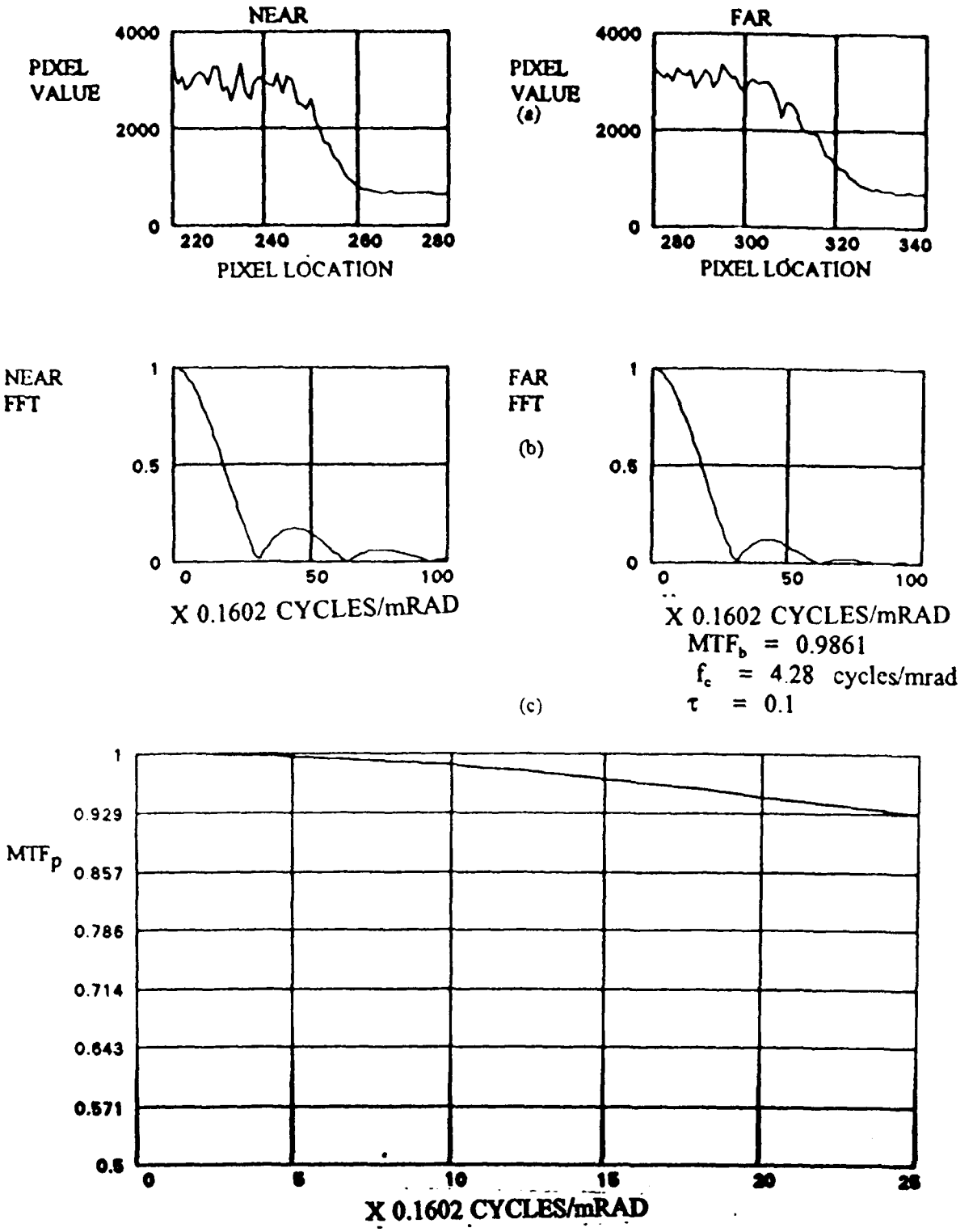

Figure 47. Data from 8:00 AM of October 31, 1992: (a) line pixel values of the black-white steps for both targets; (b) normalized, line FFTs of both targets based on the corresponding pixel values shown; (c) normalized aerosol MTF_p, derived from the ratio of the far target FFT to the near target FFT. Values for f_c, τ, and MTF_b are included.

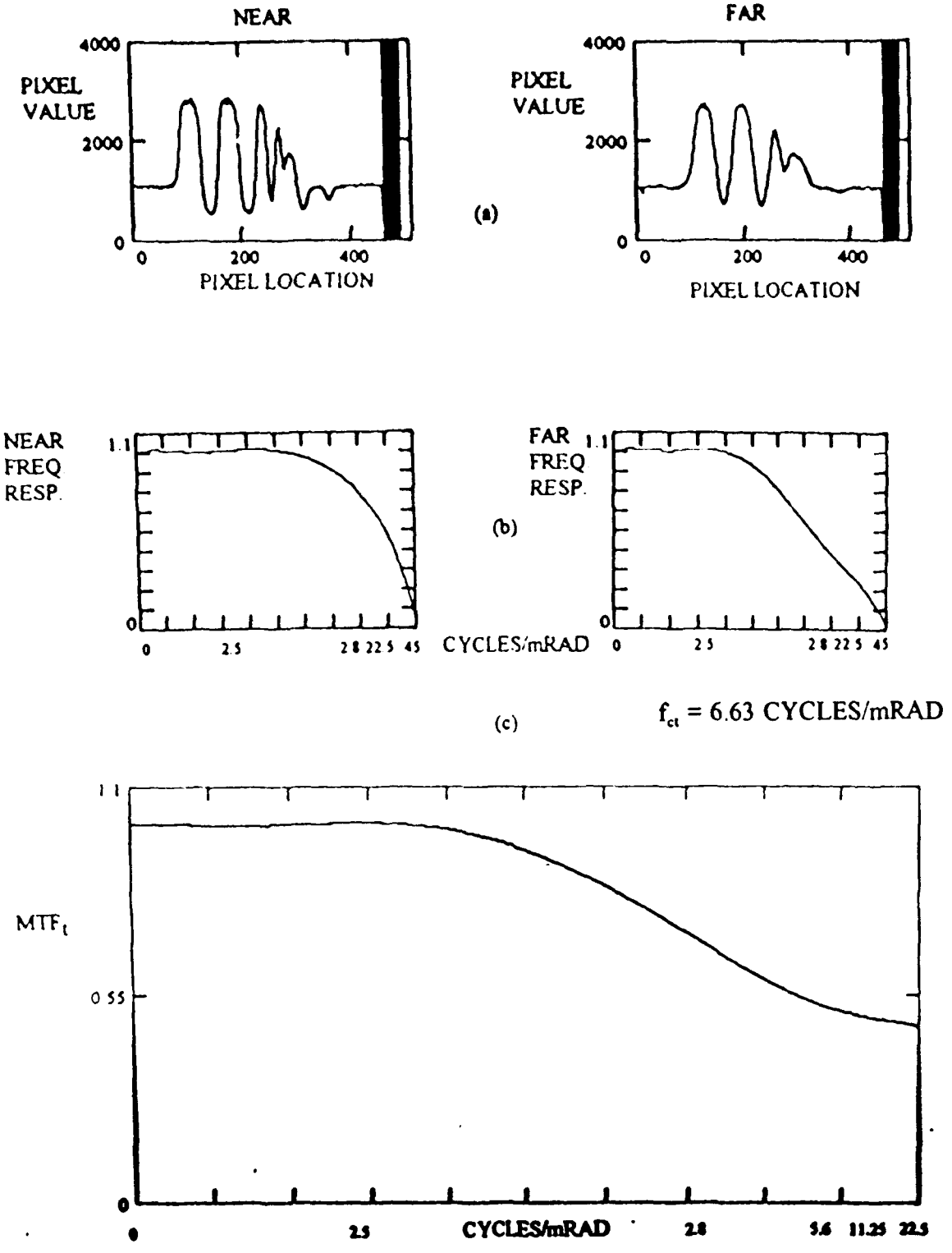

Figure 48. Data from 8:00 A.M. of October 31, 1992: (a) line pixel values of castellated black-white stripes for both targets; (b) normalized spatial frequency response of both targets based on the corresponding pixel values shown; (c) turbulence, MTF_t, derived from the ratio of the far to near target frequency response. Cutoff frequency, f_{ct}, for MTF_t is included.

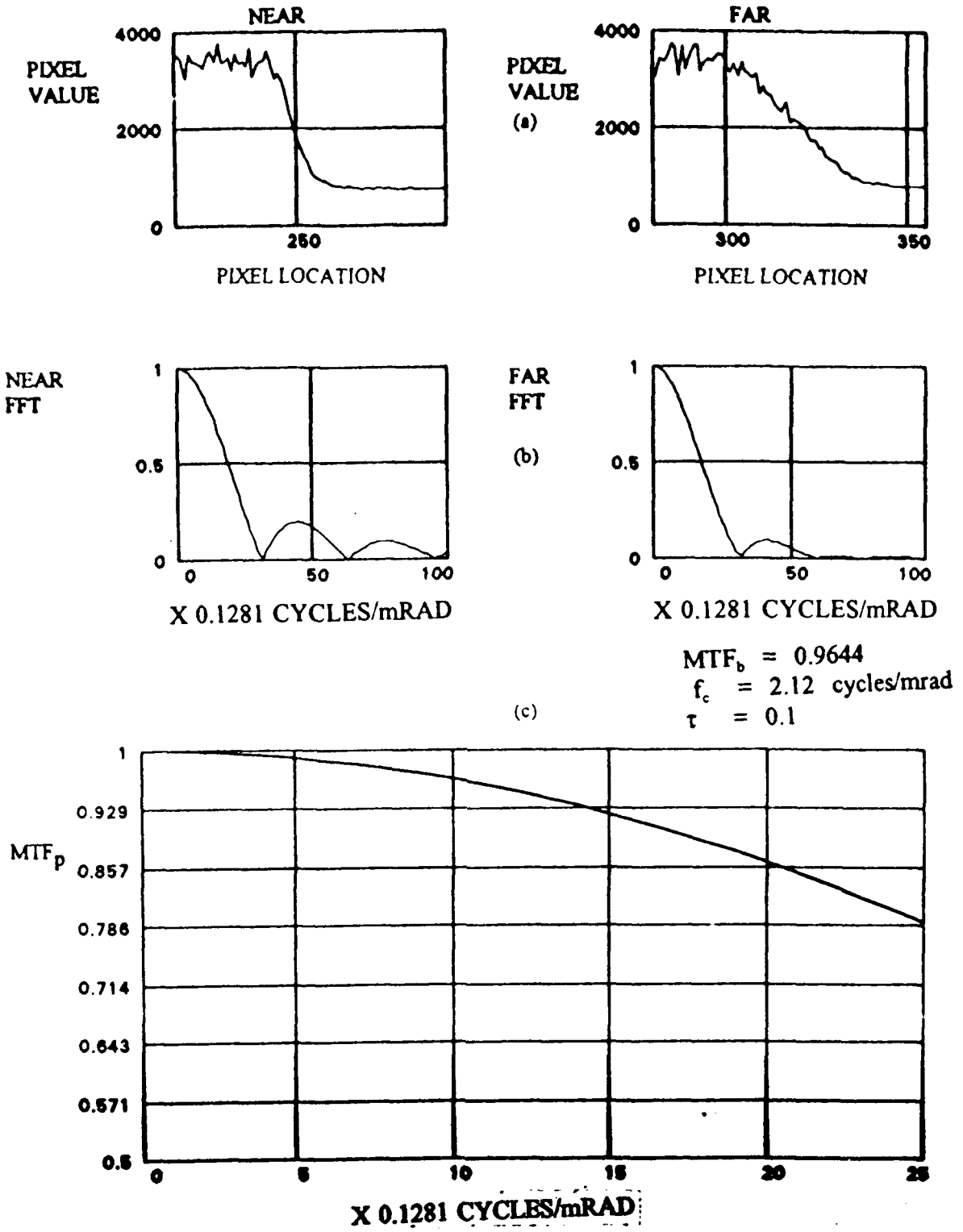

Figure 49. Data from 9:30 AM of October 31, 1992: (a) line pixel values of the black-white steps for both targets; (b) normalized, line FFTs of both targets based on the corresponding pixel values shown; (c) normalized aerosol MTF$_p$, derived from the ratio of the far target FFT to the near target FFT. Values for f_c, τ, and MTF$_b$ are included.

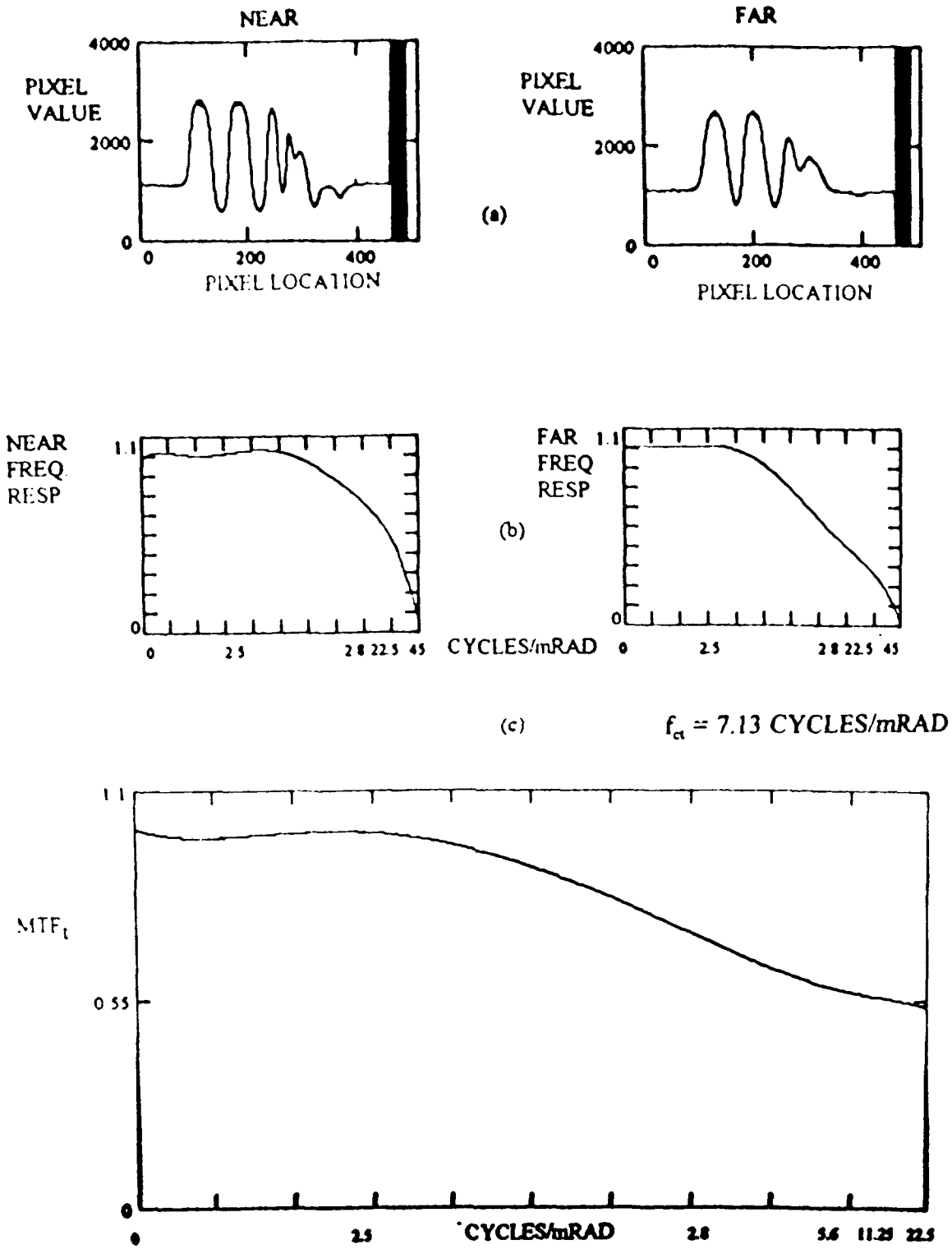

Figure 50. Data from 9:30 A.M. of October 31, 1992: (a) line pixel values of castellated black-white stripes for both targets; (b) normalized spatial frequency response of both targets based on the corresponding pixel values shown; (c) turbulence, MTF_t, derived from the ratio of the far to near target frequency response. Cutoff frequency, f_{ct}, for MTF_t is included.

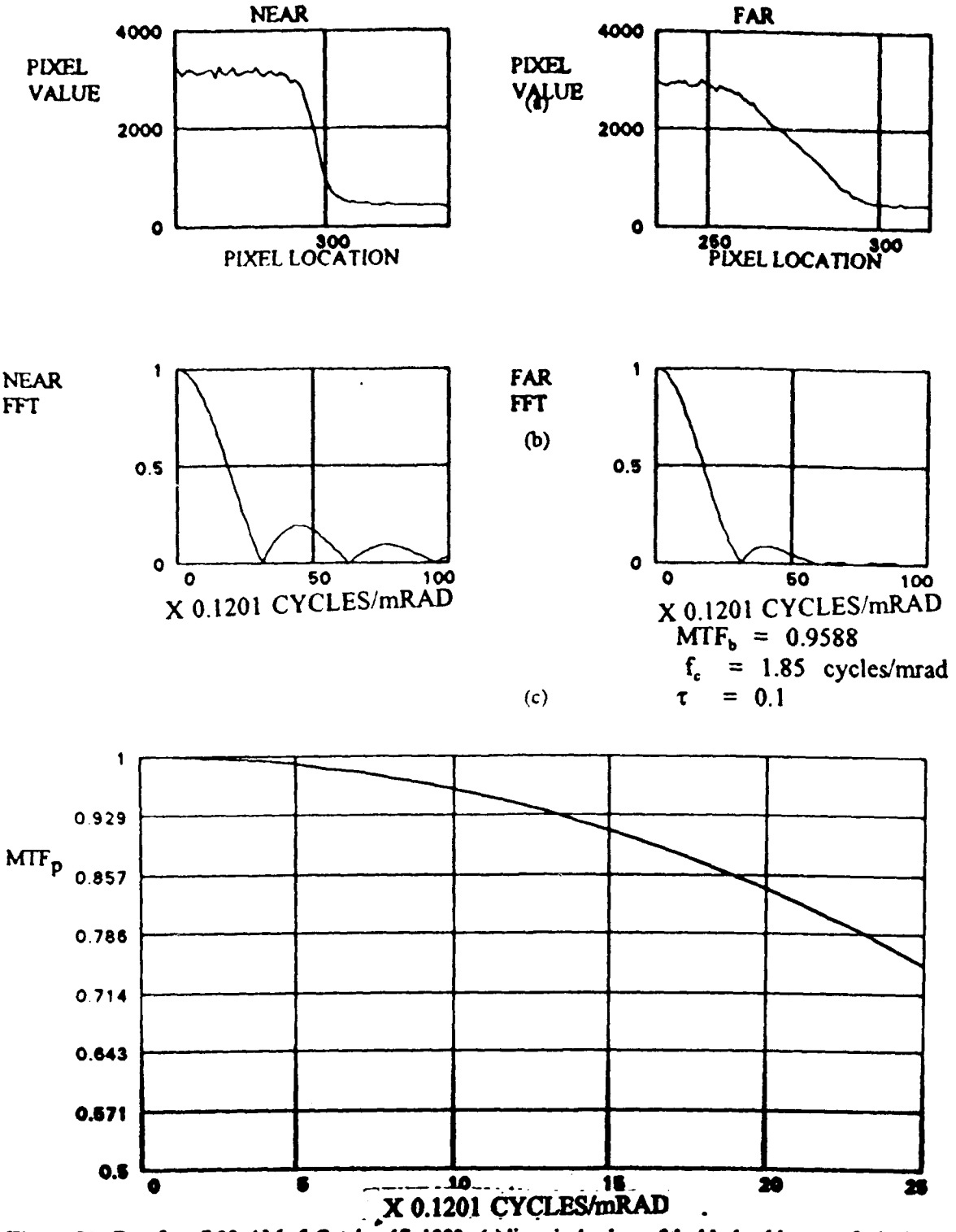

Figure 51. Data from 7:00 AM of October 17, 1992: (a) line pixel values of the black-white steps for both targets; (b) normalized, line FFTs of both targets based on the corresponding pixel values shown; (c) normalized aerosol MTF_p, derived from the ratio of the far target FFT to the near target FFT. Values for f_c, τ, and MTF_b are included.

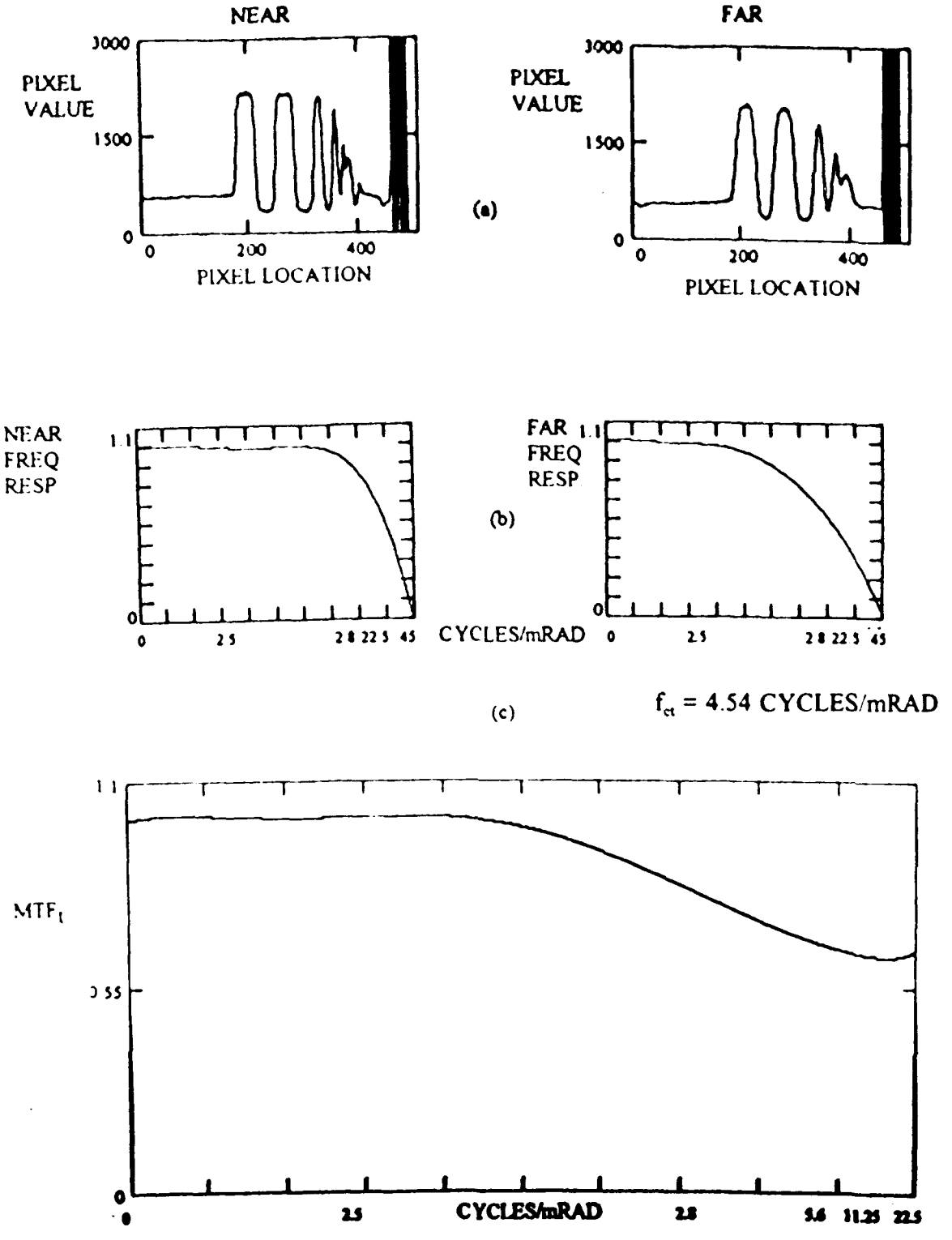

Figure 52. Data from 7:00 A.M. of October 17, 1992: (a) line pixel values of castellated black-white stripes for both targets; (b) normalized spatial frequency response of both targets based on the corresponding pixel values shown; (c) turbulence, MTF_t, derived from the ratio of the far to near target frequency response. Cutoff frequency, f_{ct}, for MTF_t is included.

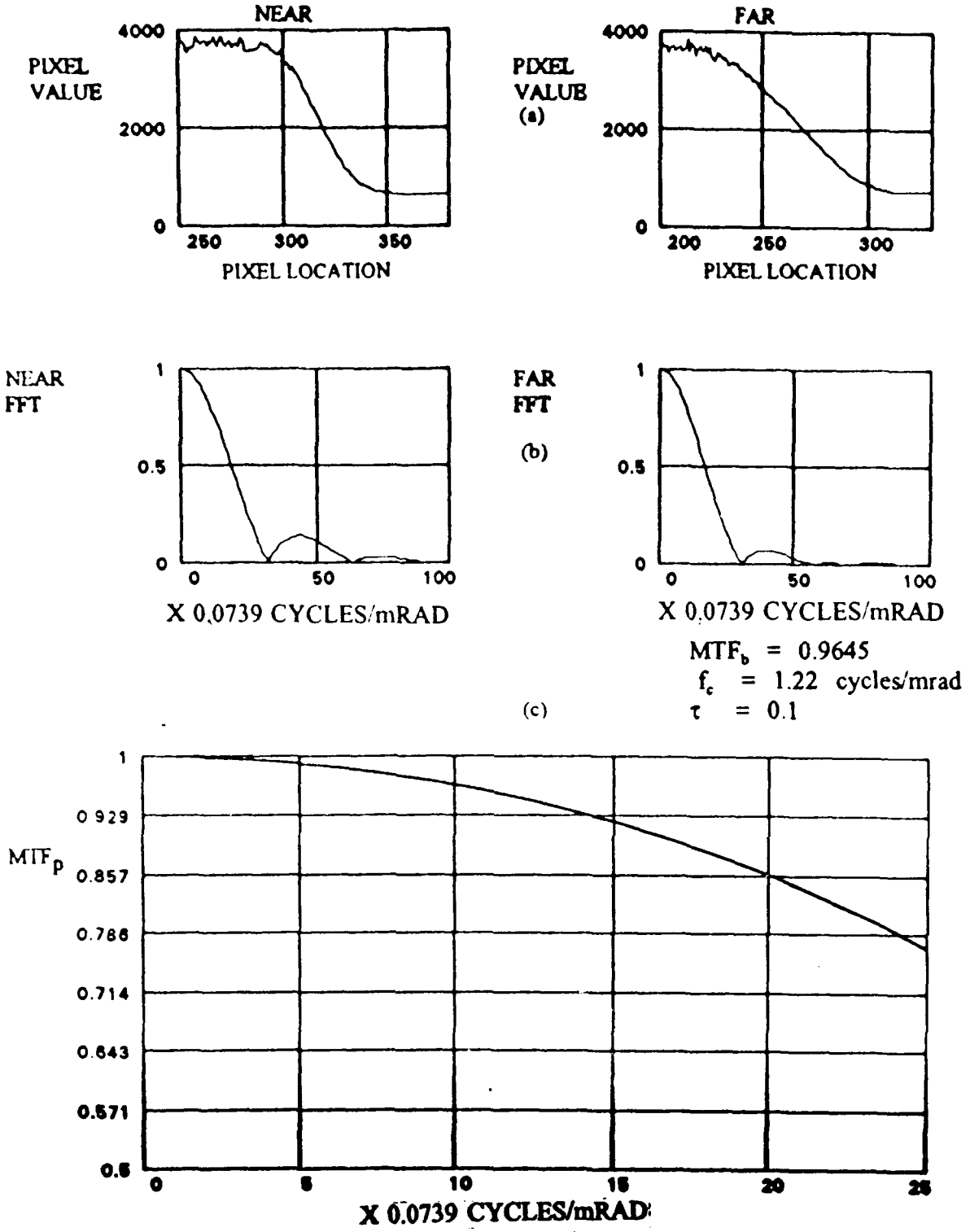

Figure 53. Data from 9:00 AM of October 17, 1992: (a) line pixel values of the black-white steps for both targets; (b) normalized, line FFTs of both targets based on the corresponding pixel values shown; (c) normalized aerosol MTF_p, derived from the ratio of the far target FFT to the near target FFT. Values for f_c, τ, and MTF_b are included.

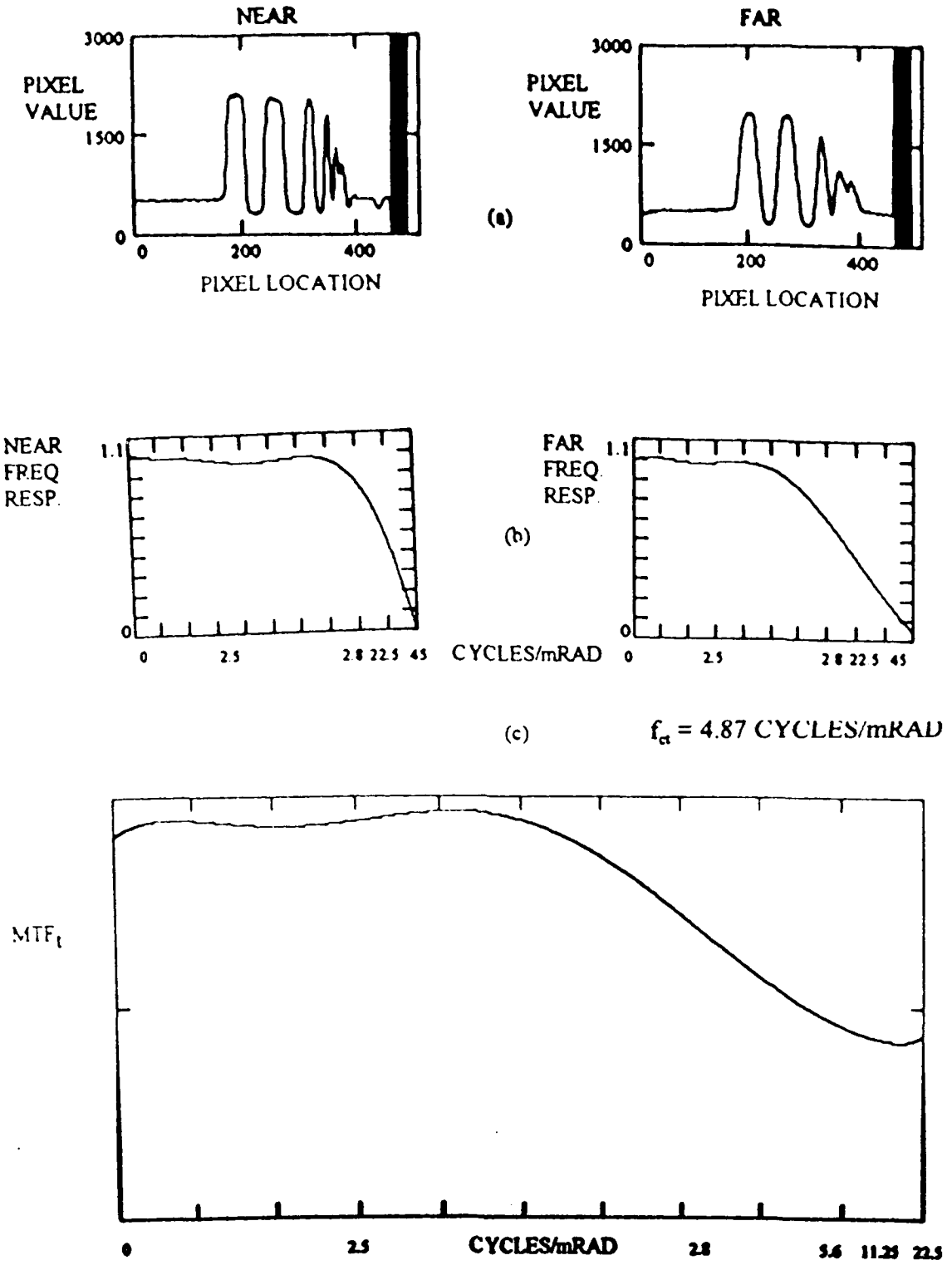

Figure 54. Data from 9:00 A.M. of October 17, 1992: (a) line pixel values of castellated black-white stripes for both targets; (b) normalized spatial frequency response of both targets based on the corresponding pixel values shown; (c) turbulence, MTF_t, derived from the ratio of the far to near target frequency response. Cutoff frequency, f_{ct}, for MTF_t is included.

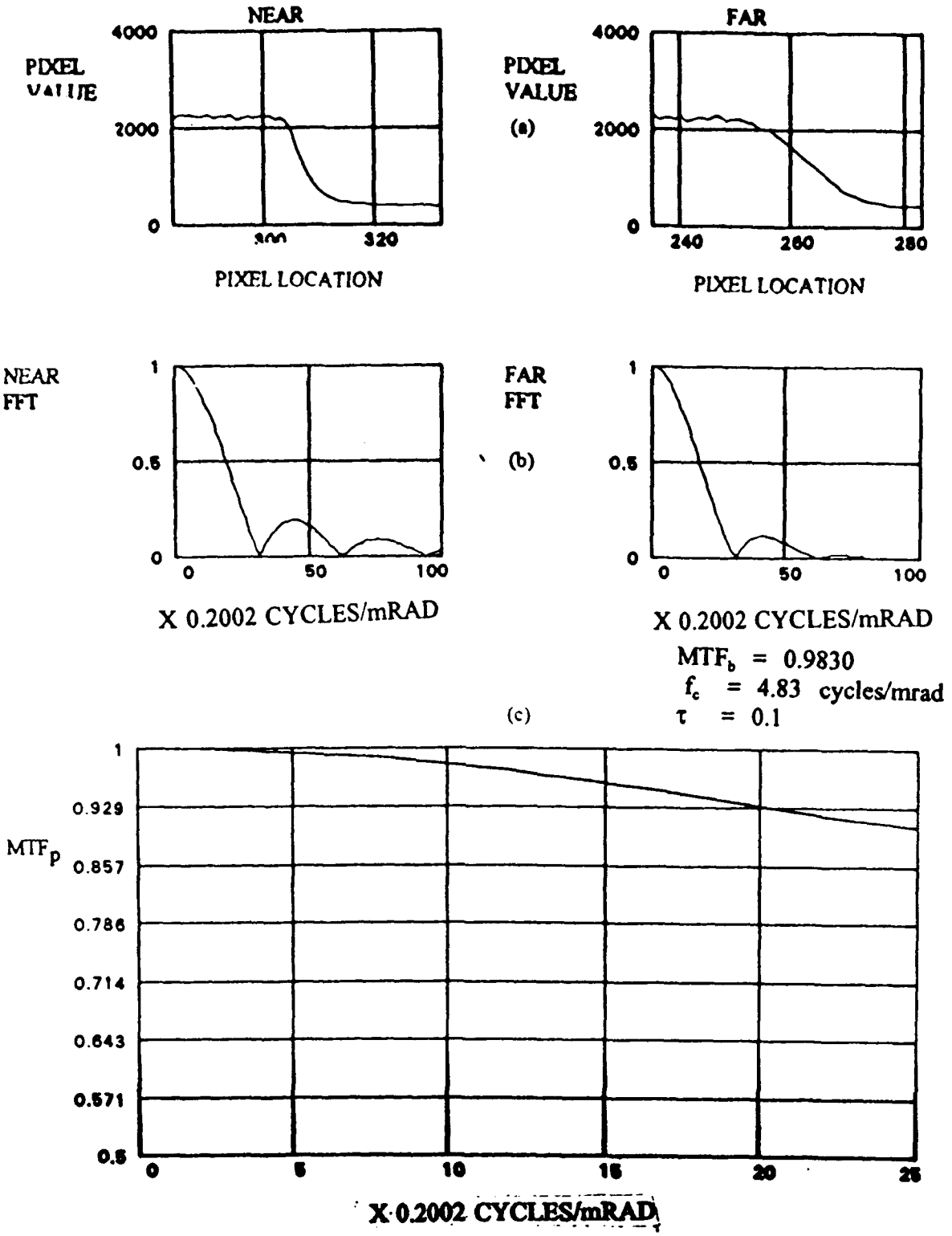

Figure 55. Data from 7:00 AM of September 5, 1992: (a) line pixel values of the black-white steps for both targets; (b) normalized, line FFTs of both targets based on the corresponding pixel values shown; (c) normalized aerosol MTF_p, derived from the ratio of the far target FFT to the near target FFT. Values for f_c, τ, and MTF_b are included.

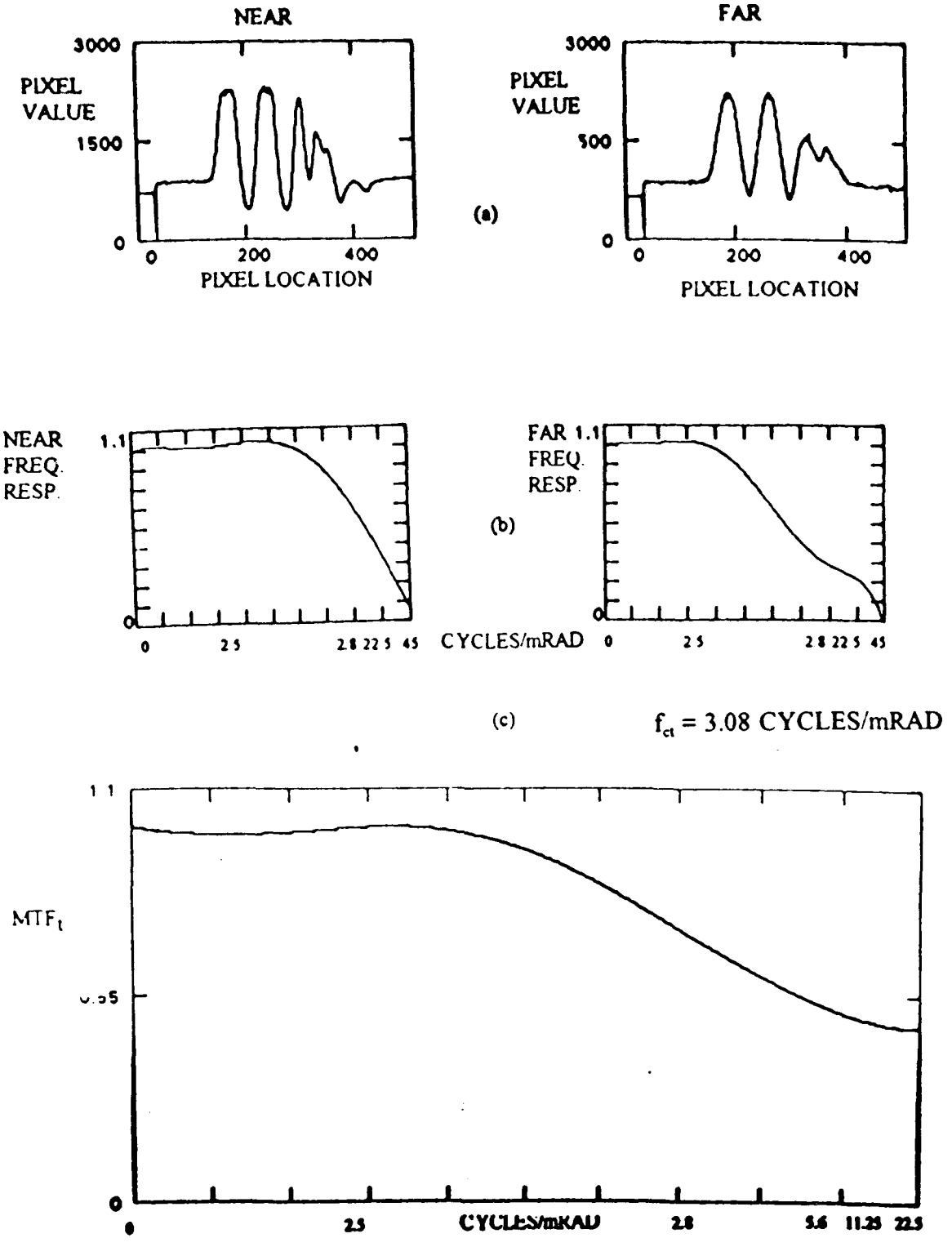

Figure 56. Data from 7:00 A.M. of September 5, 1992: (a) line pixel values of castellated black-white stripes for both targets; (b) normalized spatial frequency response of both targets based on the corresponding pixel values shown; (c) turbulence, MTF_t, derived from the ratio of the far to near target frequency response. Cutoff frequency, f_{ct}, for MTF_t is included.

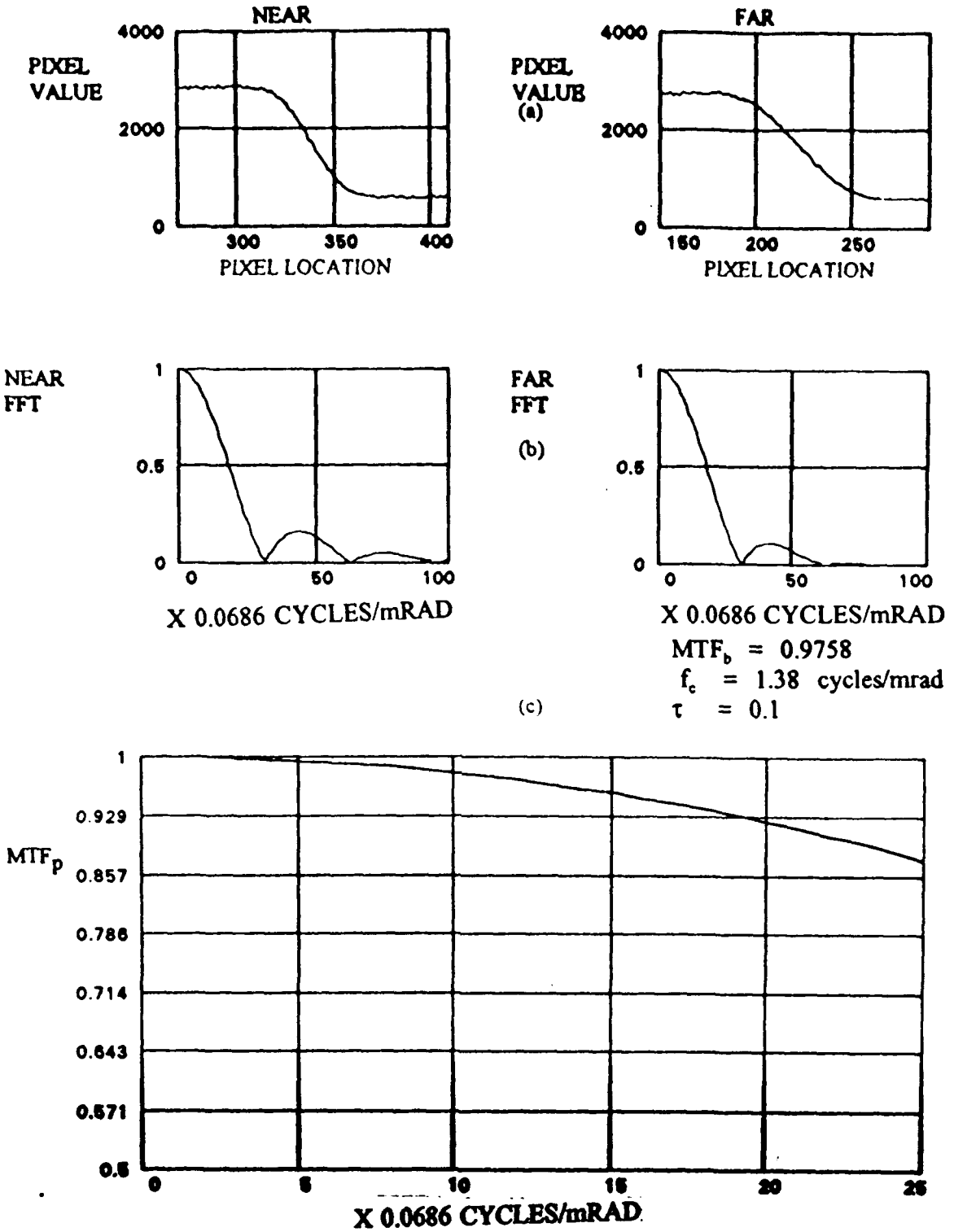

Figure 57. Data from 9:30 AM of Septemer 5, 1992: (a) line pixel values of the black-white steps for both targets; (b) normalized, line FFTs of both targets based on the corresponding pixel values shown; (c) normalized aerosol MTF_p, derived from the ratio of the far target FFT to the near target FFT. Values for f_c, τ, and MTF_b are included.

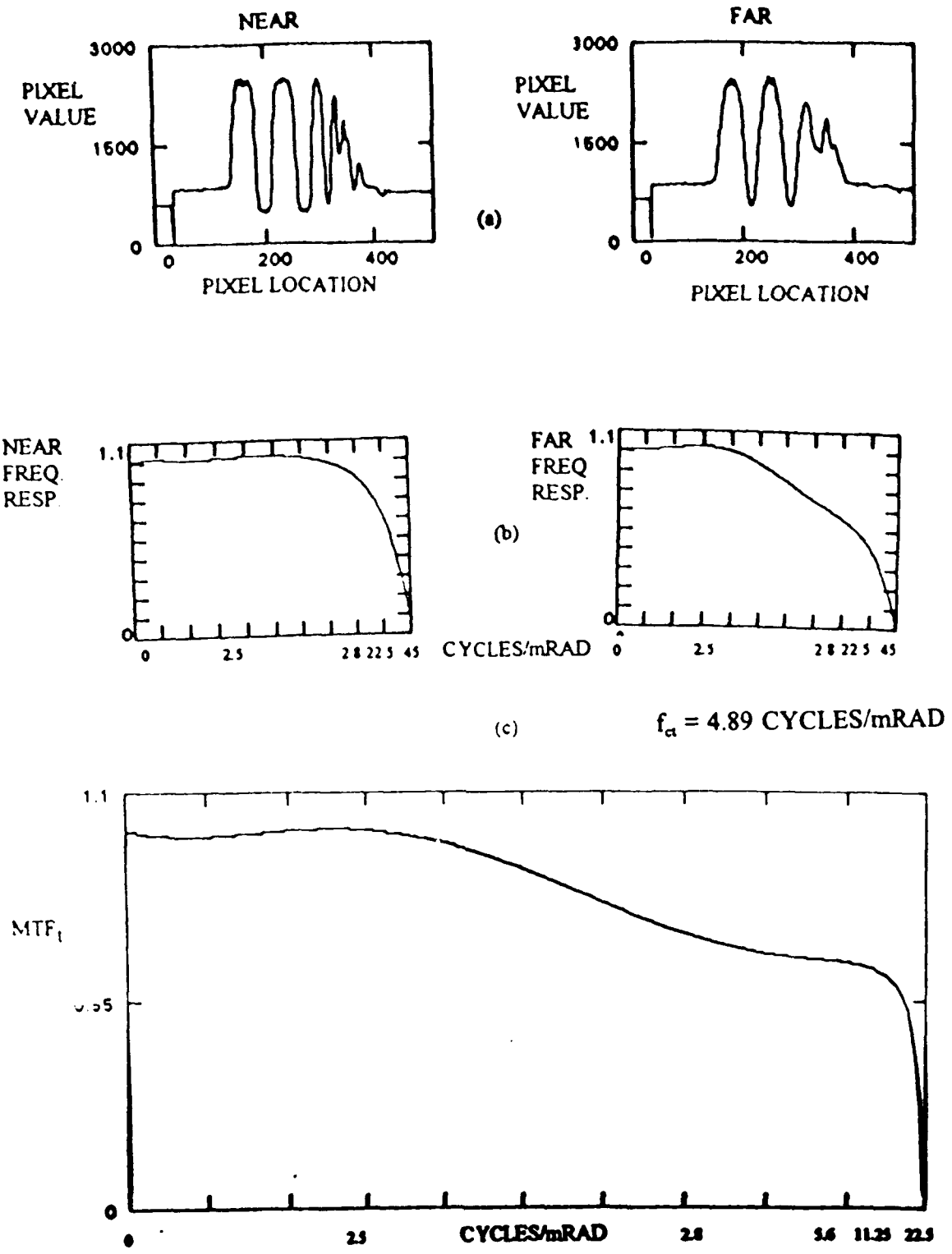

Figure 58. Data from 9:20 A.M. of September 5, 1992: (a) line pixel values of castellated black-white stripes for both targets; (b) normalized spatial frequency response of both targets based on the corresponding pixel values shown; (c) turbulence, MTF_t, derived from the ratio of the far to near target frequency response. Cutoff frequency, f_{ct}, for MTF_t is included.

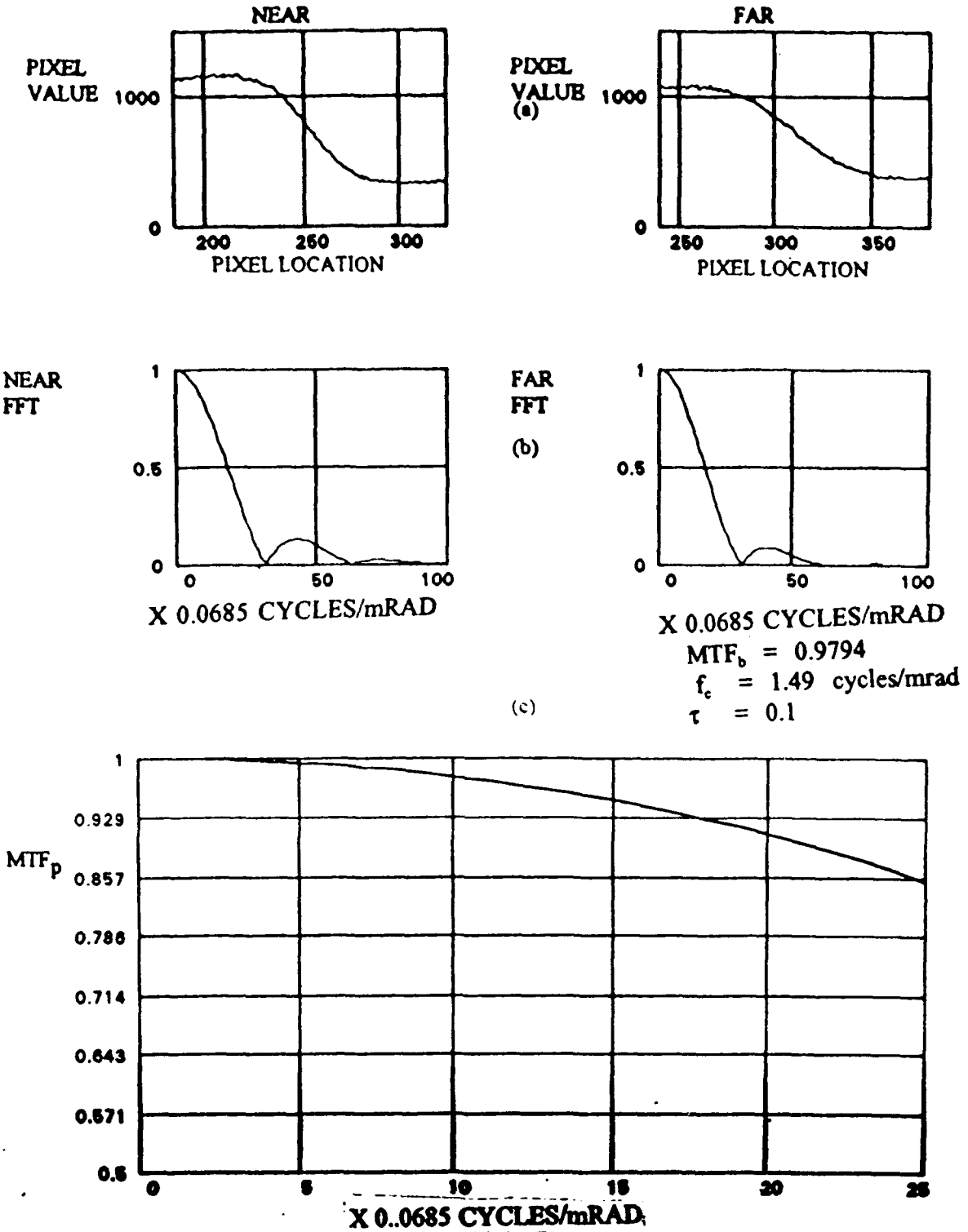

Figure 59. Data from 2:00 PM of September 5, 1992: (a) line pixel values of the black-white steps for both targets; (b) normalized, line FFTs of both targets based on the corresponding pixel values shown; (c) normalized aerosol MTF_p, derived from the ratio of the far target FFT to the near target FFT. Values for f_c, τ, and MTF_b are included.

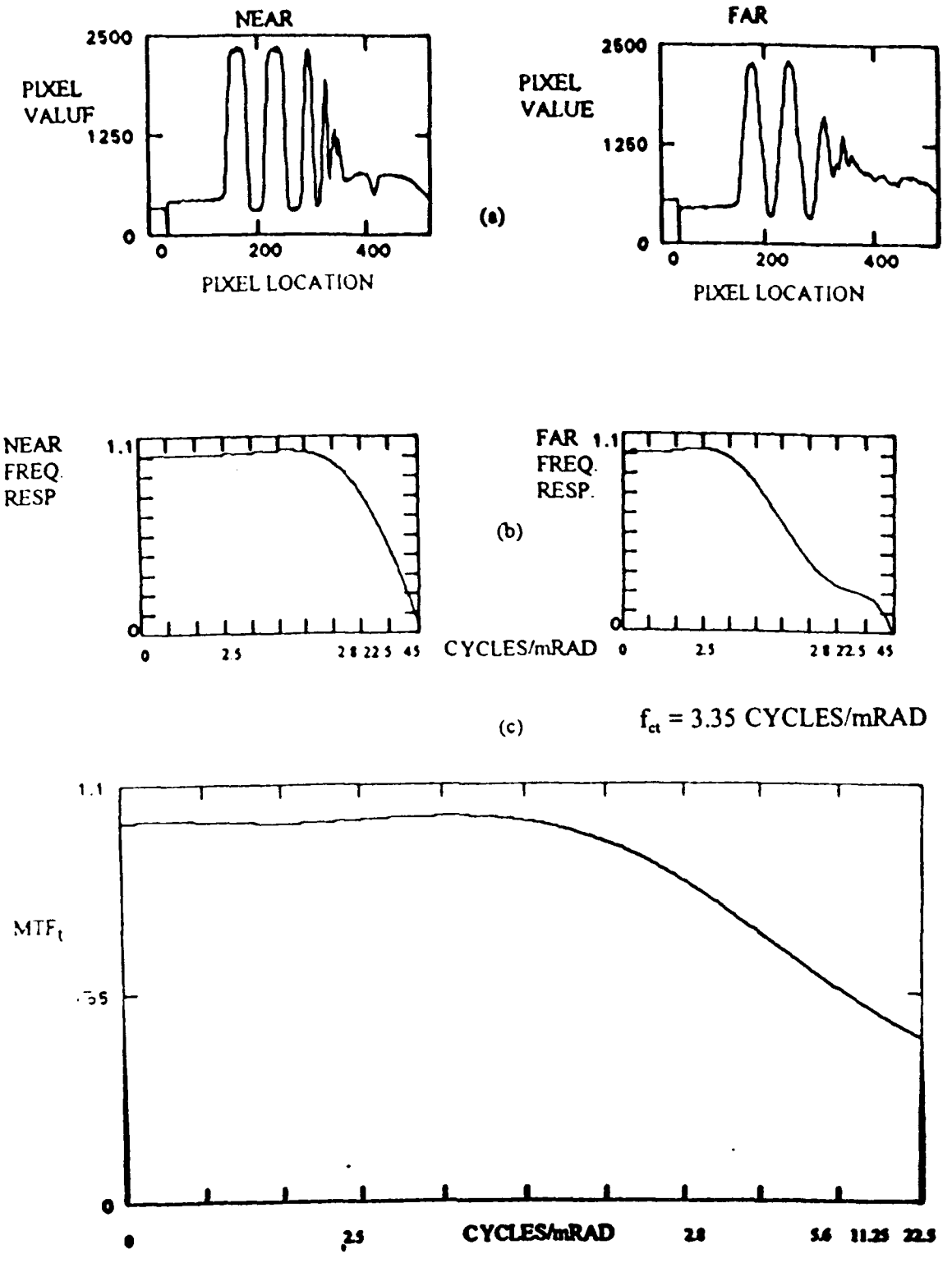

Figure 60. Data from 11:00 A.M. of September 5, 1992: (a) line pixel values of castellated black-white stripes for both targets; (b) normalized spatial frequency response of both targets based on the corresponding pixel values shown; (c) turbulence, MTF_t, derived from the ratio of the far to near target frequency response. Cutoff frequency, f_{ct}, for MTF_t is included.

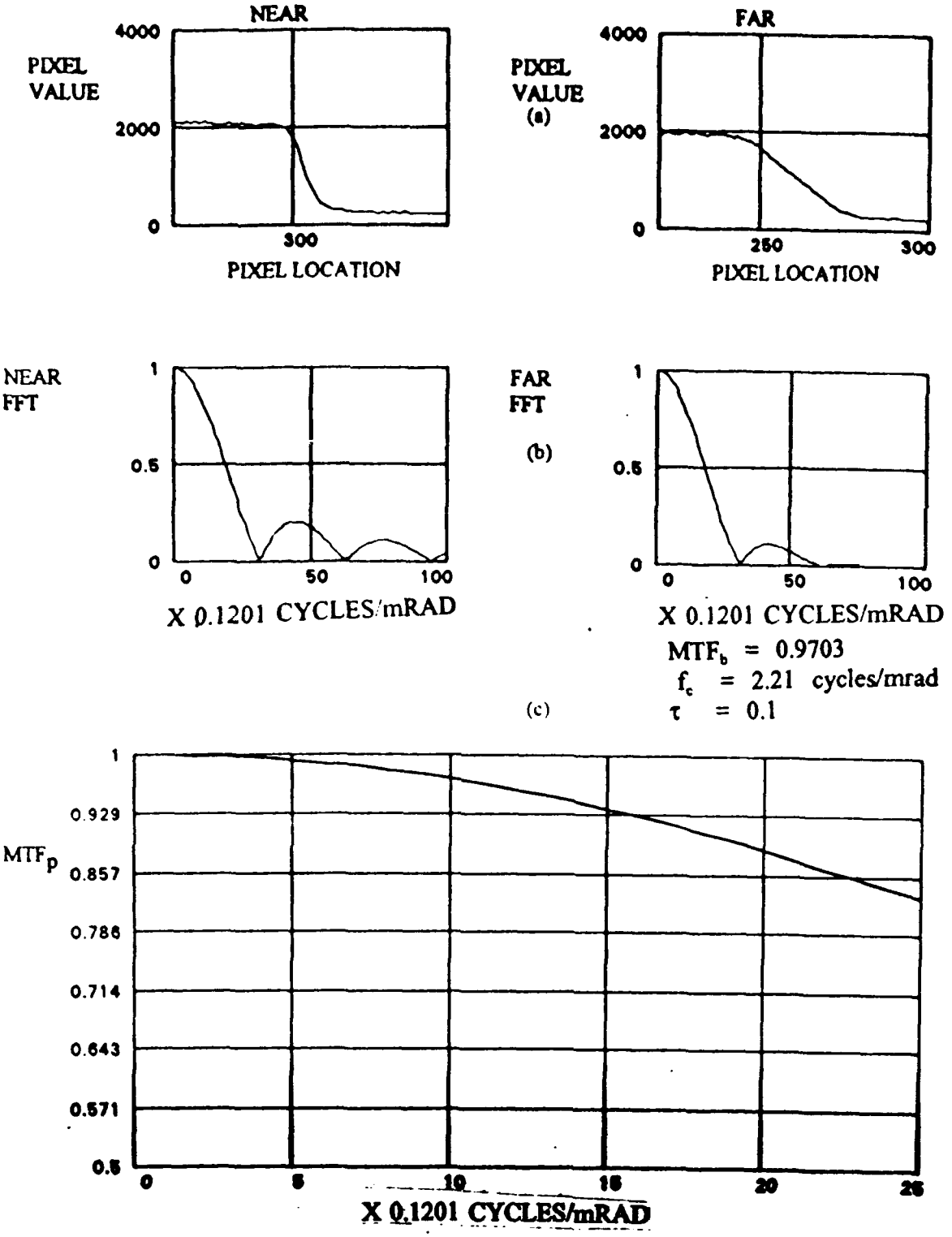

Figure 61. Data from 7:00 AM of August 26, 1992: (a) line pixel values of the black-white steps for both targets; (b) normalized, line FFTs of both targets based on the corresponding pixel values shown; (c) normalized aerosol MTF_p, derived from the ratio of the far target FFT to the near target FFT. Values for f_c, τ, and MTF_b are included.

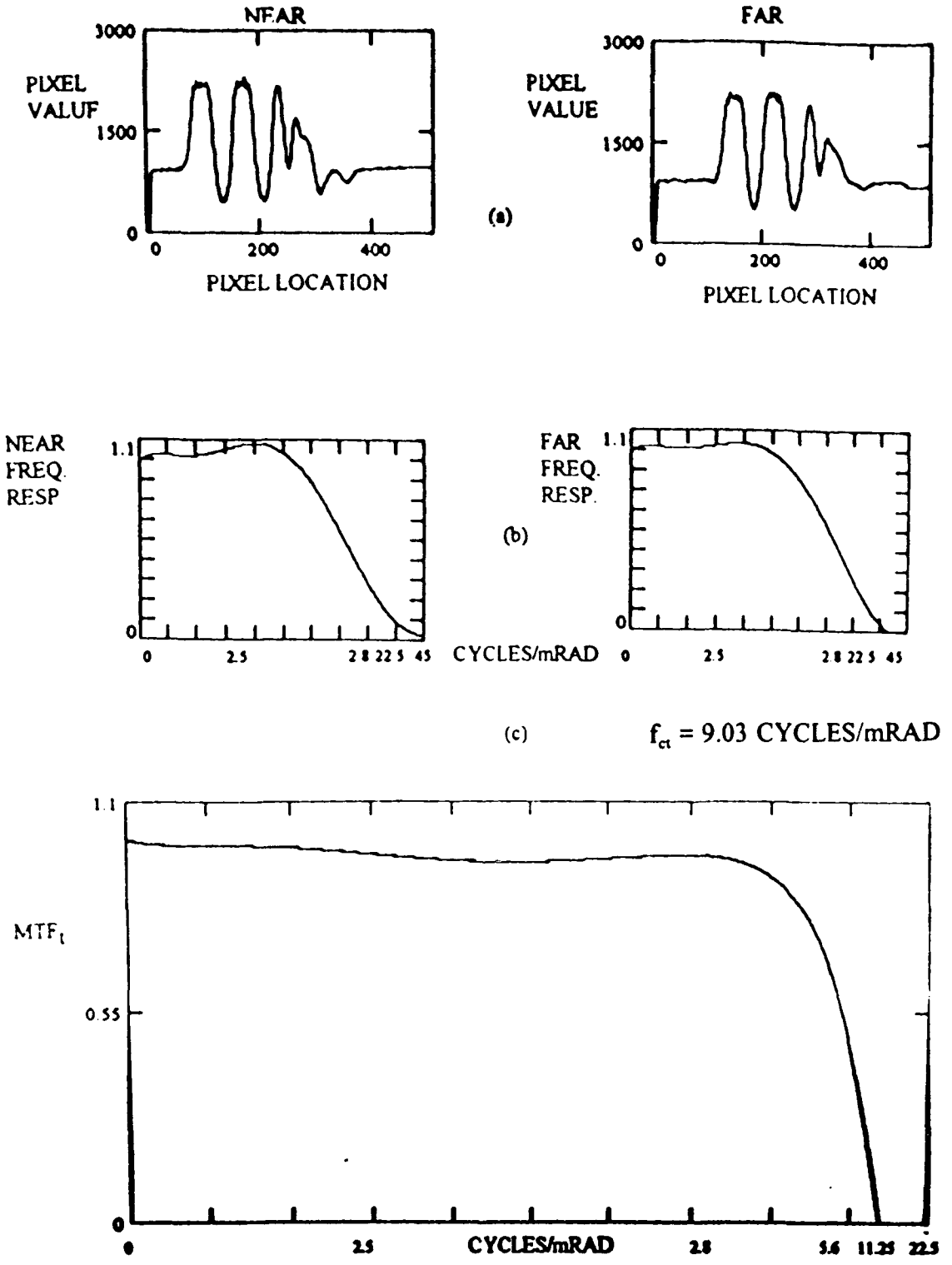

Figure 62. Data from 7:00 A.M. of August 26, 1992: (a) line pixel values of castellated black-white stripes for both targets; (b) normalized spatial frequency response of both targets based on the corresponding pixel values shown; (c) turbulence, MTF_t, derived from the ratio of the far to near target frequency response. Cutoff frequency, f_{ct}, for MTF_t is included.

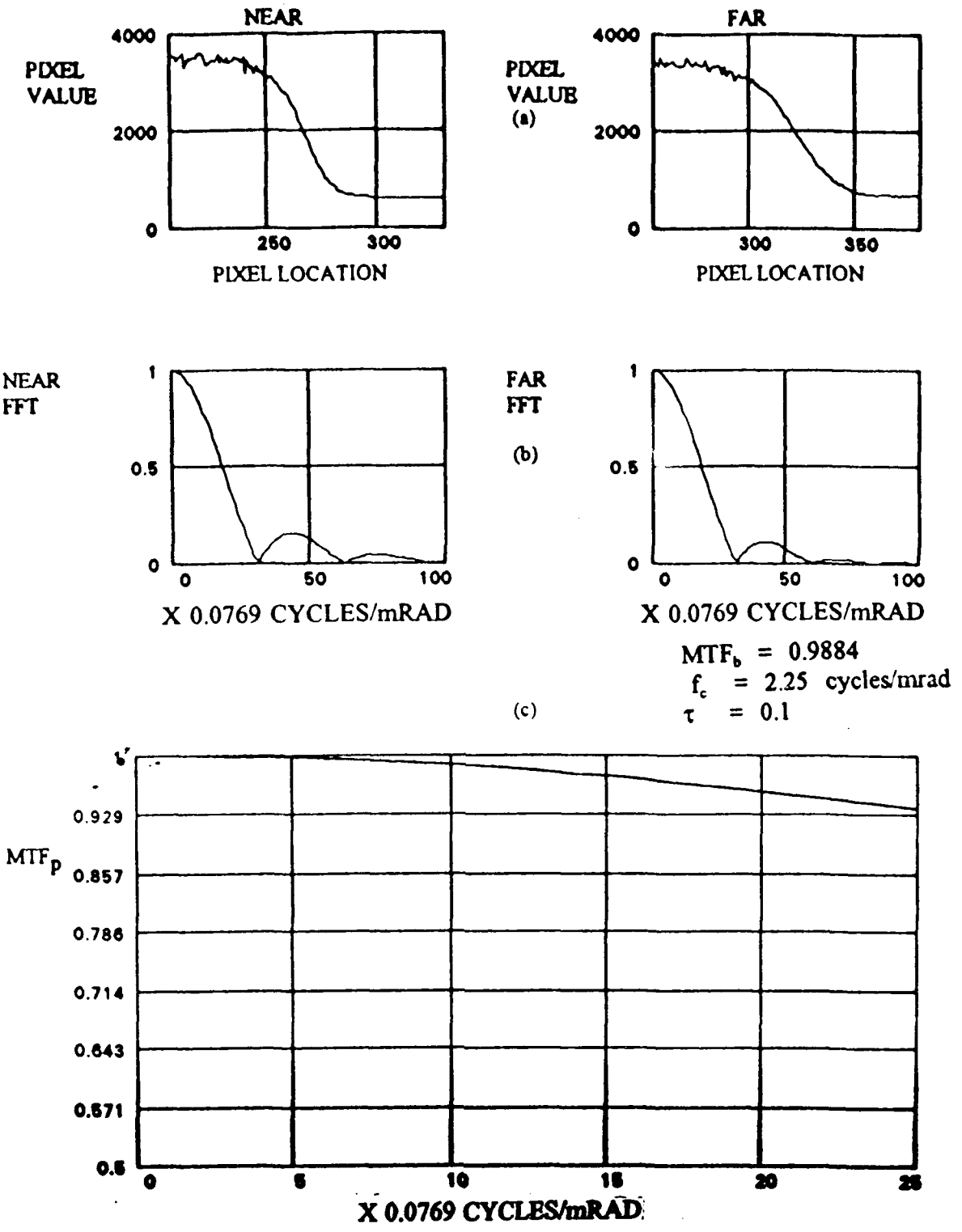

Figure 63. Data from 9:30 AM of August 26, 1992: (a) line pixel values of the black-white steps for both targets; (b) normalized, line FPTs of both targets based on the corresponding pixel values shown; (c) normalized aerosol MTF_p, derived from the ratio of the far target FFT to the near target FFT. Values for f_c, τ, and MTF_b are included.

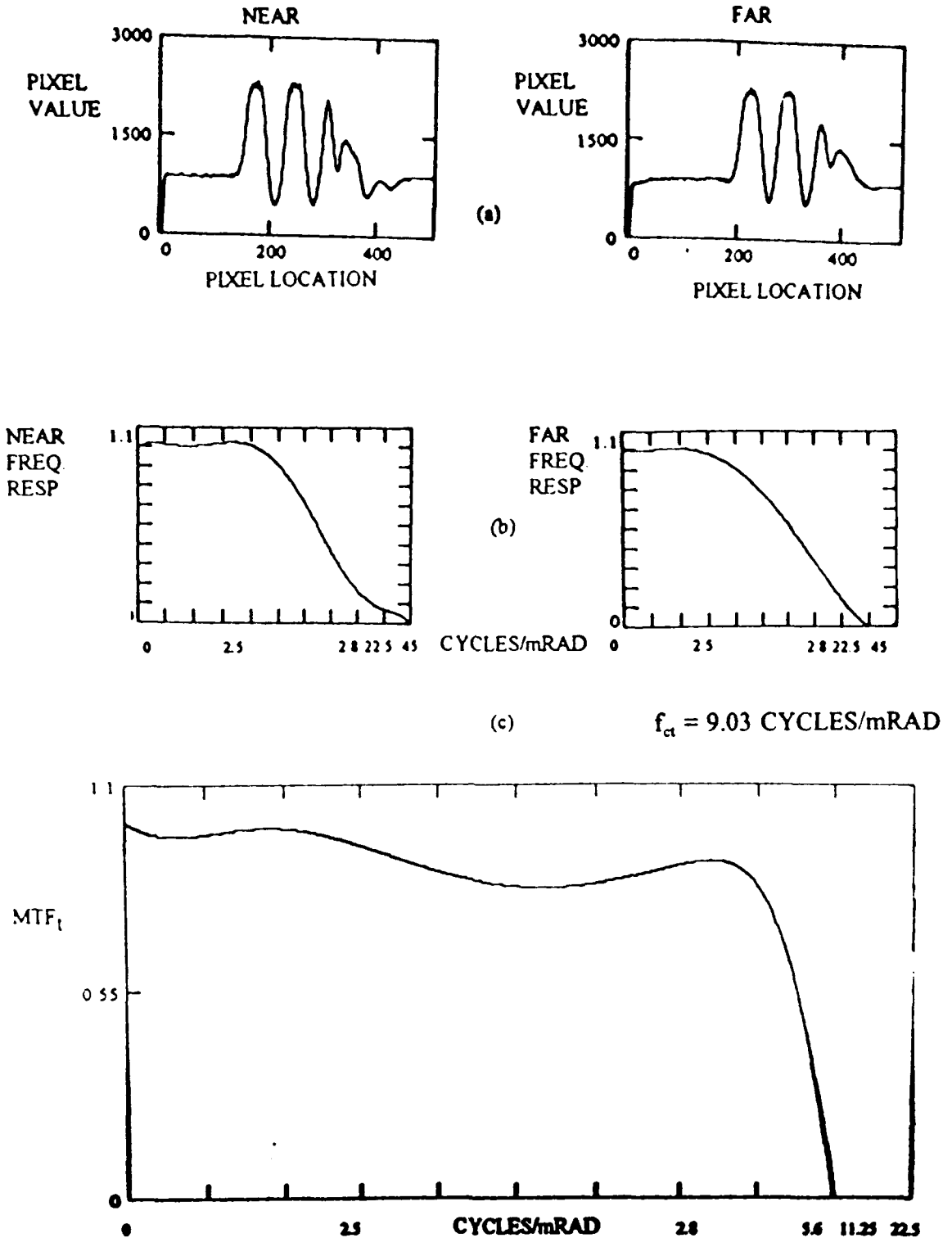

Figure 64. Data from 9:30 A.M. of August 26, 1992: (a) line pixel values of castellated black-white stripes for both targets; (b) normalized spatial frequency response of both targets based on the corresponding pixel values shown; (c) turbulence, MTF_t, derived from the ratio of the far to near target frequency response. Cutoff frequency, f_{ct}, for MTF_t is included.

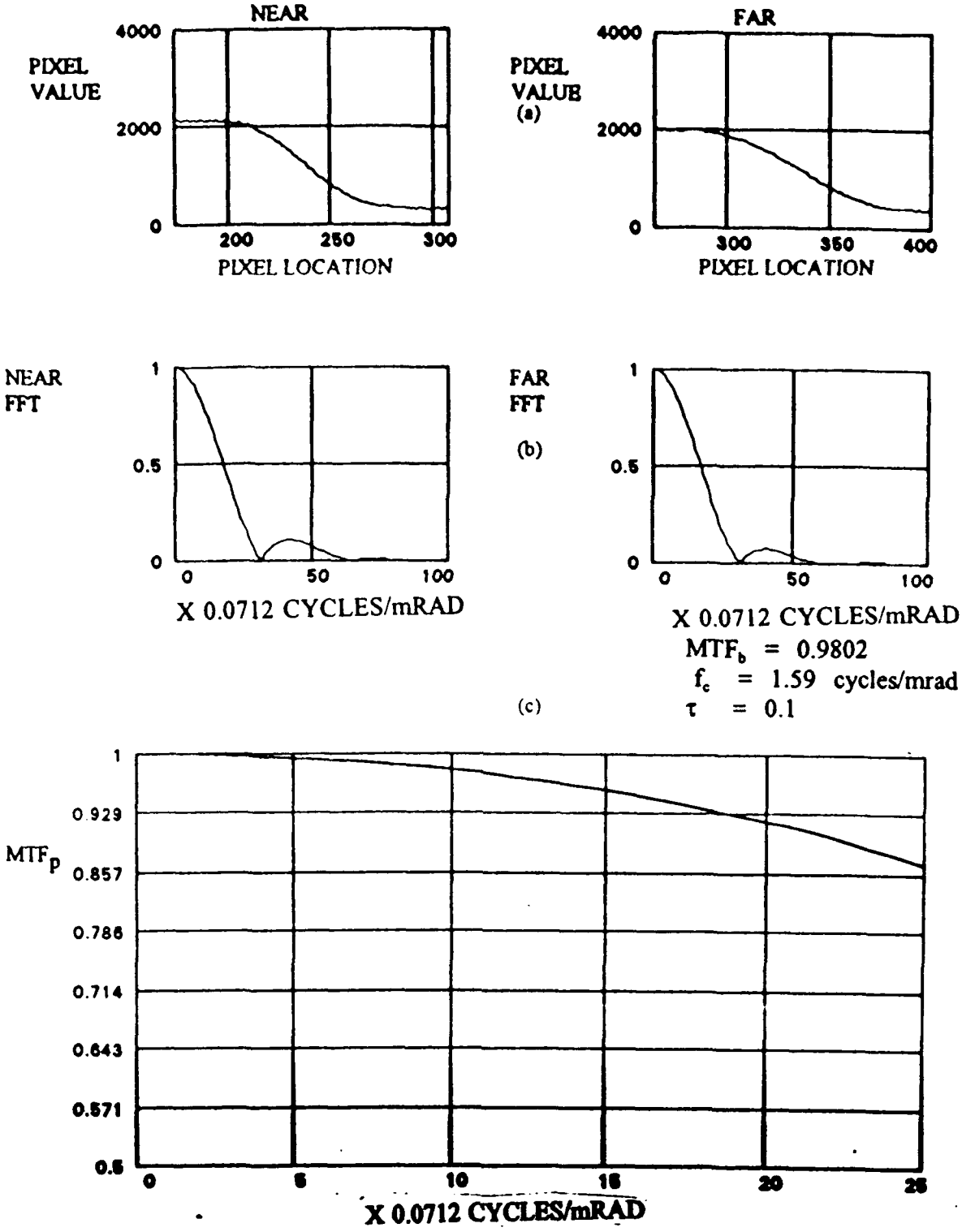

Figure 65. Data from 12:00 PM of August 26, 1992: (a) line pixel values of the black-white steps for both targets; (b) normalized, line FFTs of both targets based on the corresponding pixel values shown; (c) normalized aerosol MTF_p, derived from the ratio of the far target FFT to the near target FFT. Values for f_c, τ, and MTF_b are included.

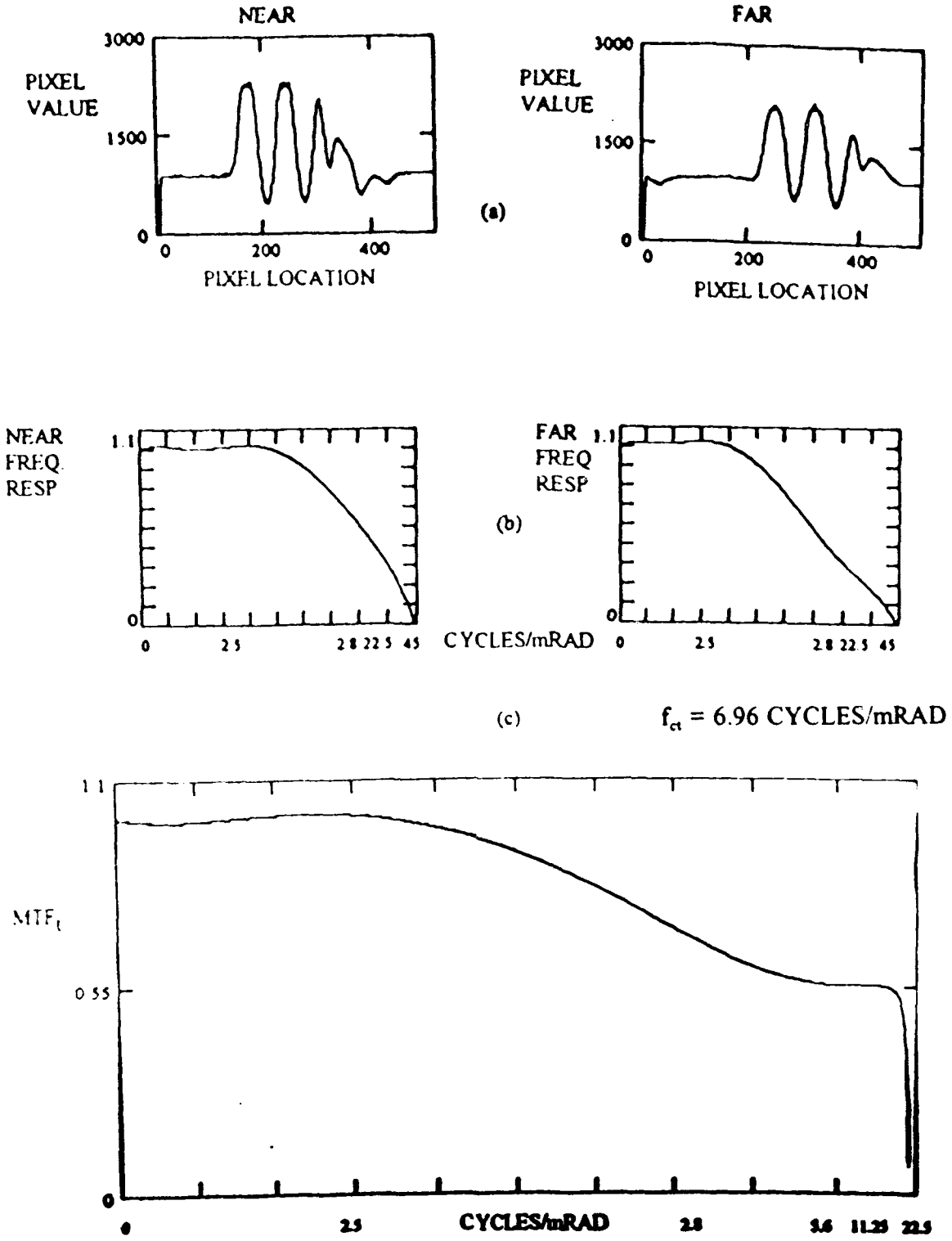

Figure 66. Data from 12:00 P.M. of August 26, 1992: (a) line pixel values of castellated black-white stripes for both targets; (b) normalized spatial frequency response of both targets based on the corresponding pixel values shown; (c) turbulence, MTF_t, derived from the ratio of the far to near target frequency response. Cutoff frequency, f_{ct}, for MTF_t is included.

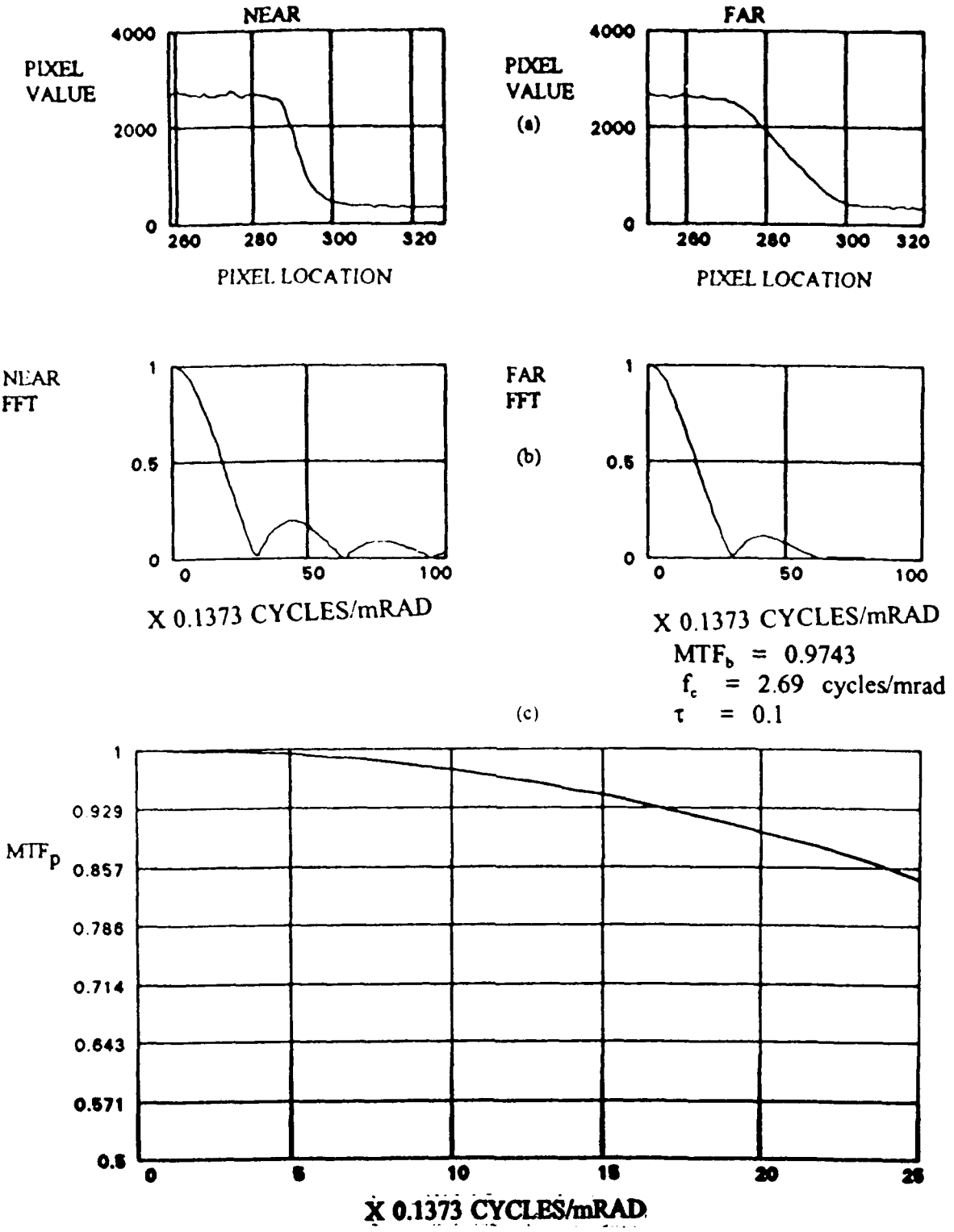

Figure 67. Data from 7:00 AM of August 25, 1992: (a) line pixel values of the black-white steps for both targets; (b) normalized, line FFTs of both targets based on the corresponding pixel values shown; (c) normalized aerosol MTF_p, derived from the ratio of the far target FFT to the near target FFT. Values for f_c, τ, and MTF_b are included.

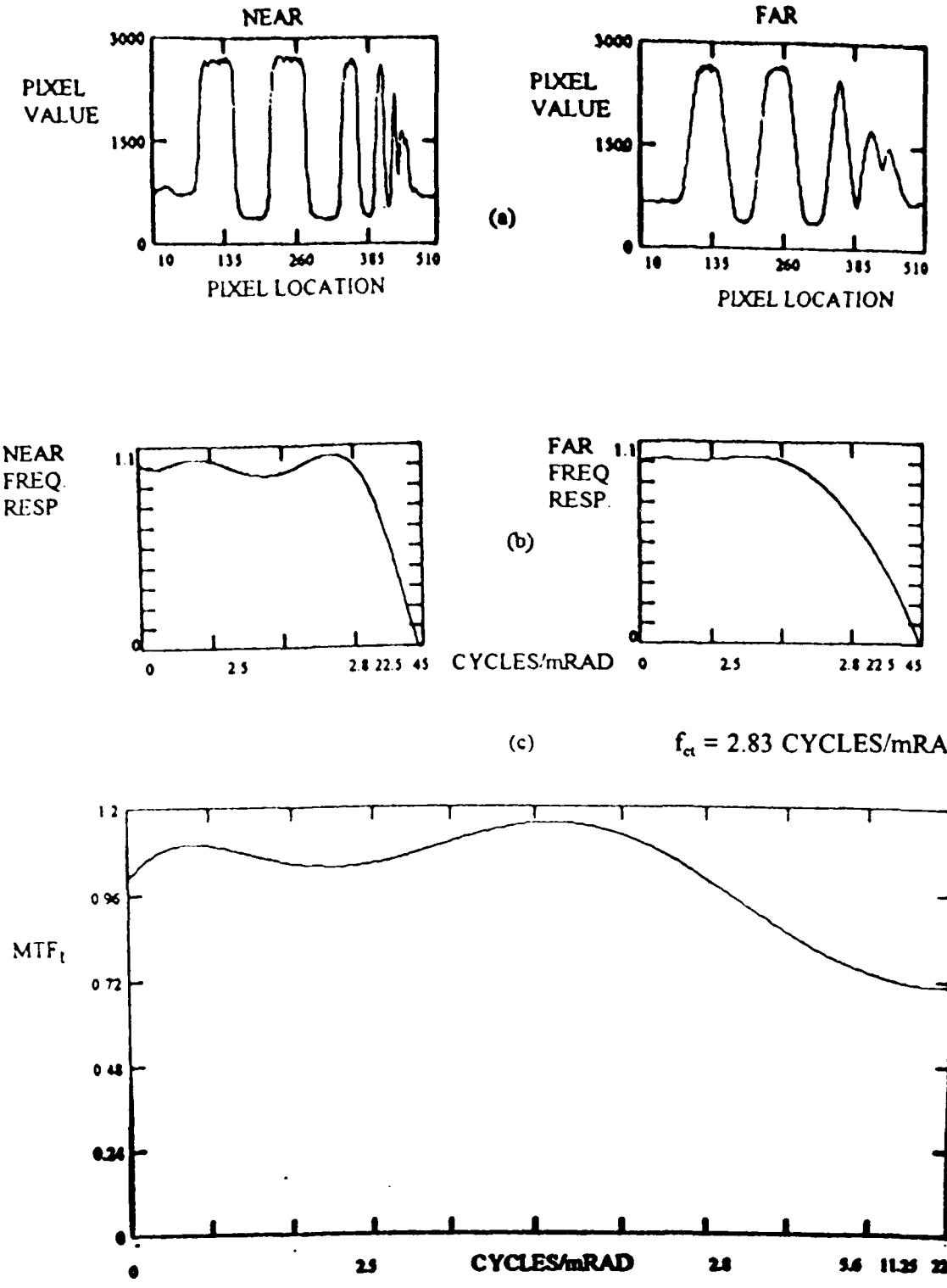

Figure 68. Data from 7:00 A.M. of August 25, 1992: (a) line pixel values of castellated black-white stripes for both targets; (b) normalized spatial frequency response of both targets based on the corresponding pixel values shown; (c) turbulence, MTF_t, derived from the ratio of the far to near target frequency response. Cutoff frequency, f_{ct}, for MTF_t is included.

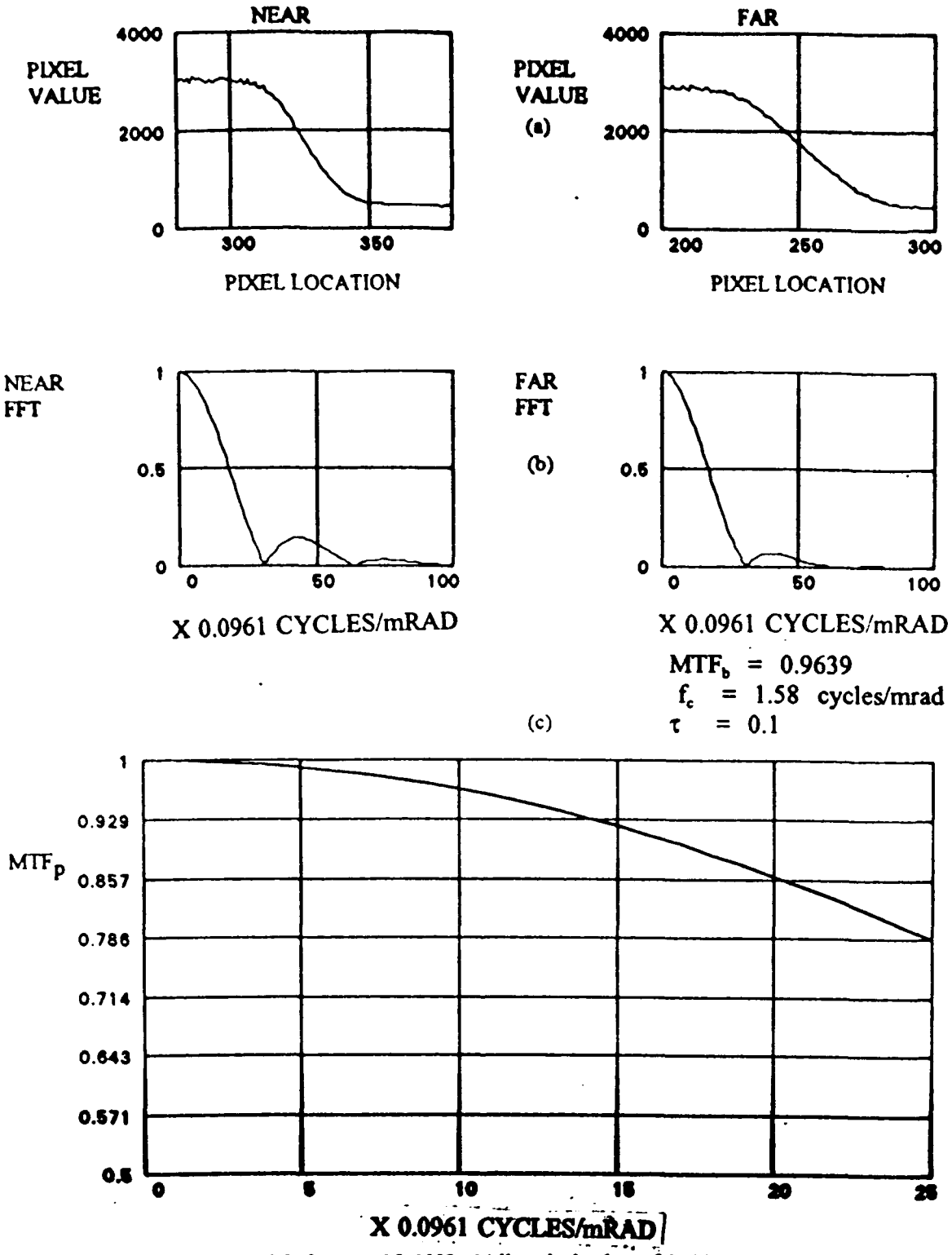

Figure 69. Data from 9:30 AM of August 25, 1992: (a) line pixel values of the black-white steps for both targets; (b) normalized, line FFTs of both targets based on the corresponding pixel values shown; (c) normalized aerosol MTF_p, derived from the ratio of the far target FFT to the near target FFT. Values for f_c, τ, and MTF_b are included.

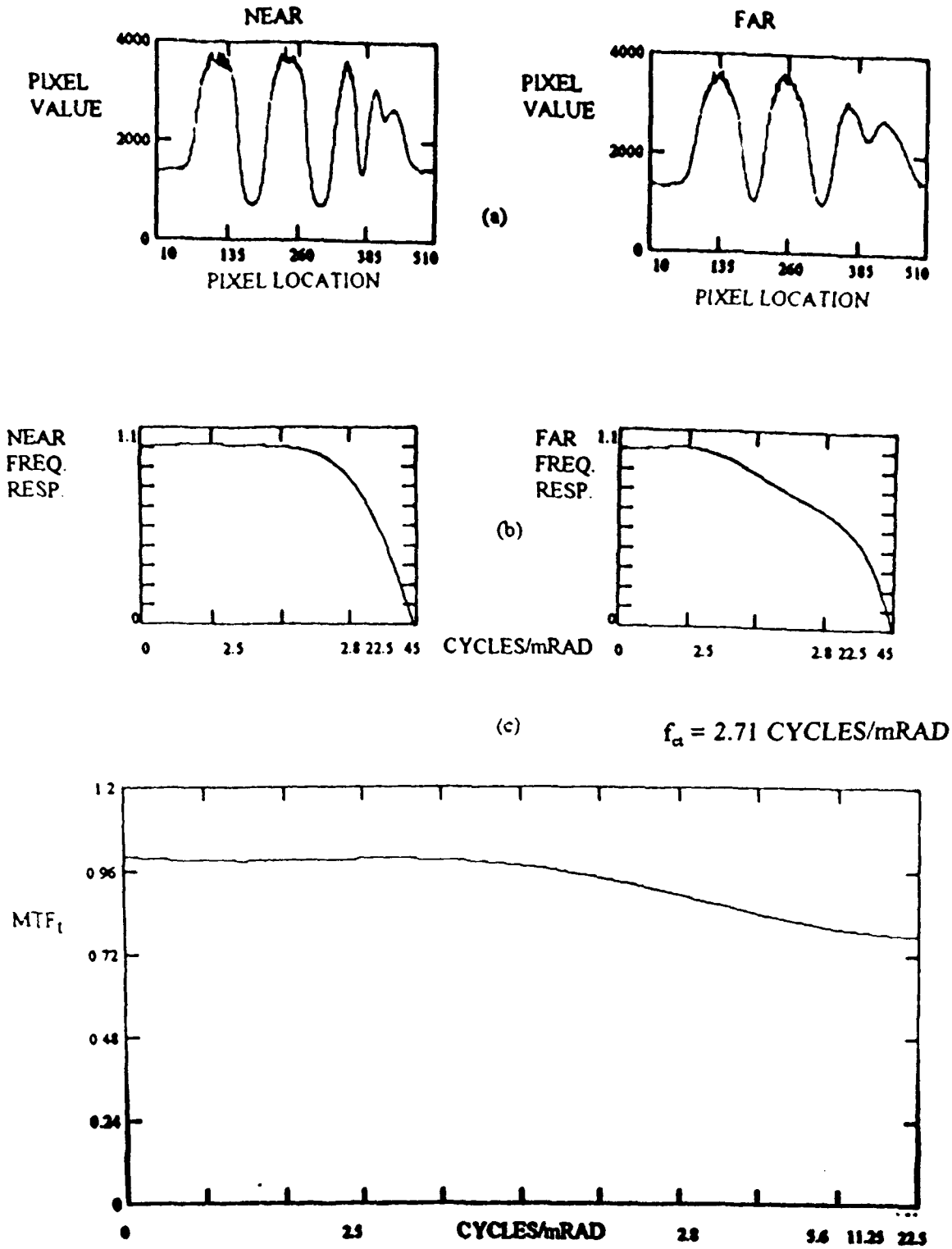

Figure 70. Data from 9:30 A.M. of August 25, 1992: (a) line pixel values of castellated black-white stripes for both targets; (b) normalized spatial frequency response of both targets based on the corresponding pixel values shown; (c) turbulence, MTF_t, derived from the ratio of the far to near target frequency response. Cutoff frequency, f_{ct}, for MTF_t is included.

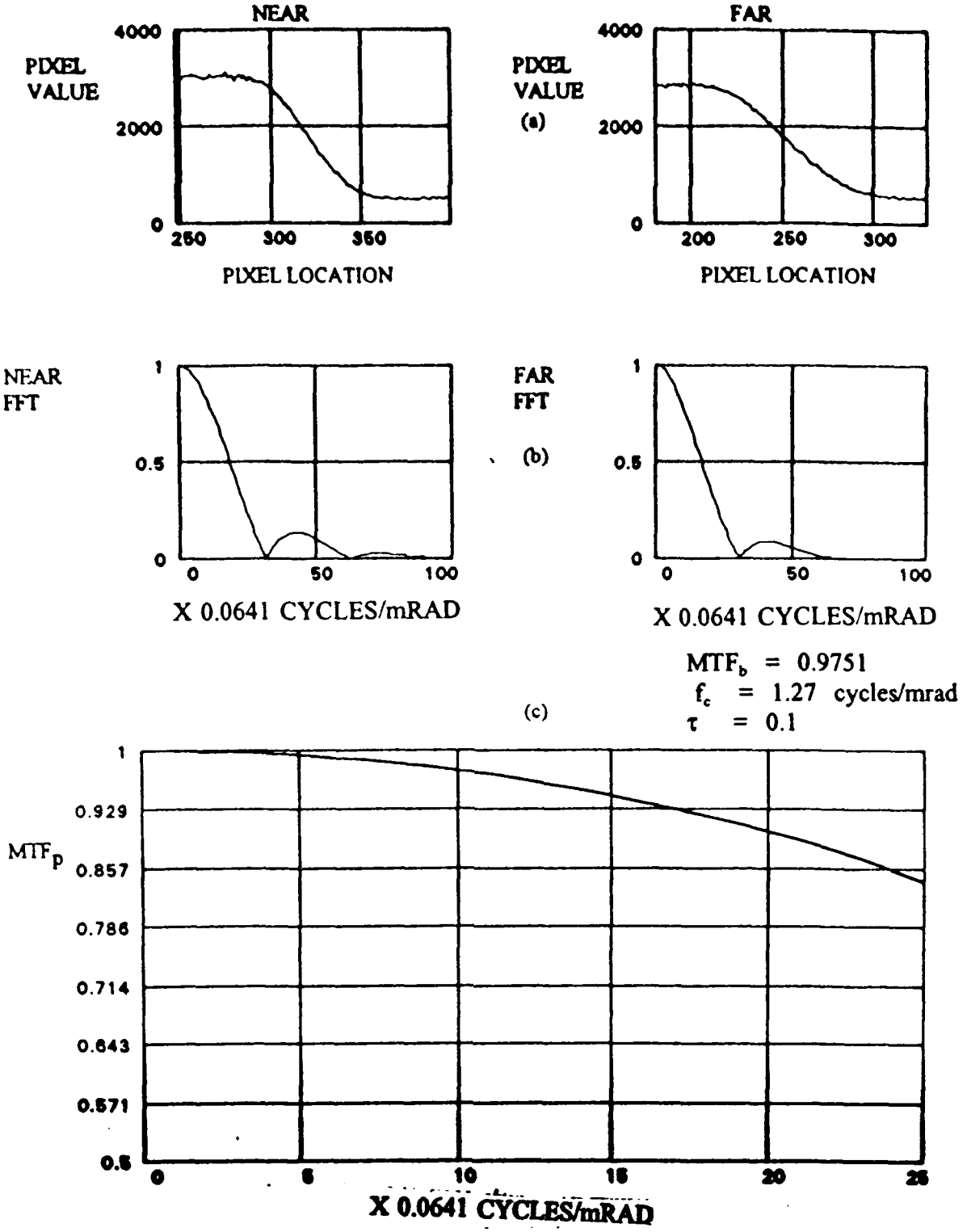

Figure 71. Data from 12:00 PM of August 25, 1992: (a) line pixel values of the black-white steps for both targets; (b) normalized, line FFTs of both targets based on the corresponding pixel values shown; (c) normalized aerosol MTF_p, derived from the ratio of the far target FFT to the near target FFT. Values for f_c, τ, and MTF_b are included.

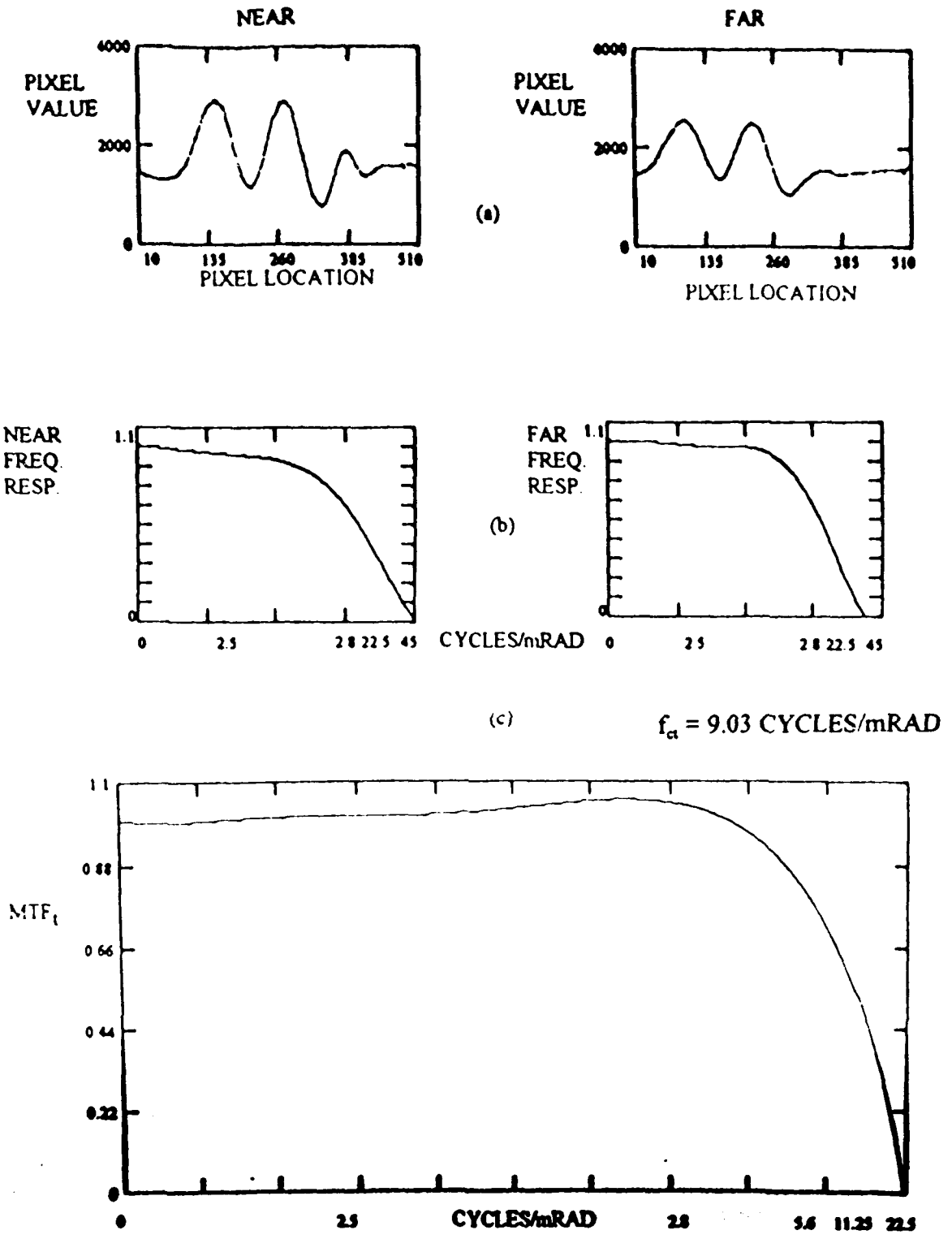

Figure 72. Data from 12:00 P.M. of August 25, 1992: (a) line pixel values of castellated black-white stripes for both targets; (b) normalized spatial frequency response of both targets based on the corresponding pixel values shown; (c) turbulence, MTF_t, derived from the ratio of the far to near target frequency response. Cutoff frequency, f_{ct}, for MTF_t is included.

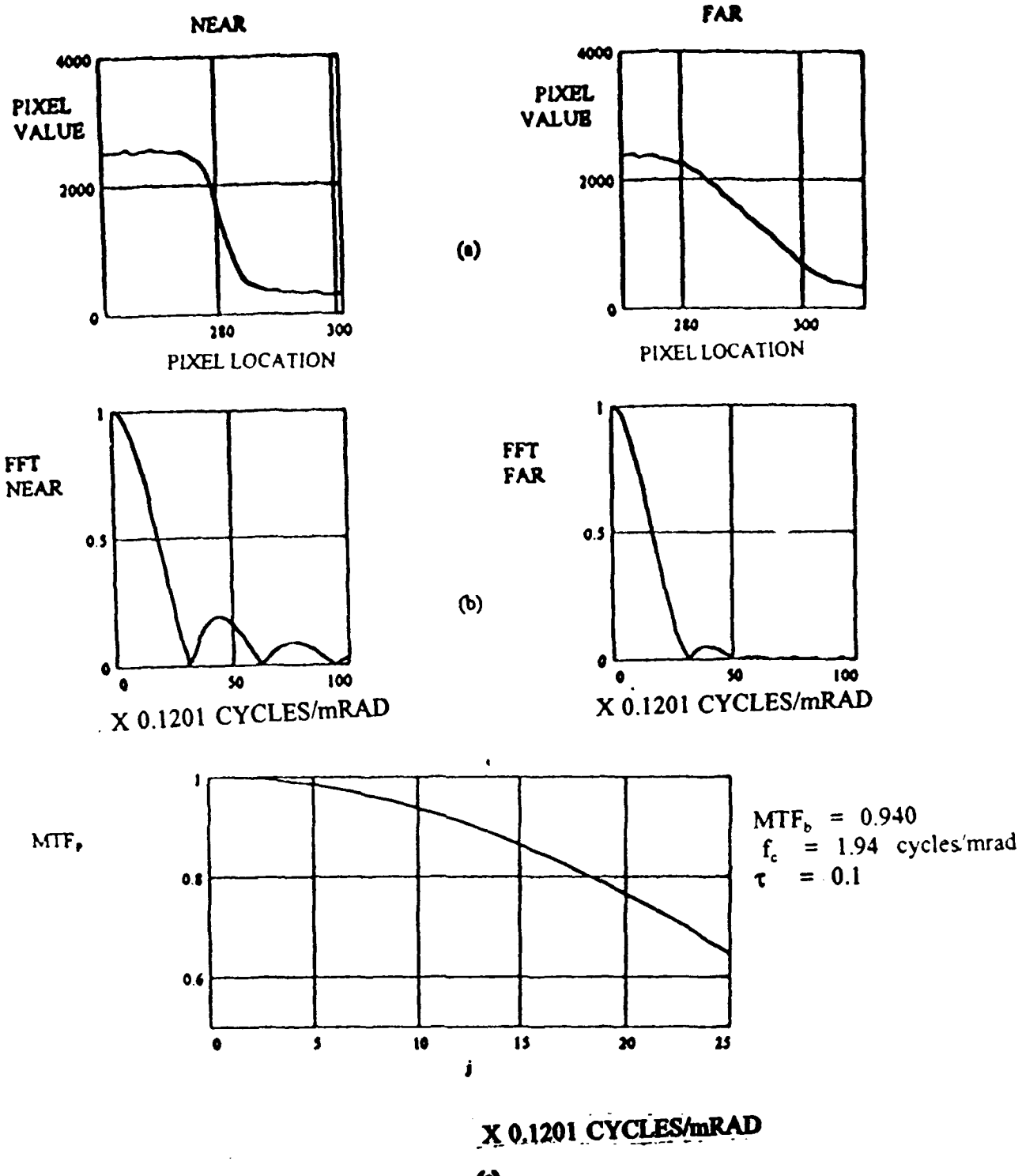

Figure 73. Data from 7:00 AM of August 21, 1992: (a) line pixel values of the black-white steps for both targets; (b) normalized, line FFTs of both targets based on the corresponding pixel values shown; (c) normalized aerosol MTF_p, derived from the ratio of the far target FFT to the near target FFT. Values for f_c, τ, and MTF_b are included.

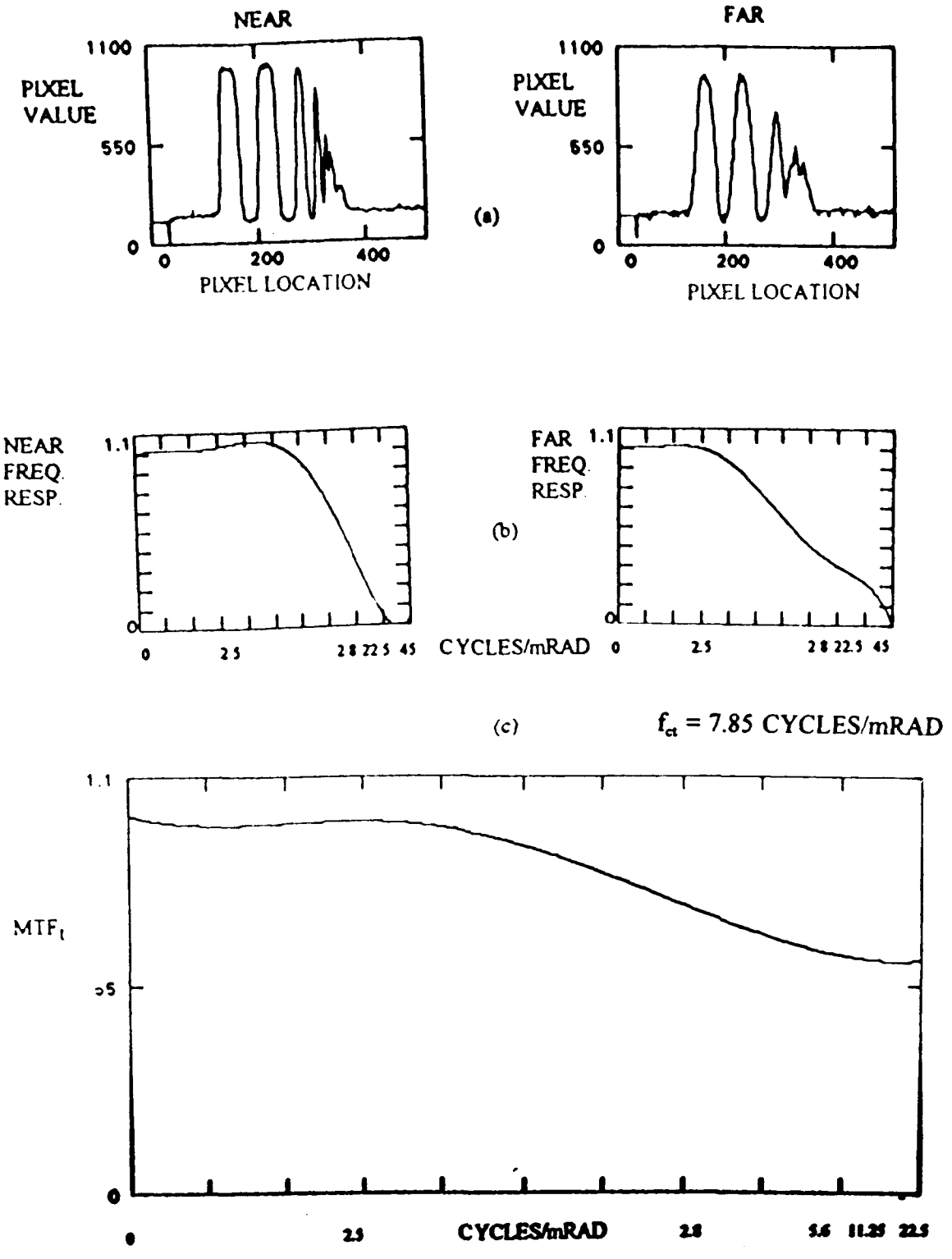

Figure 74. Data from 7:00 A.M. of August 21, 1992: (a) line pixel values of castellated black-white stripes for both targets; (b) normalized spatial frequency response of both targets based on the corresponding pixel values shown; (c) turbulence, MTF_t, derived from the ratio of the far to near target frequency response. Cutoff frequency, f_{ct}, for MTF_t is included.

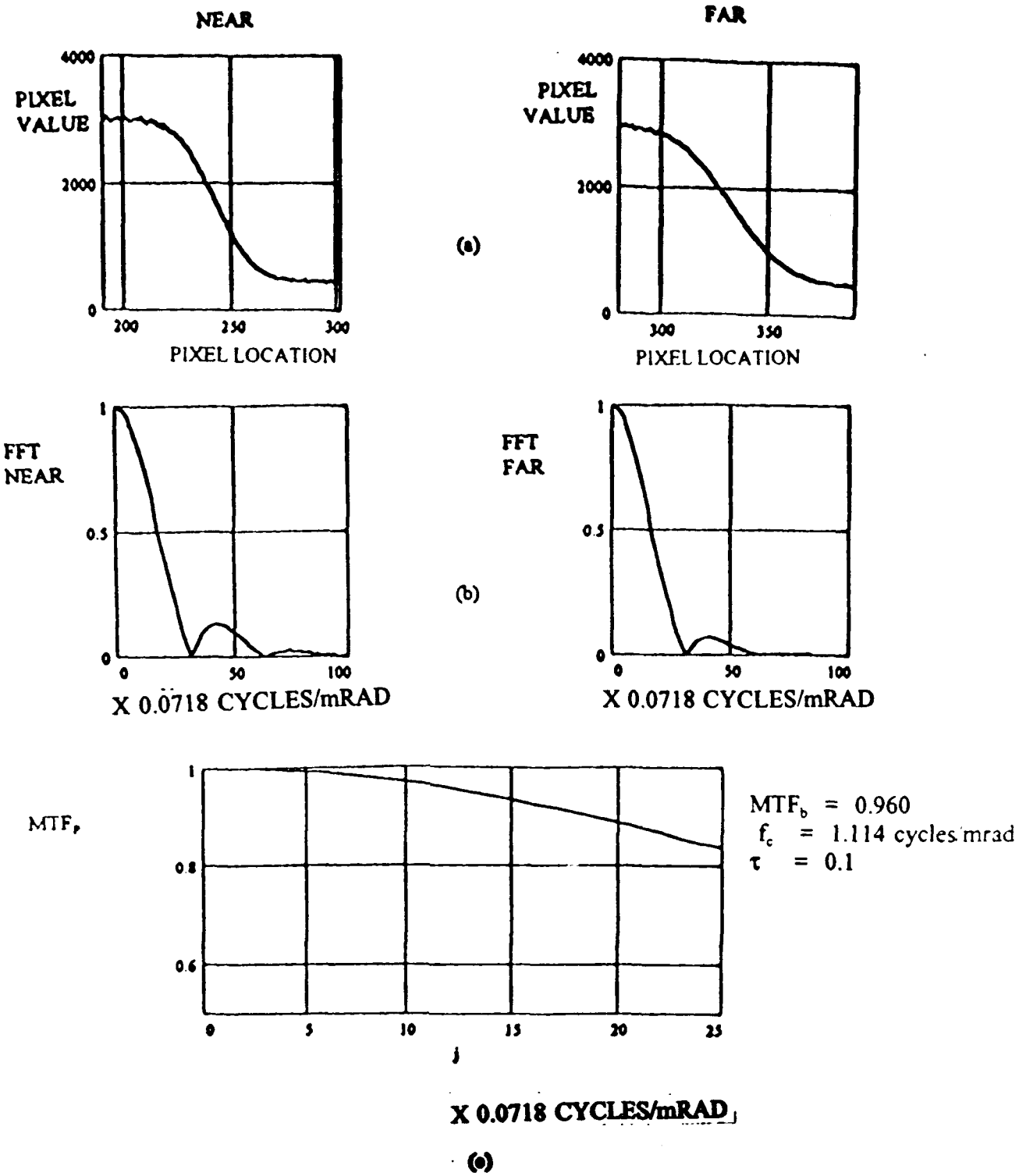

Figure 75. Data from 12:00 PM of August 21, 1992: (a) line pixel values of the black-white steps for both targets; (b) normalized, line FFTs of both targets based on the corresponding pixel values shown; (c) normalized aerosol MTF_p, derived from the ratio of the far target FFT to the near target FFT. Values for f_c, τ, and MTF_b are included.

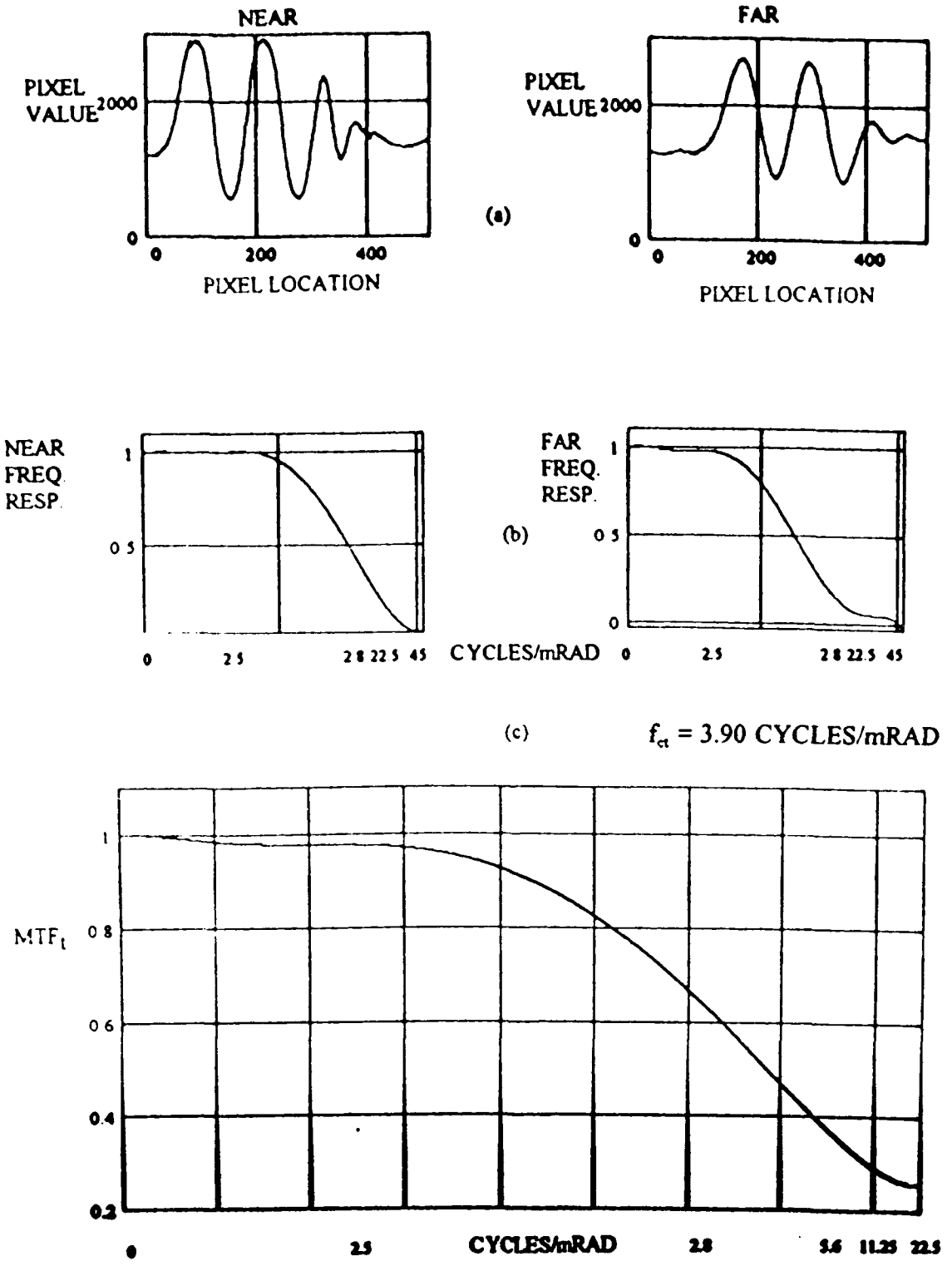

Figure 76. Data from 12:00 P.M. of August 21, 1992: (a) line pixel values of castellated black-white stripes for both targets; (b) normalized spatial frequency response of both targets based on the corresponding pixel values shown; (c) turbulence, MTF_t, derived from the ratio of the far to near target frequency response. Cutoff frequency, f_{ct}, for MTF_t is included.